

**BIOINSPIRED SURGICAL NEEDLE INSERTION MECHANICS IN SOFT
TISSUES FOR PERCUTANEOUS PROCEDURES**

A Dissertation
Submitted to
the Temple University Graduate Board

In Partial Fulfillment
of the Requirements for the Degree of
DOCTOR OF PHILOSOPHY

by
Sai Teja Reddy Gidde
August 2021

Examining Committee Members:

Dr. Parsaoran Hutapea, Advisory Chair, Department of Mechanical Engineering

Dr. Fei Ren, Department of Mechanical Engineering

Dr. Albert Kim, Department of Electrical and Computer Engineering

Dr. Santiago Orrego, External Member, Department of Bioengineering and Department of Oral Health Sciences, Temple University

©

Copyright

2021

by

Sai Teja Reddy Gidde

All Rights Reserved

ABSTRACT

Needles are commonly used to reach target locations inside of the human body for various medical interventions such as drug delivery, biopsy, and brachytherapy cancer treatment. The success of these procedures is highly dependent on whether the needle tip reaches the target. One of the most significant contributors to the target accuracy is the needle insertion force that causes needle-tip deflection, tissue deformation, and tissue damage. Recently there has been tremendous interest in the medical community to develop innovative surgical needles using biologically-inspired designs. It is well known that insects such as honeybee and mosquito steer their stingers effortlessly to a specific target and release their venom in a certain path through the skin with minimal force. These unique traits inspire this dissertation work to develop bioinspired needles and to study the insertion mechanics of these needles for reducing the insertion force, needle-tip deflection, tissue deformation, and tissue damage.

In this work, the insertion mechanics of honeybee-inspired needles with applied vibration in polyvinyl chloride (PVC) tissue phantom and chicken breast tissues was first investigated. It was observed that the insertion force was decreased by 43% and the needle tip deflection was minimized by 47% using honeybee-inspired needles. Furthermore, the insertion mechanics of mosquito-inspired needles in PVC tissue phantom and bovine liver tissues were studied. Design parameters such as maxilla design on the needle body, labrum-tip, vibration, and insertion velocity were considered. It was found that the insertion force was reduced by 60% in PVC tissues and 39% in bovine liver tissues using mosquito-inspired needles. To validate the developed bioinspired needle prototypes, a size scale

study was performed using insertion test in a PVC tissue phantom. It was confirmed that the insertion force was decreased by 38% using different needle sizes. An analytical LuGre friction model was used to explain the insertion mechanics and to confirm the experimental results.

Lastly, to investigate the effect of the insertion force reduction, the tissue deformation and the tissue damage studies were performed. Using a novel magnetic sensing system, it was observed that the tissue deformation caused by mosquito-inspired needles was decreased by 48%. A histological study was performed to quantify the tissue damage in bovine liver tissues. It was observed that the tissue damage of mosquito-inspired needles was reduced by 27% compared to standard needles.

In conclusion, this dissertation study shows that applying bioinspired needle designs and vibration during insertion into tissues reduces the insertion force, the needle-tip deflection, the tissue deformation, and the tissue damage. The outcome of this study will benefit medical communities to advance the bioinspired needles for vibration-assisted clinical procedures.

DEDICATION

I would like to express my deepest gratitude to my parents Narmada and Venkat Reddy and dedicate this thesis to them for their unconditional support and love in all my adventures especially this one.

ACKNOWLEDGMENTS

First of all, I wish to express my sincere gratitude to my advisor, Dr. Parsaoran Hutapea, for his guidance and support during this journey, who allowed me to work in his active research team and supported me throughout my Ph.D. studies. I am especially grateful for his trust in me, and the freedom he gave me to investigate diverse subjects. I truly learned a great deal on all aspects of research from conceptual ideas to the design of experiments to technical writing to be a good mentor. I am further grateful to thank my dissertation committee members, Dr. Fei Ren, Dr. Albert Kim, and Dr. Santiago Orrego for their valuable inputs.

I have been fortunate enough to work and spend time with amazing people here at Temple. I would like to thank Dr. Mohammad Kiani and Dr. Nancy Pleshko for allowing me to work in their research labs. I especially would like to acknowledge the past and current team members of the Composites Laboratory for their support and motivation.

I would like to thank the National Science Foundation (CMMI Award #1917711) Temple University Graduate School and the College of Engineering for their financial support and the opportunity to perform my research.

Finally, I would like to thank my friends and relatives back home for their support and encouragement. Most of all, I am infinitely thankful to my family, the love and trust of my parents led me to and through this pursuit. It was certainly not easy, but we did it. Last but certainly not least, thank you to my fiancée Vaishnavi for all her patience, love and understanding through this journey.

LIST OF ABBREVIATIONS

CAD – Computer-Aided Design

DPBS – Dulbecco's Phosphate-Buffered Saline

LIPMM – Laser-Induced Plasma Micro-Machining

MTJ – Magnetic Tunnel Junction

OCT – Optimal Cutting Temperature

PVC – Polyvinyl chloride

SD – Standard Deviation

NOMENCLATURE

a	Amplitude
α	Bevel-tip angle
D	Diameter of the needle
$g(v)$	Stribeck velocity parameter
E	Young's modulus
E_R	Tissue stiffness of the crack surface
E_T	Tissue stiffness
F_C	Cutting force stiffness resistance from the tissue
F_f	Friction force
F_n	Normal force
F_s	Stiffness resistance from the tissue
L	Length of the needle
$L(t)$	Length of puncture into the tissue or depth of the insertion
L_m	Length of the maxilla design on the needle (number of the maxilla on the needle)
L_r	Labrum-tip
M_a	Maxilla angle
η	at point
σ_0	Stiffness coefficient
σ_1	Damping coefficient
σ_2	The viscous relative damping coefficient
Ω	Ohm

t	Thickness of the maxilla
μ_c	The normalized coulomb friction coefficient
μ_s	The normalized static friction coefficient
μT	Microtesla
v_s	The stribeck effect velocity
v	Total velocity
v_i	Insertion speed
ω	Vibrational frequency
x	Distance between inner maxilla of the needle
x_{tip}	Position of the needle-tip
x_1	Position of the tissue before puncture
x_2	Position of the tissue after puncture
$z(\eta, t)$	Deformation due to two elements at a point η and at time t
z	Deflection of the needle

TABLE OF CONTENTS

ABSTRACT	iii
DEDICATION	v
ACKNOWLEDGMENTS	vi
LIST OF ABBREVIATIONS.....	vii
NOMENCLATURE	viii
LIST OF TABLES.....	xiii
LIST OF FIGURES	xiv
CHAPTER 1 INTRODUCTION	1
1.1 Needle Insertion Mechanics	2
1.1.1 Needle Geometry and Materials.....	4
1.1.2 Tissue Material Properties	7
1.1.3 Needle Insertion Velocity.....	9
1.1.4 Insertion Method.....	10
1.2 Research Motivation and Related Work	11
1.2.1 Bioinspired Needle Mechanics.....	11
1.3 Problem Statement	17
CHAPTER 2 EXPERIMENTS AND METHODS.....	21
2.1 Needle Insertion Force Measurement Test Method	21
2.2 Manufacturing of Tissue Mimicking Materials	22

2.3 Needle Deflection Method	24
2.4 Tissue Deformation Method.....	25
2.5 Tissue Damage Method.....	27
2.6 Statistical Analysis	31
CHAPTER 3 VIBRATION CUTTING OF HONEYBEE-INSPIRED NEEDLES	33
3.1 Honeybee-Inspired Needle Insertion Mechanics	33
3.2 Results of Vibration-Assisted Honeybee-Inspired Needles	36
3.2.1 Parametric Study.....	36
3.2.2 Needle Insertion Force Study	40
3.2.3 Needle Deflection Study.....	43
3.3 Discussions.....	44
CHAPTER 4 VIBRATION CUTTING OF MOSQUITO-INSPIRED NEEDLES	46
4.1 Mosquito-Inspired Needle Design and Modifications	46
4.2 Theoretical Analysis of Vibration Influence on Insertion Force.....	50
4.3 Results of Mosquito-Inspired Needles with Vibration.....	58
4.3.1 Parametric Study.....	58
4.3.2 Needle Insertion Force Study	64
4.3.3 Friction Force Study	66
4.3.4 Size-Scale study.....	68

4.3.5 Tissue Deformation Analysis	71
4.3.6 Ex-vivo Insertion Tests into Biological Tissue	73
4.3.7 Tissue Damage Analysis	77
4.4 Discussions.....	79
CHAPTER 5 CONCLUSION AND FUTURE WORK	82
5.1 Conclusion.....	82
5.2 Future Work	83
REFERENCES	86
APPENDIX A: COMPRESSION TESTS FOR PVC AND GELATIN PHANTOMS .	103
APPENDIX B: MATLAB CODE FOR THEORETICAL MODEL.....	105

LIST OF TABLES

Table 2.1. The Young's Modulus properties comparison of artificial [77] and biological tissues [83].	24
Table 3.1. Insertion parameters of the honeybee and mosquito used in this study.....	35
Table 3.2. Honeybee-inspired needle insertion (with and without vibration) deflection values for distance from the edge of the tissue to the center of the insertion path.	44
Table 4.1. Insertion parameters for studying the mosquito-inspired needle.	49
Table 4.2. The needle insertion vibration cutting parameters and their forces.	50
Table 4.3. The statistical data information for the area of damage in bovine liver tissue due to standard and mosquito-inspired needles.	77
Table A1. The Young's Modulus and insertion force values for different tissue-mimicking materials used in this study.....	104

LIST OF FIGURES

Figure 1.1. Forces acting during needle-tissue interaction are stiffness force (F_S), friction force (F_F) and cutting forces (F_C).....	2
Figure 1.2. A typical needle insertion process consists of insertion, relaxation, and extraction phases in soft tissue. (Insertion speed – 3 mm/sec, Insertion depth – 65 mm, Needle – 18-gauge, tip angle - 40°, tissue - PVC).....	3
Figure 1.3. A schematic representation of needle geometry consists of needle surface, diameter, and needle-tip.....	5
Figure 1.4. The schematic representation of the mosquito proboscis.....	13
Figure 1.5. The bioinspired geometry on the needle body a) jagged geometry on the side of the needle inspired from mosquito (Izumi et al. 2008), b) the standard design on the needle body with a tip angle of 30 deg (Aoyagi et al. 2008), c) the harpoon shape inspired from mosquito-proboscis (Aoyagi et al. 2008), d) the harpoon shape with different geometry to mimic the mechanism of the mosquito-proboscis (Annie L et al. 2020) and e) the honeybee-inspired barb geometry on the needle body (Mohammad et al. 2018).....	15
Figure 1.6. The schematic representation of the needle insertion with longitudinal vibration (parallel to the axis of insertion).....	19
Figure 2.1. a) The applied longitudinal vibration in the insertion direction and b) the experimental needle insertion test setup for force measurement in tissues.	22

Figure 2.2. The distance from the edge of the tissue to the center of the wound: a) top view showing the initial section and b) a schematic representation (side view) of the needle deflection. 25

Figure 2.3. A schematic representation of the tissue deformation in distance (d) during needle insertion. 26

Figure 2.4. A schematic representation of the needle insertion test setup along with the novel sensing test setup (close-up view) with a soft magnet (in red color) and MTJ sensor array for measuring tissue deformation in PVC gel..... 27

Figure 2.5. a) A schematic representation of the sectioned bovine liver tissue sample for histology after insertion tests and b) the cryotome machine which was used for sectioning the bovine liver tissue sample of 0.5 μm thickness. 28

Figure 2.6. a) The sectioned slides of the bovine liver tissue sample with a thickness of 0.5 μm and b) the hematoxylin & eosin-stained slides..... 30

Figure 3.1. a) the honeybee stinger, b) 2D drawing of the stinger (Mohammad et al. 2018), and c) a schematic representation of the honeybee-inspired needle and its parameters such as barb height, barb front angle, and the number of barbs..... 34

Figure 3.2. The microscopic view of (a) honeybee-inspired needle and (b) standard bevel-tip needle..... 36

Figure 3.3. Effect of different barb angles on honeybee-inspired needle peak force (maximum insertion force) without vibration (Barb height - 0.5 mm, insertion

depth - 60 mm, and insertion speed - 3 mm/sec). Bars sharing the same letters at the top of the bar plot is not significantly different at the 95% level, based on post-hoc Tukey tests37

Figure 3.4. Effect of different barb angles on honeybee-inspired needle peak force (maximum insertion force) without vibration (Barb height - 0.5 mm, insertion depth - 60 mm, and insertion speed - 3 mm/sec). Bars sharing the same letters at the top of the bar graph are not significantly different at the 95% level, based on post-hoc Tukey tests..... 38

Figure 3.5. Effect of different frequencies on peak force of the honeybee-inspired needle (Insertion speed - 3 mm/sec, amplitude - 5µm, insertion depth - 60 mm, barb angle - 165°, and barb height - 0.5 mm). Bars sharing the same letters at the top of the bar graph are not significantly different at the 95% level, based on post-hoc Tukey tests..... 40

Figure 3.6. The maximum insertion forces obtained from insertion tests into PVC gels using bioinspired (honeybee)and standard bevel-tip needles (Vibration - 60 Hz, amplitude - 5 µm, insertion speed - 3 mm/sec, depth of insertion - 60 mm). Bars sharing the same letters at the top of the bar graph are not significantly different at the 95% level, based on post-hoc Tukey tests. 41

Figure 3.7. The maximum insertion forces obtained from ex-vivo insertion tests into the chicken breast using bioinspired (honeybee) and standard bevel-tip needles (Vibration - 60 Hz, amplitude - 5 µm, insertion speed - 3 mm/sec, depth of insertion - 60 mm). Bars sharing the different letters at the top of the bar graph are significantly different at the 95% level, based on post-hoc Tukey tests. 43

Figure 4.1. a) The maxilla needle in mosquito-proboscis (Izumi et al. 2011) and b) the 2D representation of the proposed maxilla needle on the needle body with parameters labrum-tip (L_r), maxilla angle (M_a), length of maxilla design (L_m), length of the needle (L), the diameter of the needle (D), thickness (t), and distance between the inner maxilla (x)..... 47

Figure 4.2. a) The 3D models and b) 3D printed standard and mosquito-inspired needles and a closer view of the labrum-tip design. 48

Figure 4.3. The insertion force consists of cutting force (F_c), friction force (F_f), and stiffness resistance force from the tissue (F_s)51

Figure 4.4. The needle and tissue interaction at different stages of insertion i.e., before puncture (x_1 position), puncture and after puncture (x_2 position).....52

Figure 4.5. The cutting force during needle-tip tissue interaction with a magnitude of F_c . (α – needle-tip angle and E_R – tissue stiffness at the crack)53

Figure 4.6. The insertion force (friction and cutting force) comparison between experimental data and model with the influence of applied longitudinal vibration57

Figure 4.7. The mosquito-inspired needle design parameter on the insertion force for the parameter thickness (t) in mm (no vibration, Insertion velocity = 1 mm/sec, PVC tissue phantom with $E = 6$ kPa). Bars sharing the same letters at the top of the bar graphs are not significantly different at the 95% level, based on post-hoc Tukey tests. ...59

Figure 4.8. The mosquito-inspired needle design parameter on the maximum insertion force for maxilla angle (M_a) in deg (no vibration, Insertion velocity = 1 mm/sec, PVC tissue phantom with $E = 6$ kPa). Bars sharing the same letters at the top of the bar graph is not significantly different at the 95% level, based on post-hoc Tukey tests.60

Figure 4.9. The insertion force results for different vibrational frequencies ranging from 0 to 500 Hz. (Insertion speed – 1 mm/sec, amplitude -5 μm and depth of insertion – 60 mm)62

Figure 4.10. The insertion force results for mosquito-inspired needle by varying the insertion velocity from 1 to 10 mm/sec with a constant vibration frequency of 200 Hz and amplitude of 5 μm 63

Figure 4.11. The insertion and extraction force using standard and mosquito-inspired needles with and without vibration. (Vibration – 200 Hz, Insertion Depth – 60 mm, Insertion speed – 1 mm/sec and Amplitude – 5 μm)65

Figure 4.12. The standard deviation values for the insertion force using standard needle without vibration and mosquito needle with vibration. Bars sharing different letters are significant at the 95% level66

Figure 4.13. The insertion and extraction force using standard and mosquito-inspired needles with and without vibration. (Vibration – 200 Hz, Insertion Depth – 60 mm, Insertion speed – 1 mm/sec and Amplitude – 5 μm)68

Figure 4.14. The approximation of measured cutting force from insertion and

extraction force of the experimental data during insertion into PVC tissue phantom69

Figure 4.15. The standard and mosquito-inspired needles with different diameters (outer diameter (OD) = 1.6, 2, and 3 in mm). ($M_a = 170^\circ$, $t = 0.2$ mm, $\alpha = 40^\circ$).....70

Figure 4.16. The recorded tissue deformation using a) standard needle without vibration and b) mosquito needle with vibration72

Figure 4.17. The magnetic sensing recorded tissue deformation in distance (mm) in PVC tissue phantom with a standard needle and mosquito-inspired needle73

Figure 4.18. a) *Ex-vivo* insertion tests into bovine liver tissue and b) the average insertion force obtained from insertion tests into bovine liver tissue with the vibration of 200 Hz, an amplitude of 5 μ m, and insertion velocity of 1 mm/sec.....75

Figure 4.19. The standard deviation for insertion force into bovine liver tissue at a depth of 60 mm using both standard and mosquito-inspired needles. Bars with the different letter is significant at the 95% level76

Figure 4.20. Magnified view of the damage in different bovine liver tissue samples due to a) standard needle, b) mosquito-inspired needle and c) the schematic representation of the damaged area in bovine liver tissues (M – Mosquito-inspired and S – standard).....79

Figure A1. The compression test setup to determine the Young’s Modulus of the tissue phantom103

CHAPTER 1

INTRODUCTION

Needles are commonly used in medical procedures that include both diagnosis and therapy such as in vivo analysis using optical, Raman spectroscopy, chemotherapy, brachytherapy, photodynamic therapy, rf-based thermal ablation, biopsy, and viral or gene therapy [1-5]. There have been many research activities to design innovative surgery needles to reduce tissue damage for procedures such as blood sampling, biopsy, and brachytherapy in the prostate, liver, kidney, and other tissues [1, 2]. For example, a core needle biopsy [6] technique is commonly used to extract tissue samples. A sample of tissue is cut and taken from the organ with a needle using an ultrasound-guided percutaneous approach and is then assessed for the presence of cancerous cells by histopathological analysis or molecular profiling. The needle insertion in these procedures is highly dependent on the insertion target accuracy [7-9].

The accuracy of needle steering inside tissue is influenced by mainly the insertion force which causes the tip deflection, tissue deformation, and tissue damage [10-13]. It has been investigated decreasing the insertion force can improve the needle insertion procedure [2, 10]. Additionally, the decrease in the insertion force could potentially result in less pain, trauma, and edema caused to the patients, such that it allows them to recover in a shorter time [15].

The insertion force occurs when the needle first breaks through the tissue, and a high insertion force leads to more tissue damage [12, 16]. The insertion force consists of the cutting force (F_c), the friction force (F_f), and the stiffness resistance from the tissue (F_s)

[2] as shown in Fig 1.1. The stiffness force (F_s) occurs during needle puncture into the tissue; the cutting force (F_c) is the force at the needle-tip, and the friction force (F_f) occurs at the interface between needle during insertion after puncture. Also during needle-tissue interactions, it has been discovered that the largest contributing force to the insertion force is the friction force [17, 18].

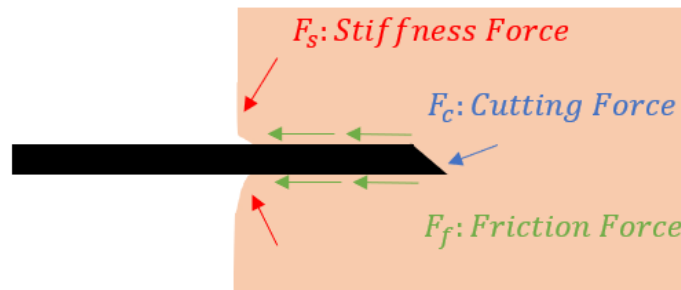


Figure 1.1. Forces acting during needle-tissue interaction are the stiffness force (F_s), the friction force (F_f), and the cutting force (F_c).

1.1 Needle Insertion Mechanics

The interaction between needle and tissue during insertion leads to different phases [2]. These phases are insertion, relaxation, and extraction as shown in Fig 1.2. A typical needle insertion into the bovine liver is shown in Fig 1.2 using an 18-gauge standard needle. During the insertion phase, the needle intersects with the tissue resulting in the first contact, and an initial crack is formed, the crack is then widened and increased by the size of the needle, and then the needle continues inside the tissue, resulting in friction and cutting (or rupture) force. In the intermediate phase, i.e., the relaxation phase happens when the needle changes the direction, resulting in force change from positive to negative. Finally, the extraction phase is due to the needle pulling out from the tissue and the extraction force is

mainly due to the frictional force. Evidently, if the tissue stiffness is larger, such as in muscle and kidney, the needle displacement will most likely be greater and the target inaccuracy will occur [19, 20].

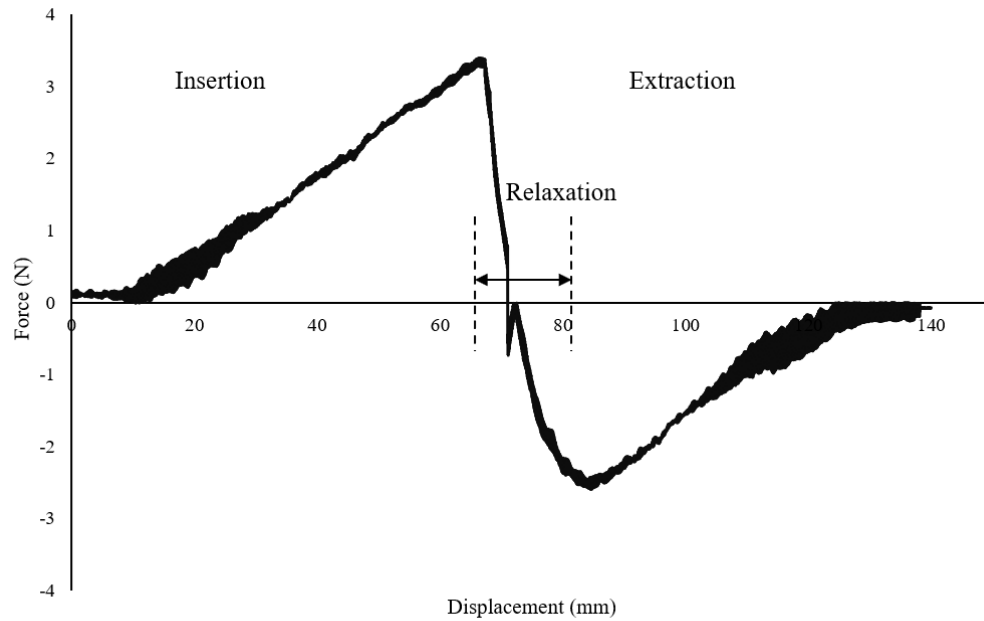


Figure 1.2. A typical needle insertion process consists of insertion, relaxation, and extraction phases in soft tissue. (Insertion speed – 3 mm/sec, Insertion depth – 65 mm, Needle – 18-gauge, tip angle - 40°, tissue - PVC)

Understanding the parameters such as needle geometry, the needle-tip, the velocity of insertion, tissue material properties, and insertion with rotation and vibration [6, 14–20] that affect the insertion force is critical in improving the insertion efficacy. Moreover, a typical procedure is generally done by inserting a needle to reach a certain target at the maximum insertion depth where the maximum insertion force occurs. It has been investigated that the target inaccuracy during a procedure can be related to the increase in the maximum insertion force [1, 28, 29]. In other words, the increase in insertion depth increases the maximum insertion force. Therefore, if the maximum insertion force is reduced, the damage to the tissue is decreased [12, 30].

1.1.1 Needle Geometry and Materials

The insertion force is highly dependent on the needle tip, size, and shape, such as shown in Fig 1.3. The geometrical effects on insertion force have been studied by many researchers [22–24]. For example, Shergold and Fleck [24] studied the mechanics of sharp and blunt tip needles and found that sharp tip needle lowers the insertion force by up to 40%. In another study, Okamura *et al.* [22] found that a change in diameter and needle shape will result in a change in the needle insertion force by 25%. Stellman [23] showed that a hypodermic needle design could reduce the insertion force by 70% and also minimize the needle deflection. Also, the effect of cutting-edge angles of the needle-tip on insertion force was investigated by Moore *et al.* [31] and found that the decrease in the cutting force is due to the cutting edge angle larger than 30°.

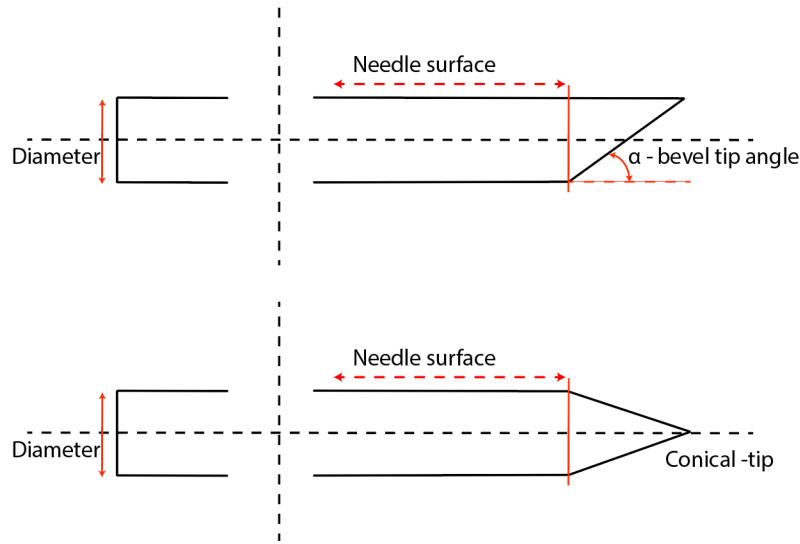


Figure 1.3. A schematic representation of needle geometry consists of needle surface, diameter, and needle-tip.

The stiffness of the needle during insertion into soft tissue plays an important role in the force behavior. For instance, a standard 16-gauge stainless steel needle has a higher impact on the force behavior compared with that of polymer needles. Polymer needles have been used to study the influence of the needle geometry on the insertion force [32, 33]. In another study, the fabrication of microneedles to mimic the mosquito-proboscis has been conducted to show the reduction in the insertion force [34]. Kim *et al.* studied the mosquito-inspired microneedle insertion in porcine skin tissue and found that the mechanophysical stimuli (i.e., 1 to 1000 Hz vibration) lower the insertion force [35].

Due to the complex shapes and geometries, the fabrication of metal bioinspired design needles is very challenging. Therefore, in this research, polymer needles were used. The polymer needles offer transparent and biodegradable functionalities for the new biomedical solutions [36, 37]. The needles were manufactured using a 3D printer, which makes the

manufacturing process easy and cost-efficient. The manufacturing of 3D printed bioinspired needles was also kept at the same limitation but the mechanical properties of polymer needles are comparatively shown to be better because of biocompatibility and biodegradability [38]. The needle needs to have mechanical properties such as high tensile strength, easy to handle, should not break unexpectedly, and cause minimal tissue reaction during needle insertion [39]. However, there is a major challenge using these polymer needles because their stiffness (measured as Young's Modulus) has a factor of 100 lower than the steel. But, the polymer needles offer shear-induced breakage due to polymer viscoelasticity [38, 40]. The shear-induced breakage for the polymer needles is dependent on its stiffness such that the force acting on the needle tends to break the polymer needle if the stiffness is lower than the tissue stiffness. An 18-gauge (outer diameter of 1.27 mm) polymer needle buckles easily in tissues with stiffness larger than 5 kPa and results in higher needle bending or deflection. Due to this reason, the needles were scaled to 3 mm to study the influence of vibration on bioinspired needle insertion force. The polymer material used for manufacturing the bioinspired needles in this study consists of 30% Acrylic monomer, 25% Isobornyl acrylate, 15% Phenol, and a small percentage of other polymers. The scale size was also studied to show the influence of vibration on the insertion force. The experiments were carried out in PVC tissues with stiffness smaller than 4 kPa.

The shape of the needle-tip also plays a vital role in minimizing the needle deflection or reducing the insertion force [11, 33, 41, 42]. The conical needles tend to create crack extensions with star-shaped cracks on the tissue which are steady and increases with an increase in insertion depth, whereas the bevel-tip needles create circular crack extensions

because of the tip-angle and the lower axial force [2]. The bevel-tip angle needles show less insertion force compared to conical tip angle needles [2, 29]. A novel compliant geometry which consists of slit shapes at the needle-tip assists in converting the longitudinal cutting to transverse cutting was investigated by Barnett *et al.* [43] to reduce the friction force. The effect of different needle-tip designs such as bevel, blunt, triangular, and cone was investigated by Shan *et al.* [44]. From all these studies, altering the needle-tip geometry and changing the design can affect the insertion force [45]. With the increase in insertion force leading to more damage to the tissue [1], it is essential to study the effect of needle geometry on the insertion force that should help in reducing the tissue damage.

1.1.2 Tissue Material Properties

The insertion force also depends on the stiffness properties of the tissue. The tissues with different layers are crucial in determining the needle insertion force as it passes through the different tissue layers such as skin, muscle, fatty, and connective tissue [1]. The needle insertion in blood sampling procedures has to go through the skin tissue, which is smaller in stiffness properties compared to porcine skin outer layer tissue. The biological tissue inhomogeneous and anisotropic properties could also affect the needle insertion force. Van Gerwen *et al.* [2] showed that there are more than 99 papers that study tissue characteristics. Among them, 38 are in artificial tissues such as gelatin, PVC, plastisol, silicone, or similar materials, 8 are in human tissues and the remaining papers were done in biological tissues. The different tissues studied in these works were shown the influence of tissue property on insertion force. The artificial tissue materials consist of homogenous properties and biological tissue materials are non-homogenous properties. For example,

the insertion force acting on the needle is lower for the tissue stiffness around 1 to 2 kPa compared to the tissue with stiffness larger than 4 kPa [2]. Similarly, when the insertion force acting on the needle is found higher in tissue with a stiffness greater than 4 kPa compared with tissue with lower stiffness, less than 3 kPa [46]. The needle insertion force is dependent on tissue stiffness. If the stiffness of the needle is higher than the tissue stiffness properties, the needle bending inside the tissue can be avoided [47].

The non-linear force curve in biological tissues is due to anisotropy and the existence of fluid [48]. But, the force curve is linear in artificial tissues and has many advantages over biological tissues in terms of reproducibility, availability, and visibility [2]. For this reason, researchers have utilized artificial tissues in studying the needle insertion mechanics [18, 32, 45, 49–52]. The needle-tissue interaction force behavior changes accordingly with the change in tissue properties. For example, Misra *et al.* [53] studied the stiffness/puncture force due to the impact of artificial gel properties and found that the force depth curve is linear in the artificial gel. From the survey done by Yang *et al.* [30], the insertion force required to insert the needle in porcine skin is larger than that of human skin tissue. However, irrespective of the tissue material, if the surface area of the needle is minimized, the insertion force can be reduced [32, 54]. This force reduction could lead to a decrease in tissue damage [12, 55].

1.1.3 Needle Insertion Velocity

The insertion velocity is another crucial parameter that contributes to the increase or decrease in the insertion force. Several researchers have studied the effect of insertion velocity on the insertion force and tissue deformation [13, 19, 56, 57]. For instance, Heverly *et al.* [57] showed that increasing insertion velocity reduces the puncture force in the porcine heart by 48%. Furthermore, the effect of insertion velocity on the insertion force was also studied by researchers using biological tissues [21, 58, 59] and artificial tissue-mimicking materials [7, 60, 61]. They found that increasing the insertion velocity results in a higher force. Mahvash and Dupont [21] also showed that an increase in the insertion velocity reduces the puncture force. Based on the physician feedback for prostate brachytherapy, Abolhassani *et al.* [19] considered the insertion velocity ranging from 1 to 20 mm/sec to study the influence of velocity on the tissue deformation. They found that increasing the velocity results in higher tissue deformation. DiMaio and Salcudean [7] showed that the friction force increases with increasing velocity but the cutting force does not increase as much compared to that of the friction force. The needle deflection also depends on the insertion velocity, which means decreasing the insertion velocity will minimize the needle deflection [1]. From all these studies, it is understood that increasing the insertion velocity will decrease the stiffness force but increases the insertion force which results in tissue damage [2, 21].

1.1.4 Insertion Method

Another parameter that influences the insertion force is the insertion method. Some examples of insertion methods are rotating needle insertion [62,63], fast needle insertion method [21,64], and applied vibration method [40, 41]. Among these procedures, the applied vibration method has been shown to lower the insertion force and particularly, the cutting force. From the literature, researchers have studied vibration tissue cutting [27,67–70], but the work addressing vibration tissue cutting using a bioinspired needle is very limited [25, 38]. The applied vibration is a periodic oscillatory response of a mechanical system in a sinusoidal waveform [71]. Barnett *et al.* studied the insertion force of the hypodermic needles at varying vibration frequencies [43]. Other researchers have also studied vibration frequency ranging from 100 Hz – 20 kHz to lower the insertion force [30, 40, 42, 43] and found that increasing the vibration will result in a higher insertion force. The advantage of using vibration leads to a decrease in the cutting force [74], which aids the reduction of the insertion force. To further study how vibration reduces the insertion force, Huang *et al.* [68] showed a 28% reduction in the maximum insertion force using a hypodermic needle (27-gauge needle). Clement *et al.* [27] showed 73% a reduction in the maximum insertion force using a hypodermic needle (25-gauge needle). The reduction in the insertion force was also achieved by applying axial or longitudinal vibration on microneedle [75] and ultrasonic vibration on hypodermic needles [68]. These forces were tested by varying frequencies and amplitudes in optimizing the vibration parameter on tissue cutting [72]. It is shown in Fig 1.1 that the insertion force is the summation of friction and cutting force. If the cutting force can be reduced with the applied vibration and the friction force is reduced by changing the needle geometry, the insertion force can

therefore be decreased. In this dissertation study, the longitudinal vibration is applied to the bioinspired needle to reduce the insertion force.

1.2 Research Motivation and Related Work

A biologically inspired solution can help to lower the insertion force caused during percutaneous procedures. Insect stingers of honeybees, wasps, scorpions, and mosquitos have sophisticated sting mechanics and morphological structures. Researchers are inspired by the unique traits of these insects that steer their stingers effortlessly to a specific target and release their venom in a certain path through the skin [29, 37–39]. The research efforts to mimic insect stingers are ongoing with penetration mechanisms such as honeybee [29, 40, 41], and mosquito [30, 37] to facilitate better needle insertion in skin tissues (higher stiffness properties) and to lower the insertion force. These mechanisms include needle geometry, needle-tip design, and vibration during insertion. For example, Mohammad *et al.* [12] investigated the honeybee stinger barb geometry on the needle body and found a reduction of 35% in PVC tissue phantom and 46% in bovine liver, and a 31% reduction in tissue damage compared to standard needles. Gidde *et al.* [20, 55] also investigated the honeybee-inspired needles with vibration and showed up to 50% reduction in PVC tissue phantom and 43% in chicken breast compared to standard needles without vibration. The insertion force can be reduced with a change in needle geometry and with needle control during insertion (applied longitudinal vibration). However, it is equally important to decrease the tissue damage caused during these procedures. Therefore, the geometry of the design in this study is designed in such a way that the extraction force can be reduced and damage to the tissue can be reduced. To implement this design on the needle body and the

vibration during insertion, it is crucial to understand the mechanics of a bioinspired (mosquito and honeybee) needle and its effect on insertion force from the literature, which is discussed in the following Section.

1.2.1 Bioinspired Needle Mechanics

Insect stingers hold promise for modernizing needle design, as the stingers have evolved and become adept at entering human tissue through various mechanical and dynamic insertion techniques [81]. Few studies in the literature discuss bioinspired needle mechanics in soft tissues [30, 55–58]. Researchers studied different bioinspired needle mechanics such as harpoon shape on the needle body to optimize the vibration tissue cutting [84], jagged shape on the microneedle [34], multiple cutting shapes on the needle-tip geometry [16], barb geometry on the needle body [29, 30], and compliant geometry (transverse cut) at the needle-tip [66] to lower the insertion force. Zhao *et al.* [85] studied the honeybee and paper wasp mechanisms into silica gel and showed 7-8 mN puncture force with an insertion velocity of 1 $\mu\text{m}/\text{sec}$. From the literature, the idea of having a honeybee-inspired barbed design on the needle body could potentially lower the force because of the removal of material. The honeybee stinger has asymmetric barbs and lays the flush against the body of the stinger [80]. It also has been shown that the barbs on the needle body surface reduce insertion force but increases the extraction force to about 70 times that of the acupuncture needle [40, 56].

Another insect-inspired mechanism is the mosquito, the most well-known and best-studied hematophagous animal. A female mosquito (males do not feed on blood) is evolved to have a biological needle-like structure known as a fascicle to penetrate human or animal

skin easily. The important tool used by the female mosquito during its penetration into the skin to suck the blood is its mouthpart known as the proboscis. Aoyagi *et al.* [67] investigated the fascicle structure using a Scanning Electron Microscope (SEM). The vibration was applied longitudinally during needle insertion to study the vibration effect on insertion force with a mosquito-inspired needle. The mosquito proboscis mechanism has exceptional ability and penetrating technique in reducing insertion force with minimal pain [45, 46, 53]. Kong and Wu [87] investigated the penetrating behavior of mosquitoes while fascicle penetrates human skin.

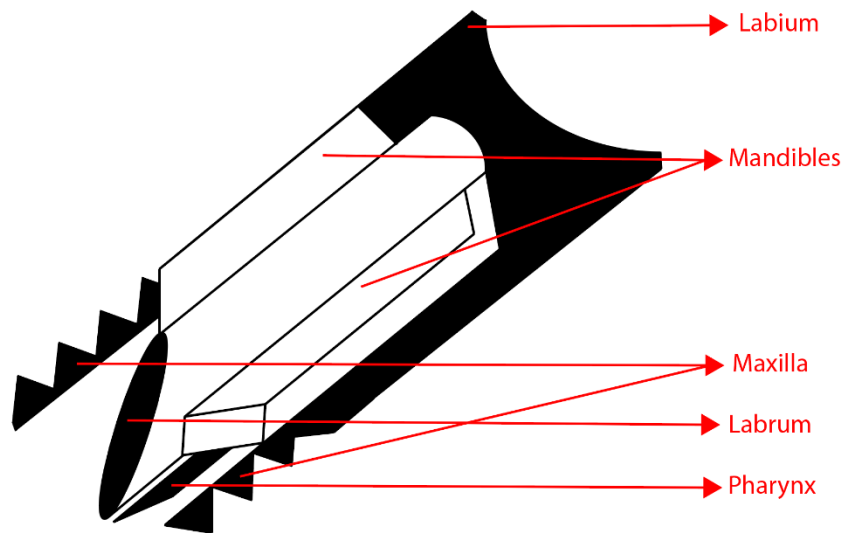


Figure 1.4. The schematic representation of the mosquito proboscis.

The proboscis consists of six elements (also called needles) such as two maxilla (used to pierce the skin tissue), mandibles (acts as a support), labrum (the tip region which is used to transport blood), and hypopharynx (which is for injecting blood-thinning saliva)

[34,36]. The two maxillas have a jagged structure, which is said to be functional for easy insertion [88]. The schematic representation of the mosquito proboscis with all the six elements is shown in Fig 1.4. Among the six elements that are shown, the maxilla which has a jagged structure is said to be functional for easy insertion along with the labrum tip. This feature of mosquito was designed on the needle body to lower insertion force. The jagged structure was carved on the needle body in this study and was symmetric throughout the design to avoid drag force. The other advantage of utilizing the maxilla design is that the extraction force can be reduced. The labrum design at the needle-tip, which has a curve shape helps in reducing the cutting force.

From the literature, the bioinspired geometry designs on the needle body are shown in Fig 1.5. The researchers studied the mechanics of the bioinspired designs for the needle body on the effect of insertion force and tissue deformation. In Section 1.1, the different phases of the needle insertion in soft tissues were discussed. The insertion force consists of cutting and friction force, which means the friction force depends on the frictional interface between the needle and tissue. If the frictional interface is reduced in the body surface, the damping coefficient will be lowered and causes a decrease in the friction force. Similarly, the cutting force that depends on the needle-tip and the insertion method such as increasing velocity should result in a higher force. With applied vibration during needle insertion, the cutting force should reduce and should lead to less effort in penetrating tissues.

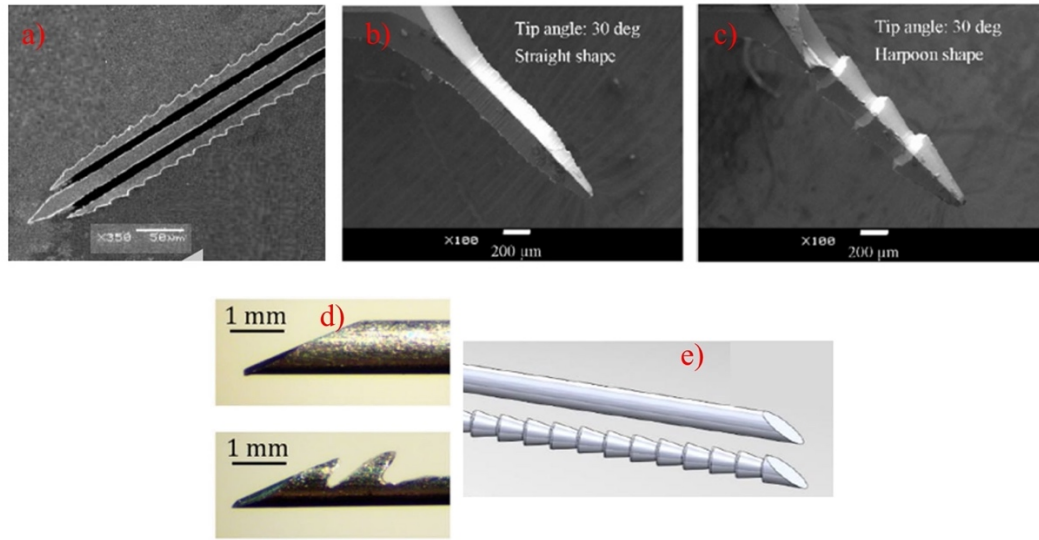


Figure 1.5. The bioinspired geometry on the needle body a) jagged geometry on the side of the needle inspired from mosquito (Izumi et al. 2008), b) the standard design on the needle body with a tip angle of 30 deg (Aoyagi et al. 2008), c) the harpoon shape inspired from mosquito-proboscis (Aoyagi et al. 2008), d) the harpoon shape with different geometry to mimic the mechanism of the mosquito-proboscis (Annie L et al. 2020) and e) the honeybee-inspired barb geometry on the needle body (Mohammad et al. 2018).

The vibration during needle insertion has been shown to improve the needle placement accuracy by the reduction in needle insertion force and needle deflection. In particular, a mosquito-inspired vibration has gained interest due to its penetrating technique in reducing insertion force with minimal pain [30], [45–47]. The vibration of the mosquito is reported to be a longitudinal direction between 15 to 30 Hz [76]. The longitudinal or axial vibration is parallel to the direction of the mosquito-proboscis bite into the human or animal skin tissue. The other important addition of vibration during needle insertion discussed by Barnett *et al.* is that the vibration lowers the needle insertion force, which allows for greater

blood sampling and also the stress specifically in animals [43]. To study the mechanics of the vibration tissue cutting for human use in percutaneous procedures, it is important to understand the mechanics and optimization of the vibration parameter during needle insertion. The mosquito vibration has been observed through the high-speed camera during its insertion into skin tissue [47, 71]. The research efforts to mimic mosquito mechanism has shown interest in the medical community to improve the needle insertion procedure and minimize the target placement error. Specifically, the vibration during mosquito proboscis has gained interest in recent times, i.e., mimicking similar vibration on a different scale in needle insertion procedures.

More studies on vibration tissue cutting are discussed in the literature. *Bi* and Lin studied the vibration effect during needle insertion [90] and found that with vibration, the needle deflection can be reduced compared to without vibration. *Gidde et al.* [54] investigated the dual bioinspired approach with honeybee needle design and mosquito vibration and showed a 47% reduction in needle deflection compared to without vibration. *Scali et al.* [78] studied the needle body geometry and actuation (using nitinol wires) inspired by wasp ovipositor and concluded that the diameter of the needle should be decreased to minimize deflection. Also, *Gidde et al.* [20] showed that mosquito-inspired needle design lowers the insertion force by 27% using a 16-gauge needle compared to the standard needle. *Yang et al.* [75] investigated the microneedle insertion with applied vibration and concluded that the force could be reduced by up to 70% compared to without vibration. The researchers previously reported the silicon and polymer jagged microneedle with an anisotropic cut in its fabrication to lower insertion force [53, 55]. According to

Kong and Wu [87], the labrum-tip (see Fig 1.4) along with the mandibles are the first to enter the skin with a mean penetration force of 18 μN . During this process, the fascicle is anchored, i.e. the tip penetrates the outer skin layer and the fascicle is repeatedly pushed forth and back within the labium at around frequency of 15 Hz [76] and 30 Hz [67]. Medical device procedures are considered minimally invasive, but due to the higher needle insertion force, their damage to the tissue can still cause injuries to the organ tissue and the patient. The problem related to the bioinspired needle with vibration tissue cutting in reducing force and damage to the tissue has not been addressed, and it is still challenging to address these problems. In this dissertation work, the focus is to lower the insertion and extraction force, tissue deformation, and damage to the tissue using a unique approach of needle geometry design on the needle body and the vibration effect. The concept of utilizing vibration is inspired by mosquito proboscis and the geometry of the needle in this study is maxilla shape and labrum-tip design [58, 62]. This study of dynamic bioinspired needle insertion will aid in developing novel methods to lower insertion force and tissue damage for percutaneous procedures. To understand more about the mosquito-inspired vibration tissue cutting, the mechanism of the mosquito-proboscis was studied, which helps to steer its stingers effortlessly and with minimal force [76]. It is understood that one of the mosquito needles has a maxilla body shape (tissue cutting during mosquito-proboscis) and the labrum-tip (used in transport the blood) plays a key role during mosquito-proboscis.

1.3 Problem Statement

The needle placement accuracy highly depends on insertion force and tissue deformation in minimally invasive procedures. As discussed in Section 1.1, reducing the

insertion force can help to minimize needle deflection and decrease tissue damage, thus improving the needle insertion procedure. However, the fundamental research in understanding the influence of vibration on bioinspired needles has yet to be performed. Although many researchers studied the vibration effect separately, the influence of vibration parameter with the mosquito-inspired needle design has not been reported. Therefore, the goal of this research is to study the effect of vibration of the mosquito-inspired needle on insertion force, tissue deformation, and tissue damage. However different bioinspired needle designs have been studied such as honeybee barb design, wasps sting, and mosquito proboscis. Nevertheless, the current novel design geometry which consists of maxilla shape on the needle body inspired from one of the six elements of mosquito proboscis (see Fig 1.4) and labrum design at the needle-tip along with applied longitudinal vibration presented in this work has not been studied. The mosquito-inspired design is not entirely the same in this study, the main features of the mosquito i.e., maxilla design (tissue cutting during mosquito proboscis) shown in Fig 1.4 and labrum design (which is a curved shape at the needle-tip) were experimentally studied. Moreover, the influence of vibration on insertion was theoretically studied. The two features of the mosquito design (maxilla and labrum) along with the vibration can be used to decrease tissue damage.

This study presents the insertion mechanics of the vibration cutting of honeybee and mosquito-inspired needles, which includes investigating the parameters of the needle insertion that can be modified to lower the insertion force, such as vibration, insertion velocity, and needle geometry. The maxilla design has been designed on the needle body

to decrease the penetration load, which results in reducing frictional force. The penetration load will be reduced because of the maxilla design geometry on the needle body, which means removal of material will result in a decrease in the load (12% reduction) and also benefits in reducing the force at the same time compared to standard needles. The weight of the standard needle is 1.20 grams, and the weight of the mosquito-inspired needle is 1.06 grams, which means the mosquito-inspired needle loses 12% of its total weight with the removal of material. But still able to lower the force with the applied vibration during insertion into tissues. The maxilla shape is designed on the needle body to reduce the frictional force and the labrum design at the needle-tip to reduce cutting force. The analysis of the vibration was also studied to understand the influence of mosquito-inspired vibration on insertion force during needle insertion. The schematic representation of the applied longitudinal vibration to the bioinspired needle during insertion into soft tissue is shown in Fig 1.6.

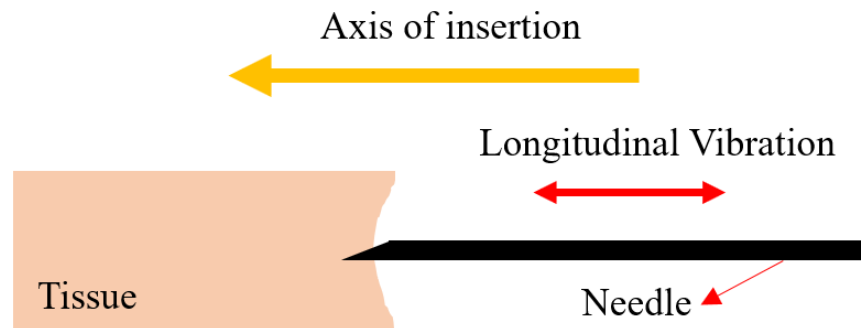


Figure 1.6. The schematic representation of the needle insertion with longitudinal vibration (parallel to the axis of insertion).

This dissertation study aims to reduce the insertion force, tip deflection, tissue deformation, and tissue damage. This dissertation is organized into four Chapters. Chapter 2 discusses the experiments and test methods utilized in this dissertation study. Chapter 3 describes the honeybee-inspired needle parametric study, the vibration effect of honeybee-inspired needles on the insertion force, and the needle-tip deflection. Chapter 4 studies the vibration cutting of mosquito-inspired needles, which includes the parametric study, the influence of vibration on insertion force, and its theoretical analysis. Moreover, the influence of vibration of a mosquito-inspired needle on insertion force, tissue deformation, and tissue damage will be discussed experimentally.

The mosquito-inspired needle insertion mechanics in soft tissues were studied to evaluate its effect on insertion and extraction force, needle deflection, tissue deformation, and tissue damage. The fundamental study presented in this dissertation will aid in advancing the bioinspired needles such that the success of needle insertion procedures can be improved for vibration-assisted clinical procedures.

CHAPTER 2

EXPERIMENTS AND METHODS

2.1 Needle Insertion Force Measurement Test Method

The needle insertion test setup in this study consists of a linear insertion motor with a six-axis Force/Torque Transducer Nano17® (ATI Industrial Automation, Apex, NC), a data acquisition system (National Instruments Corporation, Austin, TX), and a piezoelectric actuator (Physik Instrumente, Auburn, MA) that vibrated the needle in the longitudinal direction (i.e., in z-direction or parallel to the axis of insertion) with a sinusoidal waveform at a frequency of 200 Hz and an amplitude of 5 μm . The amplitude during the applied vibration was kept constant because of its cutting effect at the needle-tip that depends on cutting force [43], therefore the amplitude was set to 5 μm and the vibration was studied experimentally and theoretically (0 to 500 Hz) to study the effect of vibration on needle insertion force. The force sensor recorded the insertion and extraction forces in the z-direction. The programmable data acquisition system using LabVIEW software was used to acquire the force data. The needle guider was used to steer the needle and to decrease the possible buckling of the needle during insertion. The amplifier was used to control the low - high output voltages during the applied longitudinal vibration. Considering the needle guider friction and other errors, calibration was done on the data. To calibrate the data, the experiments were performed in airspace (without tissue) and were subtracted from the experimental data in tissues. This procedure of calibrating the data was applied to all the experiments in this study. The needle insertion test setup is shown in Fig 2.1 b) using both artificial tissue-mimicking materials and biological tissues.

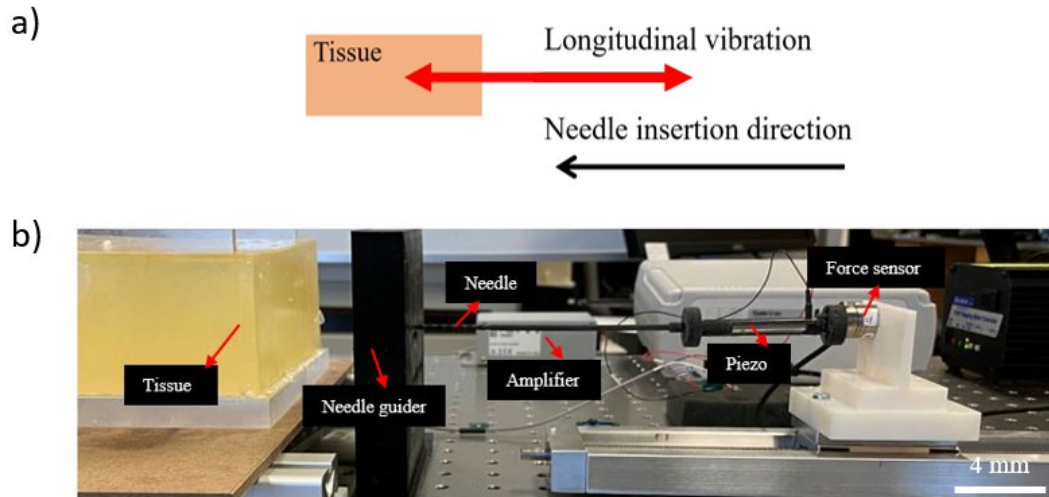


Figure 2.1. a) The applied longitudinal vibration in the insertion direction and b) the experimental needle insertion test setup for force measurement in tissues.

2.2 Manufacturing of Tissue Mimicking Materials

To fabricate the tissue-mimicking materials, a polyvinyl chloride (PVC) phantom material was used, which is commonly used to mimic tissues such as brain and liver tissues [92]. Because of its optical transparency and mechanical properties, PVC has been widely used as a tissue-mimicking material in studying needle insertion procedures [7, 49, 93, 94]. To prepare the PVC tissue phantom, the PVC polymer and softener (diethyl hexyl) solution were combined, and this mixed solution was heated to a high temperature of 100°C until it became a thick and transparent solution [50]. The components of the materials of diethyl hexyl can be adjusted to manufacture the desired stiffness properties of the tissue phantom ranging from 1.3 to 7 kPa. Moreover, this solution cannot be heated too long since overheating will change the properties of the material. After heating, the thick viscous liquid is transferred into an aluminum mold and cooled to room temperature and was

solidified by storing it in a freezer to ultimately turn into a PVC tissue phantom and a white opaque solution, which mimics the viscoelastic properties of the tissue [64, 76].

Moreover, the gelatin phantom tissue was utilized for the needle deflection study due to the lack of tissue damage seen in PVC tissue phantom [92]. In particular, the water content in the gelatin is relatively higher compared to PVC, which allowed better visibility of the location of the insertion path. Because of the lack of transparency, the insertion path was unable to be observed in the PVC. To create a gelatin phantom, 111 grams of gelatin powder and 225 ml of de-ionized degassed water were mixed in a sanitized container before adding 10 drops of Vyse defoamer solution (Vyse Gelatin Co., Schiller Park, IL, USA). The mixture of evaporated milk or water of 500 ml and 275 ml of de-ionized water was heated to 80°C and added to the above solution where it was thoroughly stirred and allowed to cool to 40°C before transferring into a phantom mold. The compression test was performed to find the Young's Modulus of the PVC tissue phantom and gelatin phantoms (see Appendix. A). All the experiments in this dissertation work were studied using PVC, except for the deflection study, where the gelatin tissue phantom was chosen due to its transparency.

Table 2.1. The Young's Modulus properties comparison of artificial [77] and biological tissues [83].

<i>Young's Modulus (E)</i>	<i>Artificial Tissues</i>	<i>Biological Tissues</i>
1.3 kPa	PVC	Bovine brain (1- 4 kPa)
1.8 kPa	PVC	Bovine muscle (2 kPa)
4.2 kPa	Gelatin	Bovine brain (1 -4 kPa)
6 kPa	PVC	Bovine liver (7 kPa)

2.3 Needle Deflection Method

To quantify the position during insertion of the honeybee-inspired needle with and without vibration, the needle deflection was studied using a gelatin tissue phantom. The insertion path in the gelatin allowed us to view the damage to surrounding tissue with a colored dye, as shown in Fig. 2.2 a). The insertion path of the tissue sample was sliced into sections and a colored dye was used to spread across the sample sections. The needle insertion path was located and each of the sections of the gelatin samples were used to determine the needle-tip deflection. A digital camera was used to image the sections and the distance from the edge of the tissue to the center of the wound was measured using ImageJ (NIH, USA) software. The total number of sectioned samples was 10 and the average of the needle-tip distance gave the final deflection. The Young's Modulus (E) of the gelatin phantom is 4.2 kPa, which was measured using a compression test that is described in Appendix A

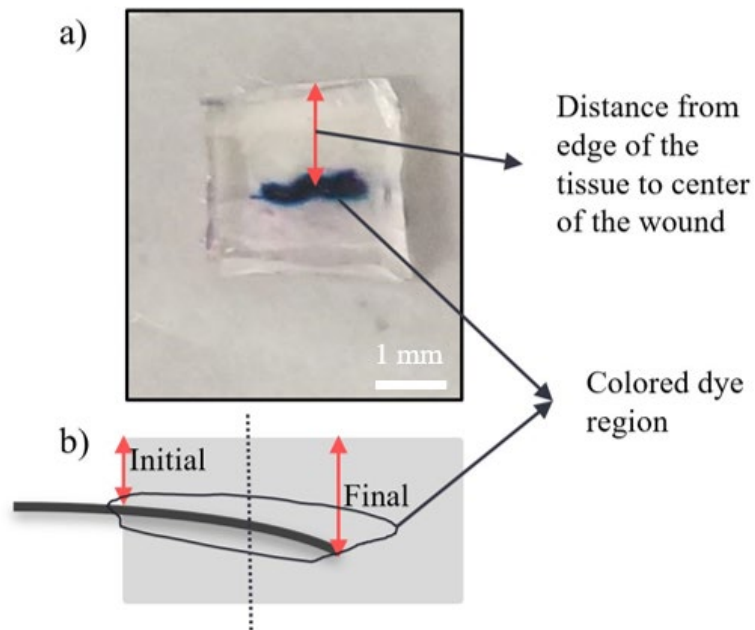


Figure 2.2. The distance from the edge of the tissue to the center of the wound: a) top view showing the initial section and b) a schematic representation (side view) of the needle deflection.

2.4 Tissue Deformation Method

A magnetic-based tissue deformation sensing system is used to examine the deformation using mosquito-inspired needles with vibration. The sensing system measures the tissue deformation by interpreting the change in a magnetic field induced by an implantable soft magnet that moves during needle insertion. This sensing method is accurate by 90% in measuring the deformation using a magnetic sensor [97]. This deformation reduction can be compared by analyzing the tissue damage, which is due to a reduction in the needle insertion force. The sensing system is calibrated using a high-speed camera (60 fps, EOS 60D, Canon). The schematic representation of the tissue deformation

during needle insertion is shown in Fig 2.3, which shows the distance (d) that is measured from the top of the tissue surface to the maximum deformation in the tissue.

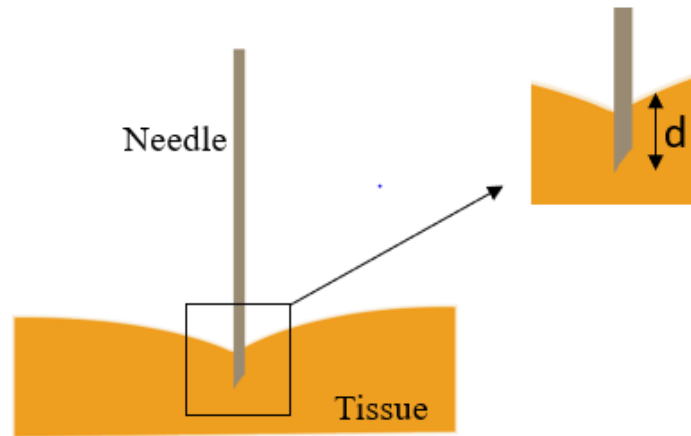


Figure 2.3. A schematic representation of the tissue deformation in distance (d) during needle insertion is measured from the top of the surface to the needle tip at the maximum depth.

The soft magnet is made of iron oxide (Fe_2O_3) nanoparticles embedded in silicone elastomer to conform with the elastic properties of the soft tissue. The disk-shaped soft magnets are prepared with a diameter of 3 mm and a thickness of 2 mm. A soft magnet is placed at 2 mm away from the needle penetration site (see Fig 2.4). An array of three highly sensitive magnetic field sensors (Micro Magnetics STJ-240) is placed directly above the soft magnet with a distance of 2 mm. As the tissue deformed due to the needle insertion, the magnetic field strength reduces by inverse cube law [98], which could be detected by the magnetic sensor array that has a sensitivity of $0.12 \Omega/\mu\text{T}$. The amount of change in the

magnetic field directly corresponds to the tissue deformation during the needle insertion.

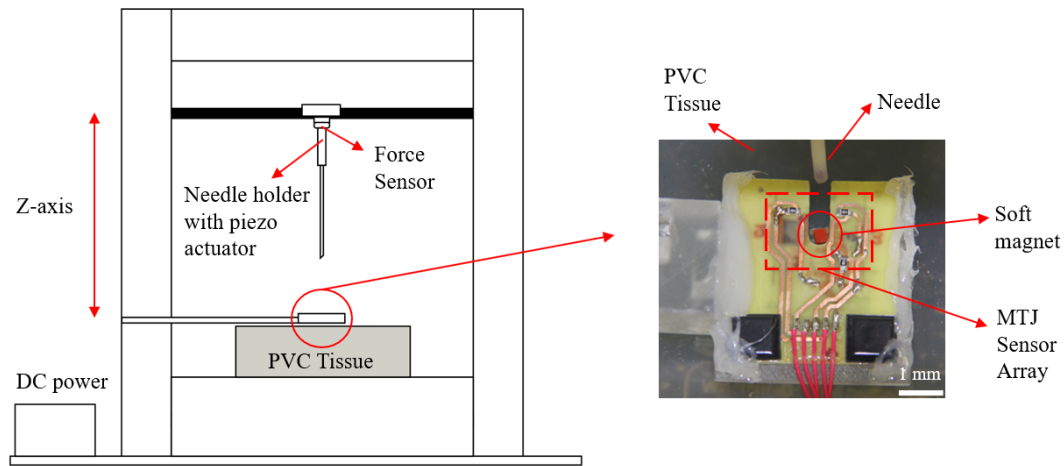


Figure 2.4. A schematic representation of the needle insertion test setup along with the novel sensing test setup (close-up view) with a soft magnet (in red color) and MTJ sensor array for measuring tissue deformation in PVC gel

2.5 Tissue Damage Method

The insertion tests were performed in bovine liver tissue using mosquito-inspired and standard bevel-tip needles. The tissue samples were cut and trimmed i.e., along the insertion path that created the insertion. Before adding formalin solution (10%), the samples (4x4 mm) were immersed three times in Dulbecco's phosphate-buffered saline (DPBS) (Thermo Fisher Scientific, Waltham, MA) solution to wash the tissue samples before dissociation. Samples were then immersed in formalin (Azer Scientific Inc, Morgantown, PA) and left in the solution for 24 hours. These samples were washed again with DPBS solution before adding the optimal cutting temperature (OCT) in the cryomold. The samples were then transferred into a cryomold, OCT was added to the tissue samples

and stored in the -80°C freezer. These frozen samples were sectioned into slices with a thickness of $0.5\ \mu\text{m}$ using a cryostat machine as shown in Fig 2.5 b).

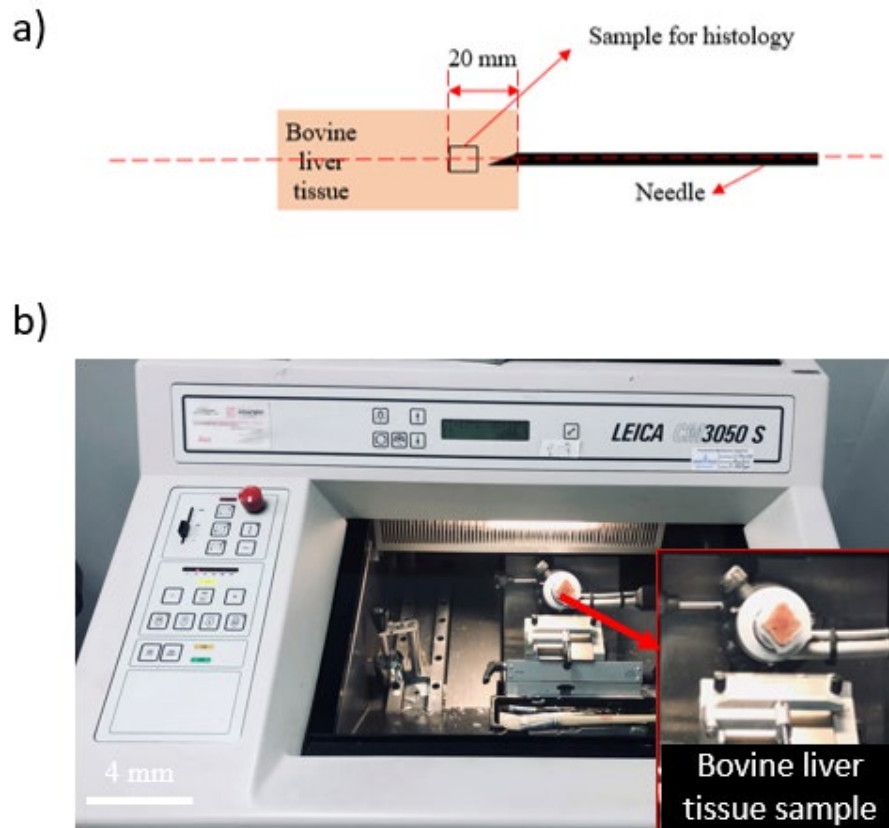


Figure 2.5. a) A schematic representation of the sectioned bovine liver tissue sample for histology after insertion tests and b) the cryotome machine which was used for sectioning the bovine liver tissue sample of $0.5\ \mu\text{m}$ thickness.

To histologically evaluate the bovine liver tissue sample, Hematoxylin solution, Eosin Y solution, xylene (all three solutions from Sigma-Aldrich Inc, USA), and ethanol (Fischer Scientific, USA) were prepared and added in the Tissue-Tek dishes. To obtain the Hematoxylin and Eosin (H & E) stain, graded ethanol from 70 to 100% was made to obtain

the desired %(v/v) concentration by diluting 100% ethanol with DI water. All the obtained prepared solutions were added to a Tissue-Tek dish to the indicated line mark for allowing the micro slides to immerse in the solution. The sectioned slides are shown in Fig. 4.7 a). were placed in a Tissue-Tek holder for the staining process. These mounted sectioned slides with a thickness of 0.5 μm were dehydrated by soaking them for 5 minutes each in 100% xylene and 50: 50 xylene: ethanol. The slides were then soaked in graded alcohols from 70 to 100% for dehydration for 5 minutes in each of the %(v/v) concentrated solutions. The slides were added to a 1%(v/v) hematoxylin for 5 minutes and washed two times with DI water. Next, the slides were added to 1%(v/v) eosin y solution for 20 seconds before washing the slides two times with DI water. This process was repeated in reverse order i.e., from 100 to 70% for 5 minutes each to rehydrate the sample slides. Finally, the samples were soaked in 100% xylene for 5 minutes to complete the staining procedure and the final stained slides are shown in Fig 2.6 b) (the stained slides).

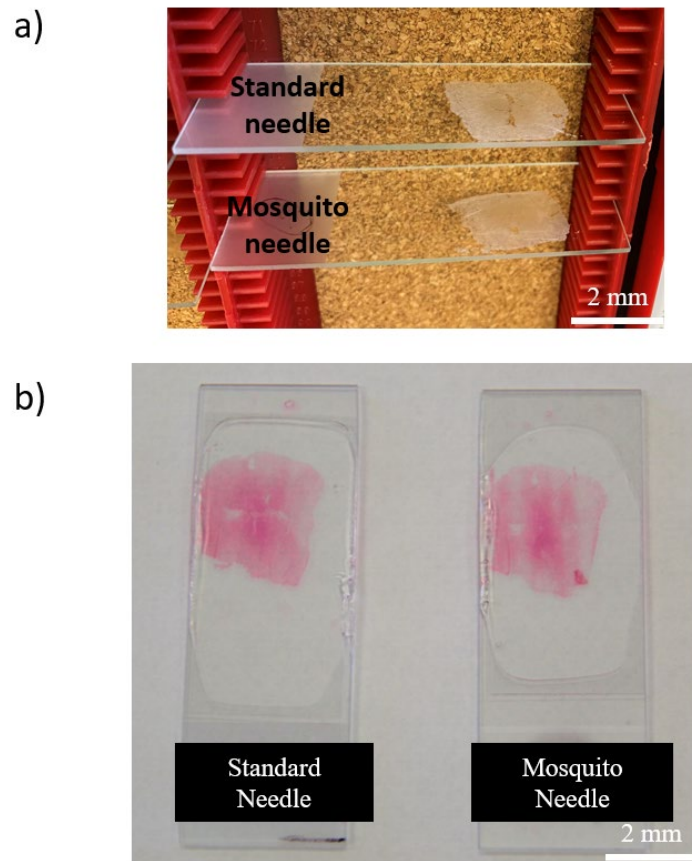


Figure 2.6. a) The sectioned slides of the bovine liver tissue sample with a thickness of $0.5\mu\text{m}$ and b) the hematoxylin & eosin-stained slides.

After finishing the staining process, the sample slides were allowed to air dry for 10 minutes and $100\ \mu\text{L}$ drops of Permount (mounting medium) were added on each slide of the sectioned stained sample. During the sample preparation before staining, all the protocols discussed were followed to achieve consistent physical characteristics in tissue sections. For example, tissue fixation in a 10% buffered formalin solution initially causes a slight change in properties, but the overall composition of the tissue remains the same [99]. This procedure was the same for both samples (see Fig 2.6). The cover slips were

added on top of the stained slides that have drops of Permout solution and the pressure was applied manually to clear out the excess Permout and the air bubbles from the slides. They were left for 24 hours to air-dry before observation. A microscope (Olympus BX53F Inverted Microscope) with a color camera of DP26 was used to observe and image the stained slides. The magnification during imaging of the slides was 4X and the exposure time was kept constant along with the brightness during the imaging process. The needle insertion area was located by defining the overview area on the slide and images were captured. These captured or snapshots of the images were studied using ImageJ (NIH) to measure the cross-sectional area of the damage caused by the needle insertion that was located on the slide in Pixels [100]. The steps that were followed to measure the cross-sectional area of the damage are within the standard procedure [86, 87, 101]. The area of the damage in the sectioned sample with 0.5 μm thickness is not different from the time the H&E staining is processed, which is why the results were compared with standard needles.

2.6 Statistical Analysis

The experimental data were analyzed using one-way Analysis of Variance (ANOVA) and post-hoc Tukey tests to compare the significance between different groups of the needle design parameters. Also, an independent *t*-test was used to test the significance of the data in Fig 4.19. For honeybee-inspired and mosquito-inspired needle insertion force analysis, multiple comparisons were made within the levels of independent variables to determine if the mean values of different factors such as maxilla angle, barb angle, thickness, insertion velocity, and vibration were statistically different. The ANOVA test

was conducted for each different data for all the figures in Chapters 3 and 4. The significance level was set at $\alpha = 0.05$ (95%) confidence interval, which means the null hypothesis can be rejected for p less than α (0.05). The analysis was done in Excel and the ANOVA test was done with the experimental data. The Tukey test was performed with the degree of freedom (df), trials (n) values from ANOVA, and the q value was found from the q-table of the Tukey test. The ANOVA test results will tell us whether the data is significant or not, but the post-hoc Tukey tests will reveal the significant difference within the groups. The difference between the two means of the data provides the significance of the data. This significance factor is plotted with letters A, B, C, and D to show the significance of the data within the groups. The bar graph plots with the same uppercase and lowercase letters indicate that they are not significantly different, and the different letters indicate the significance at the 95% confidence level based on post-hoc Tukey tests.

CHAPTER 3

VIBRATION CUTTING OF HONEYBEE-INSPIRED NEEDLES

In this Chapter, the vibration cutting of the honeybee-inspired needles in PVC, gelatin phantom, and chicken breast were experimentally studied in detail and compared with standard bevel-tip needles to show its effect on the maximum insertion force and the needle-tip deflection.

3.1 Honeybee-Inspired Needle Insertion Mechanics

The insertion mechanics of the honeybee-inspired stinger mainly consists of barb geometry. Considering the drawback of honeybee barb stingers, the design of the needle in this study utilized the symmetric barbs around the needle body. In Fig 3.1 a-b, it is shown that the barb geometry on the honeybee stinger is asymmetric and has sharp edges. The geometry design of the barbs reduced the insertion force significantly by 35%. The extraction force for a honeybee-inspired needle can be lowered because of the gap space that allowed for the easy extraction [82]. In our study, the barbs were carved on the needle body surface, so that the extraction force can be reduced with the vibration [30, 42]. The parameters that were studied are barb front angle and barb height. Previous research studies have shown that increasing or decreasing the parameters will affect the insertion force [32]. However, the barb front angle and barb height were experimentally studied due to their significant contribution in reducing the insertion force [54]. The barb back angle is shown to be dependent on the barb front angle and barb height. The number of barbs can be increased or decreased depending on the depth of insertion. Therefore, parameters such as barb back angle of 90° , number of barbs of 10, and barb tip thickness of 0.15 mm were

kept constant according to the study by Mohammad *et al.* (see Fig 3.1 for the parameters) [12].

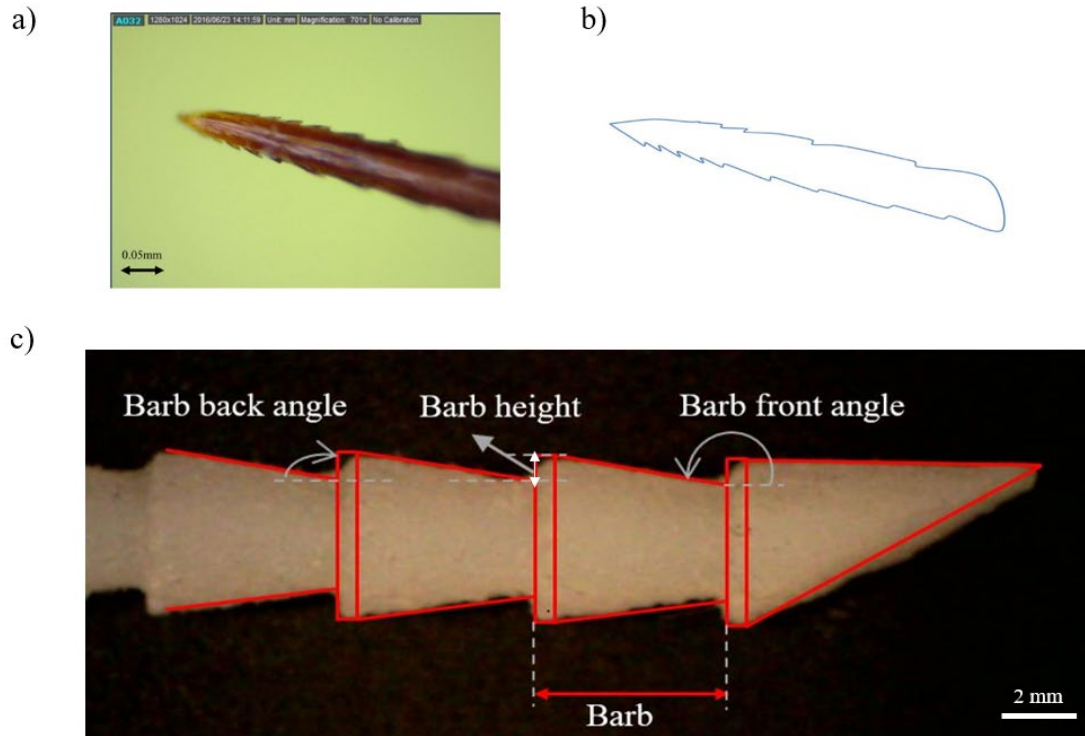


Figure 3.1. a) the honeybee stinger, b) 2D drawing of the stinger (Mohammad et al. 2018), and c) a schematic representation of the honeybee-inspired needle and its parameters such as barb height, barb front angle, and the number of barbs.

The addition of vibration to the honeybee-inspired needle during its insertion into tissue lowers the insertion force. Studies have shown that vibration-assisted needle insertion assists in increasing the needle placement [90] and reduces the cutting force [19, 55], ultimately decreasing the insertion force. This vibration parameter inspired from the mosquito proboscis helps to facilitate better needle insertion [76]. Furthermore, due to its

penetrating technique in reducing the insertion force, it also assists in minimizing the damage [45, 46, 53]. This penetrating process of the mosquito vibration was added to the honeybee-inspired needle to further reduce the maximum insertion force. The maximum insertion force with an amplitude of 5 μm is $1.84 \text{ N} \pm 0.11 \text{ N}$ compared to the amplitude of 10 μm i.e., $2.15 \text{ N} \pm 0.15 \text{ N}$. The maximum insertion force increases with increasing amplitude. The honeybee-inspired needle was compared with the standard needle, and both the needles were modeled using CAD software and 3D printed (see Fig. 3.2). This study experimentally investigated the effect of barb front angle, barb height, and vibration frequency on the maximum insertion force. The importance of adding the honeybee-inspired barb design is that to utilize the advantage of barb design geometry on the needle body and at the same time, to experimentally study which design parameters are mostly influencing the maximum insertion force.

Table 3.1. Insertion parameters of the honeybee and mosquito used in this study.

Needle Length – 180 mm, Needle diameter – 4 mm		
<i>Parameters</i>	<i>Insect-inspired from</i>	<i>Values</i>
Barb front angle	Honeybee	140°,145°,150°,155°,160° and 165°
Barb height	Honeybee	0.1, 0.2, 0.3, 0.4 and 0.5 (all in mm)
Vibration Frequency	Mosquito	60, 70, 80, 90 and 100 (all in Hz)



Figure 3.2. The microscopic view of (a) honeybee-inspired needle and (b) standard bevel-tip needle.

3.2 Results of Vibration-Assisted Honeybee-Inspired Needles

The insertion tests were performed in PVC tissue phantom, Young's Modulus (E) of 1.3 kPa, using a honeybee-inspired needle to study parameters such as barb front angle, barb height, and vibration. The insertion tests were also performed in chicken breast ($E = 20$ kPa). Lastly, the needle-tip deflection was studied in gelatin using the honeybee-inspired needle.

3.2.1 Parametric Study

The maximum insertion force was measured with different barb front angles (Fig. 3.3) and the barb heights (Fig. 3.4). The average maximum insertion force of the five trials of both barb front angle and barb heights are shown. The maximum insertion force is defined as the peak force that is recorded at the maximum depth of insertion. The maximum

insertion force lowers with an increase in barb front angle and similarly, increasing barb height also resulted in the maximum insertion force reduction. Both the parameter study conjectured that increasing the barb angle or barb height results in less frictional force [82] and thus decreasing the maximum insertion force. The post-hoc Tukey tests were also performed to compare the differences in the mean data within the groups. Bars shown in Fig 3.3 with the same uppercase letters are not significant, which means the p -value (0.09) is greater than alpha (0.05). Bars showing the different uppercase letters are significant with a p -value (0.03) is less than alpha (0.05). However, it is shown that increasing the barb front angle will result in a lower maximum insertion force.

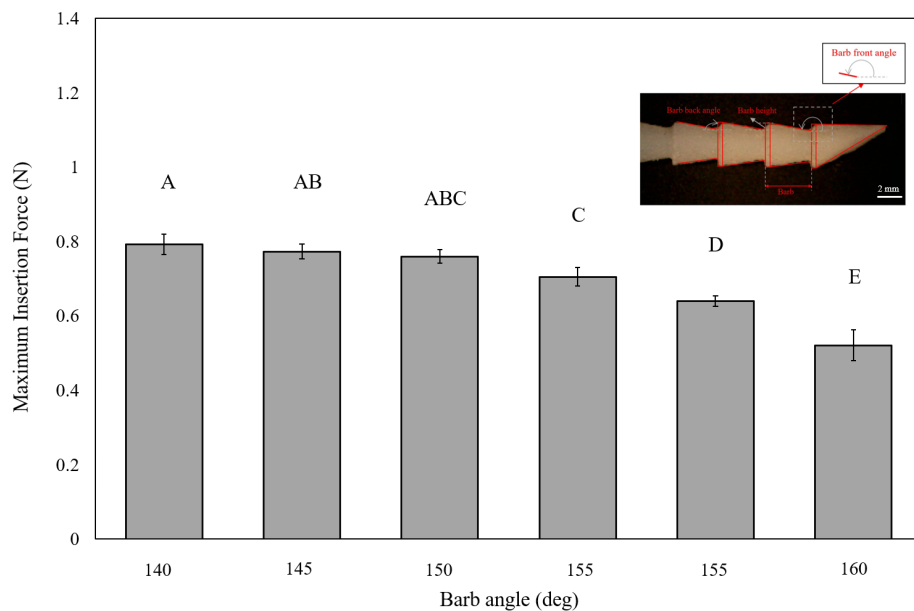


Figure 3.3. Effect of different barb angles on honeybee-inspired needle peak force (maximum insertion force) without vibration (Barb height - 0.5 mm, insertion depth - 60 mm, and insertion speed - 3 mm/sec). Bars sharing the same letters at the top of the bar graph are not significantly different at the 95% level, based on post-hoc Tukey tests.

Figure 3.3. Effect of different barb angles on honeybee-inspired needle peak force (maximum insertion force) without vibration

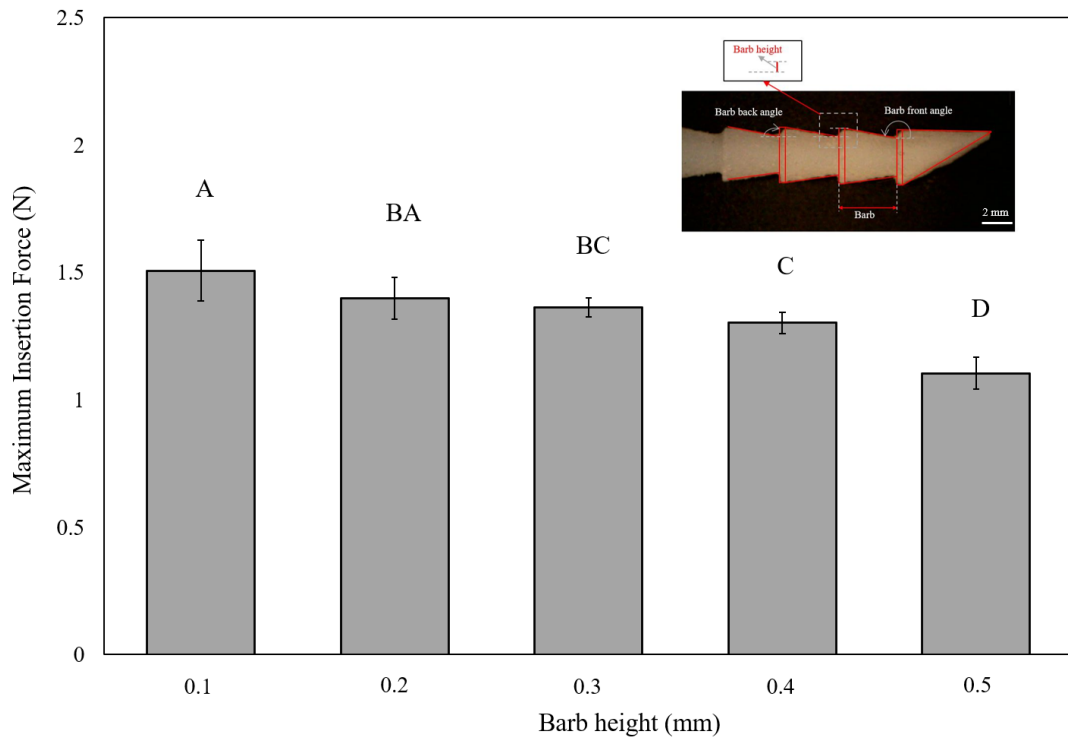


Figure 3.4. Effect of different barb heights on insertion force of the honeybee-inspired needle without vibration (Insertion speed - 3 mm/sec, barb angle - 165°, and insertion depth - 60 mm). Bars sharing the same letters at the top of the bar graph are not significantly different at the 95% level, based on post-hoc Tukey tests.

Similarly, the post-hoc Tukey test revealed a significant difference between the mean data of different groups in Fig 3.4. Bars with different uppercase letters are significant with a p -value (0.02) less than alpha (0.05) and with the same letters are not significant (p -value greater than alpha of 0.05). It is shown that increasing the barb height lowers the maximum

insertion force. The final parameter studied was the mosquito vibration applied to the honeybee-inspired needle and discussed at what vibration frequency effect will reduce the insertion force. Since a mosquito vibration lies between 15 - 30 Hz [36, 69, 76] and increasing frequency could result in a higher force. However, to mimic this on a larger scale, empirical tests were done to determine the lowest frequency that affected the insertion force measurements, while still being below 100 Hz to be representative of the mosquito. Between the vibrational frequency of 15 and 60 Hz, there is a small difference of 0.012 N in the maximum insertion force. This is because the diameter of the needle is 4 mm and the vibration effect is 15 Hz. Therefore, the vibration frequency ranging from 60 to 100 Hz with an amplitude of 5 μm was studied. The vibration addition decreases maximum insertion force but increases with further increase in vibration due to more cutting effect that results in higher cutting force. The difference between cutting and friction force is presented in Chapter 4, Section 4.4.3. The results for this analysis are shown in Fig. 3.5, which indicates that increasing the vibration to 100 Hz lowers the maximum insertion force for a honeybee-inspired needle. The post-hoc Tukey tests showed a significant difference between the means of the data. The p -value for significant data is less than alpha (0.05) and the data with different uppercase letters are significant with the p -value (0.032) greater than alpha of 0.05.

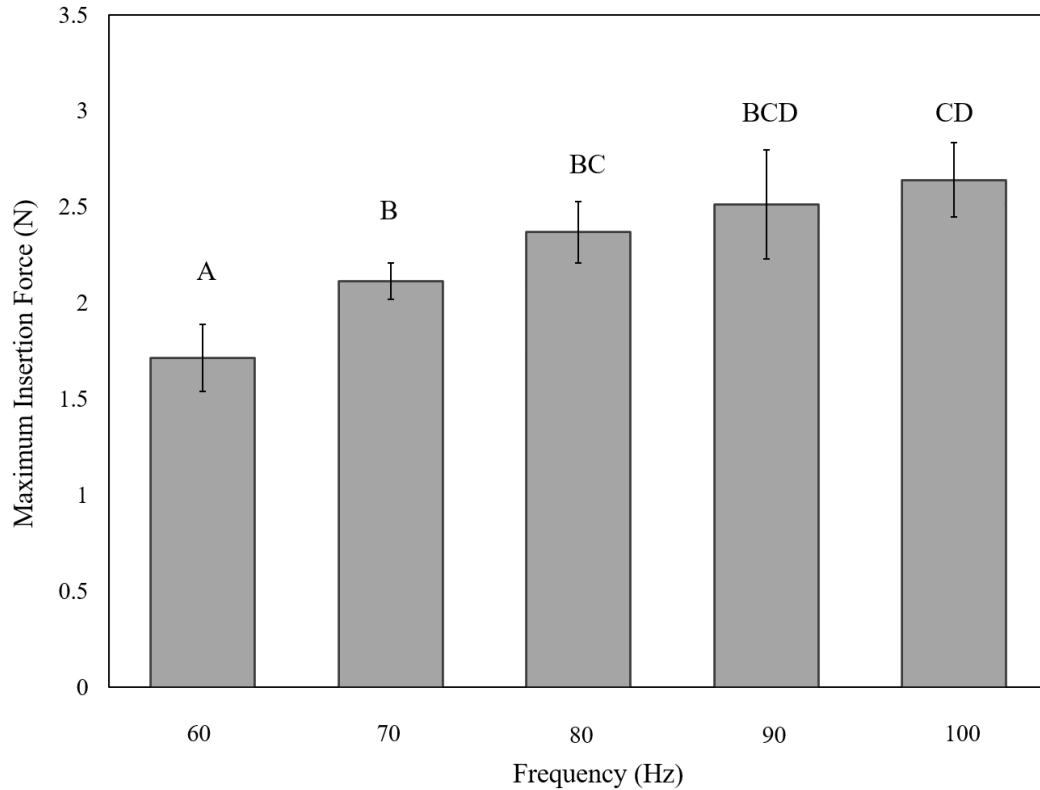


Figure 3.5. Effect of different frequencies on peak force of the honeybee-inspired needle (Insertion speed - 3 mm/sec, amplitude - 5 μ m, insertion depth - 60 mm, barb angle - 165 $^{\circ}$, and barb height - 0.5 mm). Bars sharing the same letters at the top of the bar graph are not significantly different at the 95% level, based on post-hoc Tukey tests.

3.2.2 Needle Insertion Force Study

The insertion tests were performed in PVC tissue phantom ($E = 3.5$ kPa) and the chicken breast ($E = 20$ kPa) using a horizontal needle insertion test setup (see Chapter 2, Section 2.1) [53] with a honeybee-inspired needle. The honeybee-inspired needle parameters consist of a barb front angle of 165 $^{\circ}$, a barb height of 0.5 mm, and a vibration frequency of 60 Hz with an amplitude of 5 μ m. The maximum insertion force data in PVC tissue phantom using a vibratory honeybee-inspired needle (with and without vibration)

and standard bevel-tip needle without vibration are shown in Fig. 3.6. The maximum insertion force results for the chicken breast are shown in Fig 3.7. The maximum insertion force in the chicken breast using a honeybee-inspired needle (without vibration) was found to be a mean of 6.97 N, whereas the final average insertion for the honeybee-inspired needle (with vibration) was 3.99 N. The applied vibration actuation during honeybee-inspired needle insertion reduces the amount of force required for needle penetration. The significant difference between the means of the data is presented in Fig 3.6 and the bars with different uppercase letters are significant at the 95% confidence level. This significant experimental data with a honeybee-inspired needle with vibration decrease the maximum insertion force by 50% compared to standard needles without vibration.

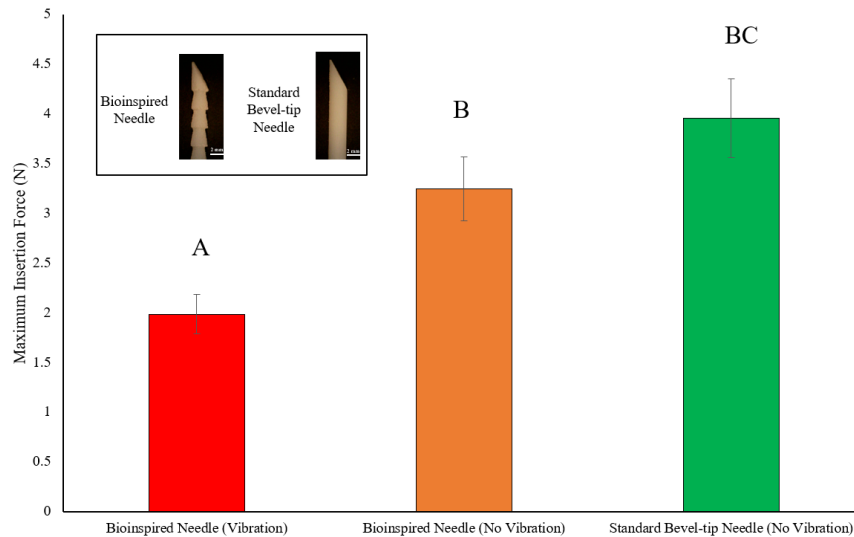


Figure 3.6. The maximum insertion forces obtained from insertion tests into PVC gels using bioinspired (honeybee) and standard bevel-tip needles (Vibration - 60 Hz, amplitude - 5 μ m, insertion speed - 3 mm/sec, depth of insertion - 60 mm). Bars sharing the same letters at the top of the bar graph are not significantly different at the 95% level, based on post-hoc Tukey tests.

It has been demonstrated that having vibration actuation during a honeybee-inspired needle reduces maximum insertion force in the chicken breast compared to a standard needle without vibration. The experimental results were also examined in PVC tissue phantom and found that the maximum insertion force decreases with vibration. The vibration-assisted insertion for the honeybee-inspired needle lowers the maximum insertion force compared to the standard needle without vibration due to reduction in cutting (vibration effect) and friction (barb geometry) force. The cutting and frictional force difference and their effect are presented in Chapter 4 Section 4.4.3. The experimental data shows that with the vibration of a honeybee-inspired needle, the maximum insertion force reduces significantly by 43% in the chicken breast. The post-hoc tests also revealed a significant difference between the means of the data shown in Fig 3.7. The bar plot with different uppercase letters is shown to be significant with a p -value (0.03) less than alpha of 0.05.

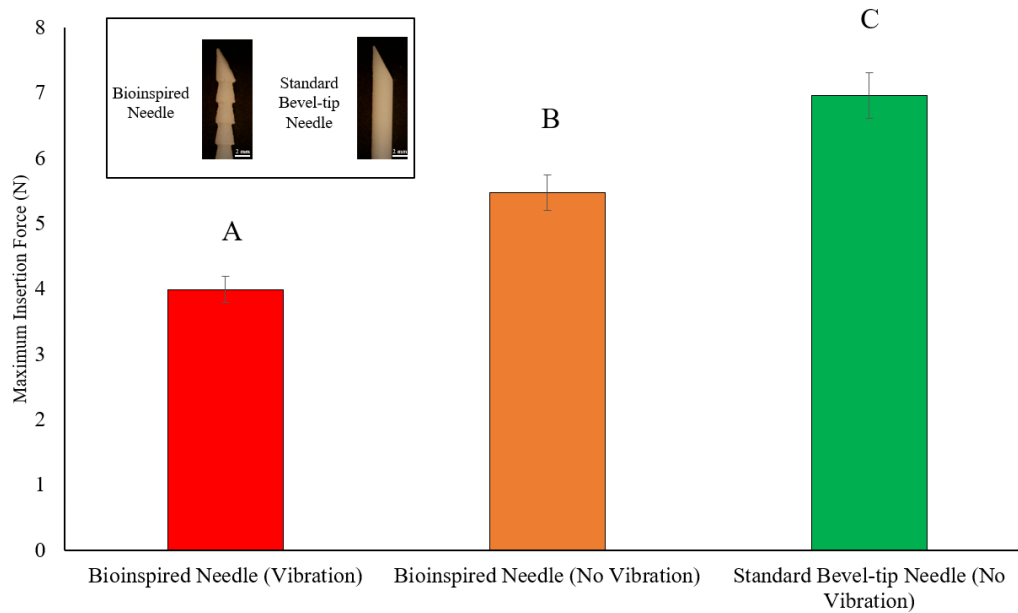


Figure 3.7. The maximum insertion forces obtained from ex-vivo insertion tests into the chicken breast using bioinspired (honeybee) and standard bevel-tip needles (Vibration - 60 Hz, amplitude - 5 μ m, insertion speed - 3 mm/sec, depth of insertion - 60 mm). Bars sharing the different letters at the top of the bar graph are significantly different at the 95% level, based on post-hoc Tukey tests.

3.2.3 Needle Deflection Study

In addition to the insertion force measurements, the needle-tip deflection was studied in gelatin phantom (see Appendix A for $E = 4.2$ kPa) to determine the effect of vibration on the deflection of a honeybee-inspired needle. This deflection study helps in understanding the influence of vibration effect on the honeybee-inspired needle other than the insertion force. The design parameters during this study are as follows: barb front angle of 165° , a barb height of 0.5 mm, and vibration frequency of 60 Hz with an amplitude of 5 μ m. The maximum insertion force in gelatin with vibration ($2.94 \text{ N} \pm 0.08 \text{ N}$) is lower than

the force without vibration ($3.44 \text{ N} \pm 0.07 \text{ N}$). The initial and final distance measured values and the standard deviation values for distance from the edge of the tissue to the center of the wound are presented in Table 3.2. The data analysis for the needle deflection with t-test showed that the p -value (0.04) is less than alpha (0.05) with two different groups (standard and honeybee-inspired needles).

Table 3.2. Honeybee-inspired needle insertion (with and without vibration) deflection values for distance from the edge of the tissue to the center of the insertion path.

<i>Group</i>	<i>Initial deflected distance (mm)</i>	<i>Final deflected distance (mm)</i>	<i>Total distance (mm) = Final - Initial</i>
with vibration	7.87 ± 0.03	9.31 ± 0.08	1.44 ± 0.10
without vibration	6.84 ± 0.05	9.56 ± 0.02	2.72 ± 0.03

3.3 Discussions

In this Chapter, a honeybee-inspired needle with vibration effect on maximum insertion force and needle-tip deflection was designed and experimentally studied. The fundamental objective of this study was to utilize the vibration effect in tissues. The honeybee-inspired needle design parameters were experimentally modified to study their effect on the maximum insertion force. The removal of material from the needle with the increase in barb front angle shows a significant reduction in the maximum insertion force. The vibration parameter on the honeybee-inspired needle was also studied to determine the

effect of vibration frequency ranging from 60 to 100 Hz on the maximum insertion force. The experiments were performed in PVC tissue phantom with a stiffness of 3.5 kPa and found that the maximum insertion force decreased by 50% compared to standard needles. Similar to the insertion force reduction, the needle-tip deflection was also reduced with the vibration effect. However, the honeybee-inspired needle diameter in this study is 4 mm, the results are compared with the standard needles of the same diameter. From the literature, the results shown by the researchers using the scaled-up diameter of the needles have shown a similar effect on the insertion force [32].

In addition to the insertion force study, a needle deflection was studied with and without vibration effect during insertion into soft tissues. Comparisons between the experimental data show good correspondence, with an error of 10%, and prove that the effect of vibration decreases the maximum insertion force, which also resulted in a 47% reduction in needle-tip deflection. The limitation of utilizing the tissue-mimicking material in this study is PVC because of its viscoelastic properties compared to the biological tissues, which is why the insertion tests were also performed in the chicken breast ($E = 20$ kPa). The other limitation is the transparency of the artificial tissues because gelatin tissue is more transparent compared to PVC tissue phantom. For this reason, gelatin phantom is utilized for locating the needle insertion path, which gave the total distance of 1.44 mm in needle deflection with vibration. More investigations are needed to determine the influence of vibration on the insertion force using theoretical analysis which consists of the cutting and frictional force, which are discussed and compared with experimental data in Chapter 4.

CHAPTER 4

VIBRATION CUTTING OF MOSQUITO-INSPIRED NEEDLES

In this Chapter, the vibration cutting of mosquito-inspired needles is experimentally studied in artificial and biological tissues. In the earlier Chapter, it was found that the influence of vibration of a honeybee-inspired needle has a significant reduction on the maximum insertion force. The influence of vibration and the mosquito-inspired needle design on the maximum insertion force, tissue deformation (using novel magnetic sensing system), and tissue damage (histological evaluation) were studied.

4.1 Mosquito-Inspired Needle Design and Modifications

The labrum-tip and maxilla shape were designed on the needle body to penetrate tissues with minimal damage due to the lower insertion force [45, 46]. From the literature, it is shown that the maxilla design has a jagged shape on the mosquito proboscis [34]. Therefore, the symmetric maxilla shape was carved on the needle body surface, which has a 360° revolved feature to minimize the friction and drag force. The modified design parameters of the mosquito-inspired needle are shown in Fig. 4.1(b). The mosquito-inspired needle parameters minimize the disadvantages of the maxilla design but maintain the feature in our presented design. The maxilla needle has a sharp edge and is asymmetric, but the symmetric shape was designed and experimentally modified to study their effect on the maximum insertion force.

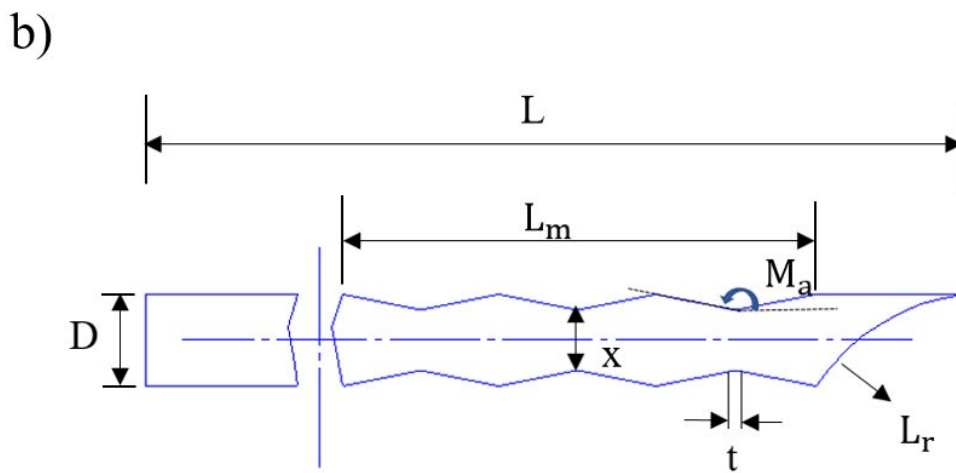
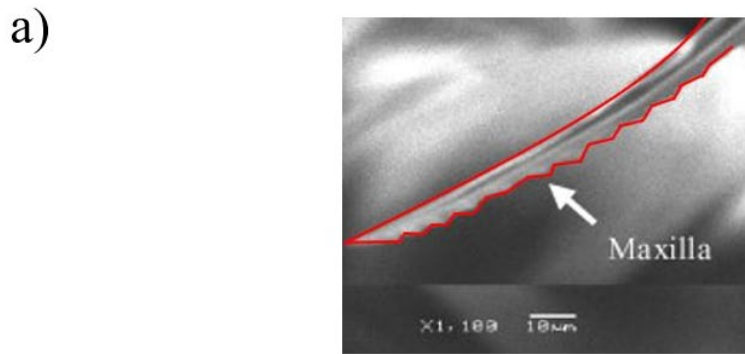


Figure 4.1. a) The maxilla needle in mosquito-proboscis (Izumi et al. 2011) and b) the 2D representation of the proposed maxilla needle on the needle body with parameters labrum-tip (L_r), maxilla angle (M_a), length of maxilla design (L_m), length of the needle (L), the diameter of the needle (D), thickness (t), and distance between the inner maxilla (x).

The design parameters in the proposed needle are labrum-tip (L_r), maxilla angle (M_a), length of maxilla design (L_m), thickness (t), and distance between the inner maxilla (x). The thickness (t) is between each maxilla shape on the needle body, L is the total length of the needle and D is the diameter of the needle. The limitation for the thickness parameter in the needle design is that it cannot exceed 0.3 mm because the needle will lose its stability

and can cause needle bending during insertion. Needle bending will also depend on the needle-tip, as the needle deviates in the direction of the tip shape. For this reason, the needle-tip is designed with a radius of 35 mm rather than a bevel angle. This curved shape is inspired from one of the elements of mosquito proboscis. Studies have shown that the bevel angle tends to deviate with the direction of the bevel, but the presented labrum-tip design minimizes the bending and reduces the cutting force. This mosquito-inspired needle design study is compared with the standard bevel-tip needles. The needles were modeled using CAD software and both the mosquito and standard needles were manufactured using a high-resolution 3D printer (Object Connex 350, Stratasys, Inc., Eden Prairie, MN) as shown in Fig 4.2.

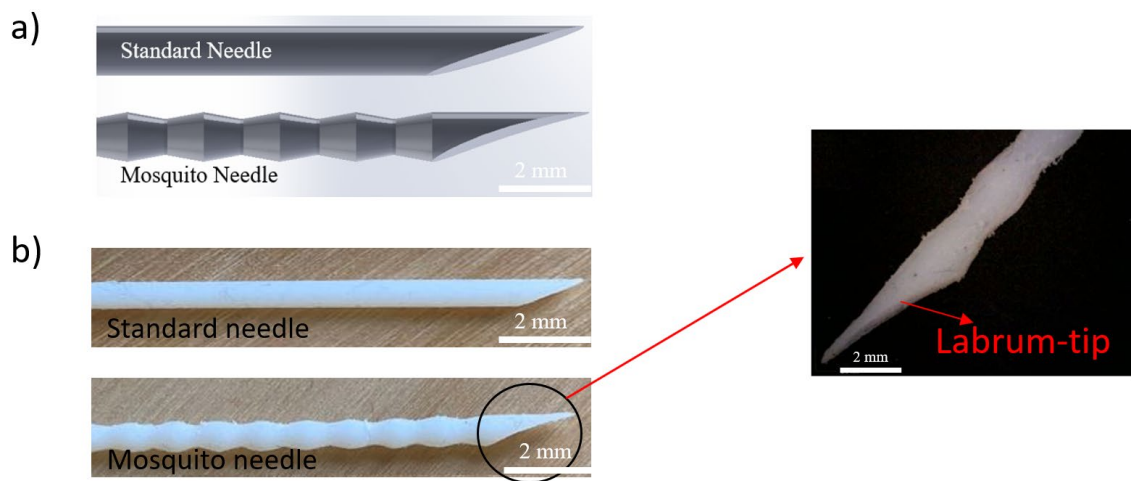


Figure 4.2. a) The 3D models and b) 3D printed standard and mosquito-inspired needles and a closer view of the labrum-tip design.

The experiments were carried out in tissues using a mosquito-inspired needle and standard bevel-tip needle to validate the results. The insertion velocities in this work were divided into sections (insertion velocity of 1,3,5,7 and 10 mm/sec) to study the effect of vibration. The increase in insertion velocity gradually decreases the puncture force and tissue displacement but increases the friction force [2]. Also, the higher insertion velocity can potentially reduce friction force in tissues with stiffness less than 3 kPa, but the damage to the tissue will result in a higher impact [92]. However, the effect of insertion velocity using a mosquito-inspired needle with vibration has not been reported. Therefore, the variation in insertion velocity with vibration was studied and the tests were performed in PVC tissue phantom.

Table 4.1. Insertion parameters for studying the mosquito-inspired needle.

Needle Length – 180 mm, Needle diameter – 3 mm	
<i>Parameters</i>	<i>Values</i>
Maxilla angle	110°, 130°,150°, and 170°
Thickness	0.1, 0.15, and 0.2 (all in mm)
Vibration frequency	100, 150, 200, 300, 400 and 500 (all in Hz)
Insertion velocity	1, 3, 5, 7 and 10 (all in mm/sec)

The parameters that are involved during vibration tissue cutting of mosquito-inspired needles are the vibration frequency, amplitude, needle-tip geometry, depth of insertion, and speed of insertion (see Table 4.2). Each of these parameters during needle insertion that

affects the insertion force (cutting and friction force) is discussed in the theoretical model presented in Section 4.3. The important parameters during vibration cutting are the insertion depth and the vibration that is applied longitudinally, which is why the increase in insertion force is seen using the mosquito-inspired needle and standard needle (Section 4.4).

Table 4.2. The needle insertion vibration cutting parameters and their forces.

<i>Parameter</i>	<i>Units</i>	<i>Type of forces</i>
Applied Vibration	Hz	Insertion Force (Cutting and Friction)
Amplitude	μm	Cutting Force
Insertion Speed	mm/sec	Insertion Force (Cutting and Friction)
Depth of Insertion	mm	Insertion Force (Cutting and Friction)
Needle-tip radius	mm	Cutting Force
Needle-tip angle	degree	Cutting Force

4.2 Theoretical Analysis of Vibration Influence on Insertion Force

The major force component during needle-tissue interactions is the friction force [17], which mainly depends on the frictional interface between the needle and tissue. The total force consists of stiffness, friction, and cutting force [13, 24, 28] (see Fig 4.3). The stiffness force occurs during the needle puncture, which means during puncture of the tissue. The cutting force acts after the puncture to slice the tissue and make the path for the needle [1, 69]. The friction force occurs along the needle shaft i.e., between two contact surfaces

(needle and tissue). Among these forces, the friction force is the largest contributor (see Chapter 4, Fig 4.12), and was also studied experimentally with the mosquito-inspired needle. The total force that acts during needle-tissue interactions is given as

$$F_{Total\ Force} = F_{stiffness} + F_{friction} + F_{cutting} \quad (1)$$

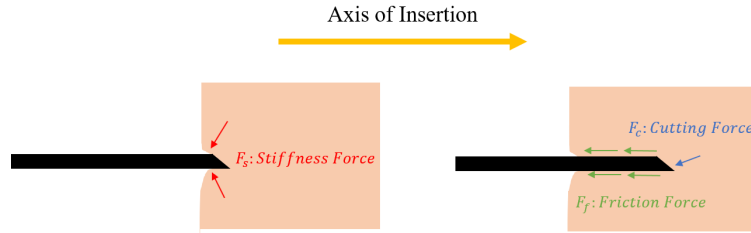


Figure 4.3. The insertion force consists of cutting force (F_c), friction force (F_f), and stiffness resistance force from the tissue (F_s).

The stiffness force, in this case, is for a linear stiffness model (which is equivalent to zero) after puncture compared to cutting and friction force. For example, in Fig 4.13, it is shown that the puncture force (also called the stiffness force), is less than the friction force. Furthermore, it is evident from our experimental data (see Fig 4.16) that the deformation seen is linear. If the tissue properties are non-homogenous, then the deformation will be non-linear which can be presented as a non-linear model [103]. The general form of the stiffness force on the needle is considered as a small number, which is less than 1% compared to the insertion force, which means the stiffness force is considered before puncture [103] and its relationship is given as

$$F_{stiffness} = \begin{cases} 0 & x_{tip} < x_1 \\ 0 & x_{tip} > x_3 \end{cases} \quad (2)$$

In the above equation, x_1, x_3 are the positions of the tissue surface before and after the needle puncture, as shown in Fig 4.4.

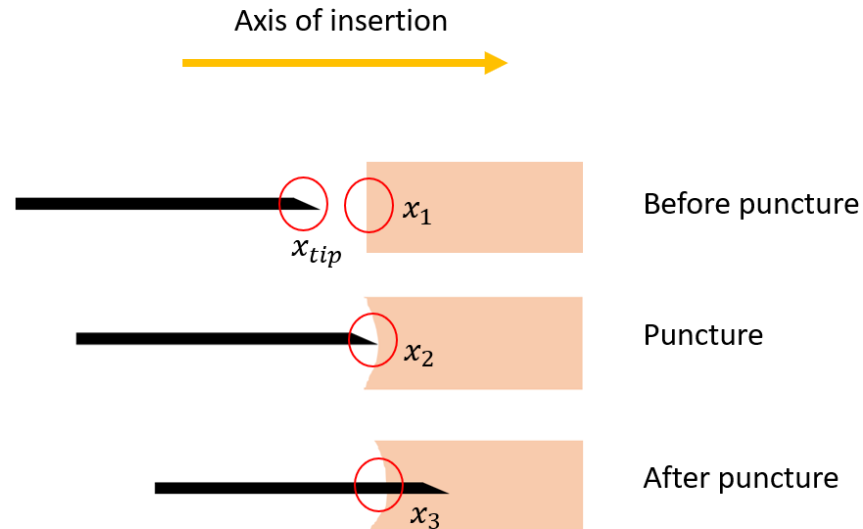


Figure 4.4. The needle and tissue interaction at different stages of insertion i.e., before puncture (x_1 position of the tissue surface), puncture (x_2), and after puncture (x_3 position of the tissue surface).

The cutting force occurs when the needle cuts the tissue and makes the path, which means the needle-tip plays an important role when cutting the tissue. The estimated cutting force from the experimental data can also be found using insertion and extraction force. The insertion force is the summation of friction and cutting force that occurs after puncture force and during extraction, there is no cutting, which means only friction force exists. Therefore, the cutting force was calculated by subtracting extraction force (no cutting force) from insertion force, which results in cutting force (see Fig 4.13 for approximate cutting force). Based on the tissue cutting that begins after the puncture, the cutting force

for high insertion depth decreases with insertion depth because the needle load inside the tissue is more [103] and is given as

$$F_{cutting} = \frac{4 \tan\left(\frac{\alpha}{2}\right) E_R^2}{b E_T} \quad (3)$$

In the above equation, α represents the tip angle, E_T represents the tissue stiffness and E_R represents the stiffness of the crack surface and b represents the insertion depth. The schematic representation of the cutting force during needle-tip tissue interaction is shown in Fig 4.5.

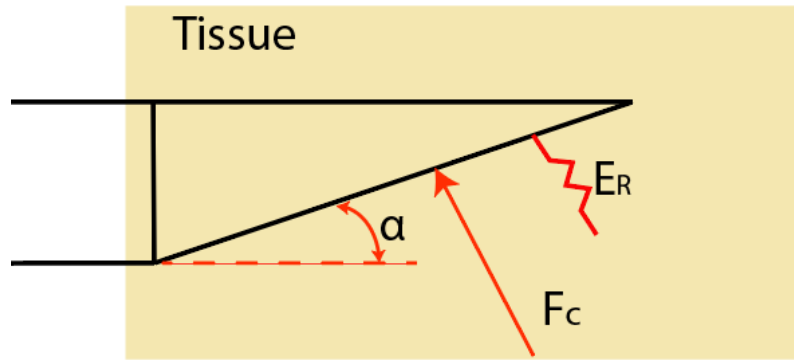


Figure 4.5. The cutting force during needle-tip tissue interaction with a magnitude of F_C . (α – needle-tip angle and E_R – tissue stiffness at the crack)

The friction force is the biggest force contributor in the total insertion force, it also depends on the cutting force (F_C). Minimizing the frictional effects could potentially reduce friction force, thus reducing the insertion force. From the experimental results (see Fig 4.9), it was observed that varying or minimizing the vibration parameter values could lower insertion force but increase with the increase in vibration [30, 67]. Reduction in insertion force leads to a decrease in the soft tissue deformation [91], which is important in needle-

based procedures [104]. A mathematical model is needed to justify various design parameters such as needle geometry, insertion velocity, and vibration that affect the reduction in the insertion force. The researchers have proposed several models to explore friction [82, 83] and its effects and found that friction is a complex nonlinear phenomenon and its response is not instantaneous but has internal dynamics, which is why models like the LuGre friction model have been widely used in the literature [82, 83, 102]. This friction model will relate to the impact of the design parameter variations during needle insertion, such that the force and vibration relationship will be studied. The relationship between the vibration parameters and the coefficient of friction in the LuGre model is presented. The LuGre friction model responds on dynamics properties and assist friction compensation. The differential form of the governing LuGre model equation [106] is given as

$$\frac{dz}{dt}(\eta, t) = v - \frac{|v|}{g(v)}z \quad (4)$$

Where v is the relative velocity between two surfaces. The first term represents the deflection, which is proportional to the integral of the relative velocity. The second term describes the deflection z .

$$F_{friction}(t) = \int_0^{L(t)} df(\eta, t) \quad (5)$$

$z(\eta, t)$ – deformation of the two elements (needle and tissue) at point η at time t , v represents the relative velocity of the needle and tissue, and $L(t)$ – length of puncture into the tissue.

When v is constant, the deflection (z) is in a steady state and the function g is positive and depends on properties and lubrication. If the velocity (v) increases, $g(v)$ will decrease,

which corresponds to steady-state behavior. The friction force occurs along the needle shaft during its interface with the tissue and is due to the Coulomb friction and tissue adhesion [26]. The friction force generated from bending of the two elements (needle and tissue) with the parameters like stiffness coefficient (σ_0) and damping coefficient (σ_1) is associated with z . To account for viscous friction, the viscous relative damping coefficient (σ_2) is added. These coefficients are responsible during needle-tissue interaction which results in needle bending and thus leading to friction force [26]. The equation (6) for the friction force is characterized by the stribek effect (g), and the parameter $g(v)$ has been proposed to describe the stribek effect velocity (see eq 4). The friction force is described as

$$F_f = F_n \left(\sigma_0 z + \sigma_1 \frac{dz}{dt} + \sigma_2 v \right) \quad (6)$$

$$\sigma_0 g(v) = \mu_c + (\mu_s - \mu_c) e^{-\left(\frac{v}{v_s}\right)^2} \quad (7)$$

Where μ_c is normalized Coulomb friction coefficient, μ_s is the normalized static friction coefficient and v_s is the Stribek effect velocity. The deflection (z) can be described as

$$z = \frac{v}{|v|} g(v) \quad (8)$$

If vibration is applied longitudinally during needle insertion, the total velocity (v) can be expressed as the summation of vibration and insertion speed (v_i) in terms of sinusoidal form can be described as

$$v = 2\pi(a\omega)\cos(\omega t) + v_i \quad (9)$$

where a represents the amplitude and ω is the frequency given, substituting v in Eq (8) gives,

$$z = g(a\omega + \cos(\omega t) + v_i) \operatorname{sgn}(a\omega + \cos(\omega t) + v_i) \quad (10)$$

$$\frac{dz}{dt} = v_i - \sigma_0 \left(\frac{|v|}{g}\right) z \quad (11)$$

Combining all the equations i.e., for insertion force (cutting and friction forces), the insertion force (F) is given as

$$F = F_{stiffness} + F_{friction} + F_{cutting} \quad (12)$$

$$F = F_n \left(\sigma_0 z + \sigma_1 \frac{dz}{dt} + \sigma_2 v \right) + \frac{4 \tan\left(\frac{\alpha}{2}\right) E_R^2}{E_T} \quad (13)$$

The above equation (11) was plotted in MATLAB along with the force acting on the needle and compared with experimental results to show the influence of vibration on the insertion force. The plot shown in Fig 4.6 gives the relationship between vibration and insertion force ($F_f + F_c$) for a standard needle. The parameter values for the Eq.13 are between the needle and tissue with σ_0 of 0.0521 N/mm^2 , σ_1 of $0.0145 \text{ N. sec/mm}^2$, σ_2 of $-0.0051 \text{ N. sec/mm}^2$, μ_c of 1.0611 N/mm and μ_s of 0.294 N/mm [103]. The tip angle (α) is 40° , E_T and E_R in this model is same because of the linear stiffness model. It is understood from the model that increasing the vibration results in higher insertion force for a standard needle with a bevel-tip angle. The model plot is not linear because of the incremental insertion force at different vibration frequencies. The influence of vibration of a standard needle (16-gauge) reduces the cutting force, which is dependent on the stiffness properties of the tissue (E_T and E_R), but with the increase in vibration, the total velocity (v)

also increases, which results in a higher cutting force. For this reason, the insertion force with a vibration frequency ranging from 200 to 500 Hz is higher. Similarly, the friction force also plays an important role such that if the friction between the needle and tissue can be decreased by decreasing the penetration load (see Chapter 3, Fig 4.13), the friction force can be reduced. This reduction in friction force depends on Coulomb friction, static friction, and damping coefficients. The cutting force parameter is dependent on the stiffness of the tissue or the crack inside the tissue. When the stiffness of the tissue becomes homogenous, the cutting force parameter will become a constant or small number that results in friction force (in total insertion force).

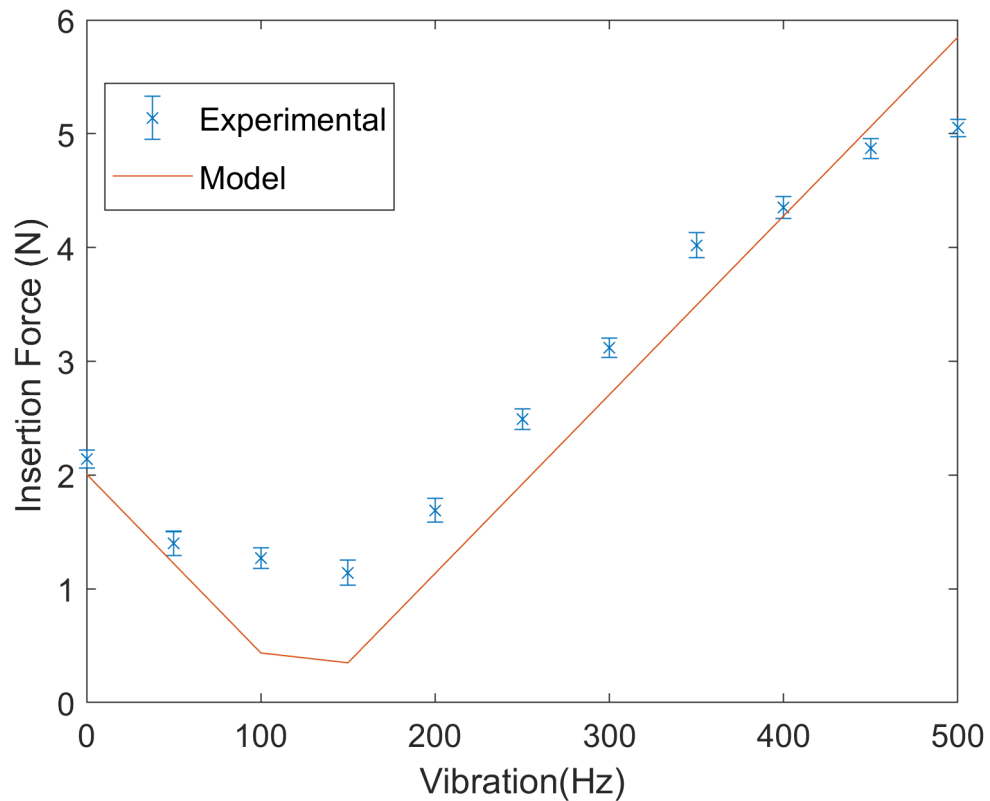


Figure 4.6. The insertion force (friction and cutting forces) comparison between experimental data and model with the influence of applied longitudinal vibration.

4.3 Results of Mosquito-Inspired Needles with Vibration

4.3.1 Parametric Study

The effect of mosquito-inspired needle design parameters on the maximum insertion force was explored in this Section, while other design parameters are kept constant. The effect of the thickness (t) and maxilla angle (M_a) on the maximum insertion force of the needle was studied before evaluating the parameters that contribute to force reduction. The labrum-tip radius ($L_r = 35$ mm) and distance between the inner maxilla ($x = 2.20$ mm) is constant because the parameter 'x' depends on the maxilla angle. Figure 4.7 shows the average of three trials for the insertion tests of mosquito-inspired needles with different thicknesses ($t = 0.1, 0.15,$ and 0.2 in mm). The maximum insertion force decreases with an increase in thickness. The final thickness value chosen for the needle is 0.2 mm. Similarly, with $t = 0.2$ mm, Fig. 4.8 shows the average of three trials of the insertion tests in PVC ($E = 6$ kPa) with different maxilla angles ($M_a = 110, 130, 150$ and 170 in deg). The increase in maxilla angle resulted in a lower insertion force because of the extra removal of material from the needle body surface. Higher maxilla angle showed less maximum insertion force. Therefore, the final values considered were 0.2 mm of thickness and 170° of maxilla angle. The experimental data with parameter modification showed the influence of thickness and maxilla angle on the maximum insertion force. The data analysis was performed to test the significance of the data using ANOVA. The post-hoc Tukey tests revealed the difference between the means of the data for thickness $0.1, 0.15,$ and 0.2 mm. The bar plot shown in Fig 4.7 with the same uppercase letters is not significant with a p -value (0.07) greater than the alpha of 0.05 . Moreover, the difference between the data is not significant, but the

increase in thickness resulted in a lower maximum insertion force using mosquito-inspired needles without vibration.

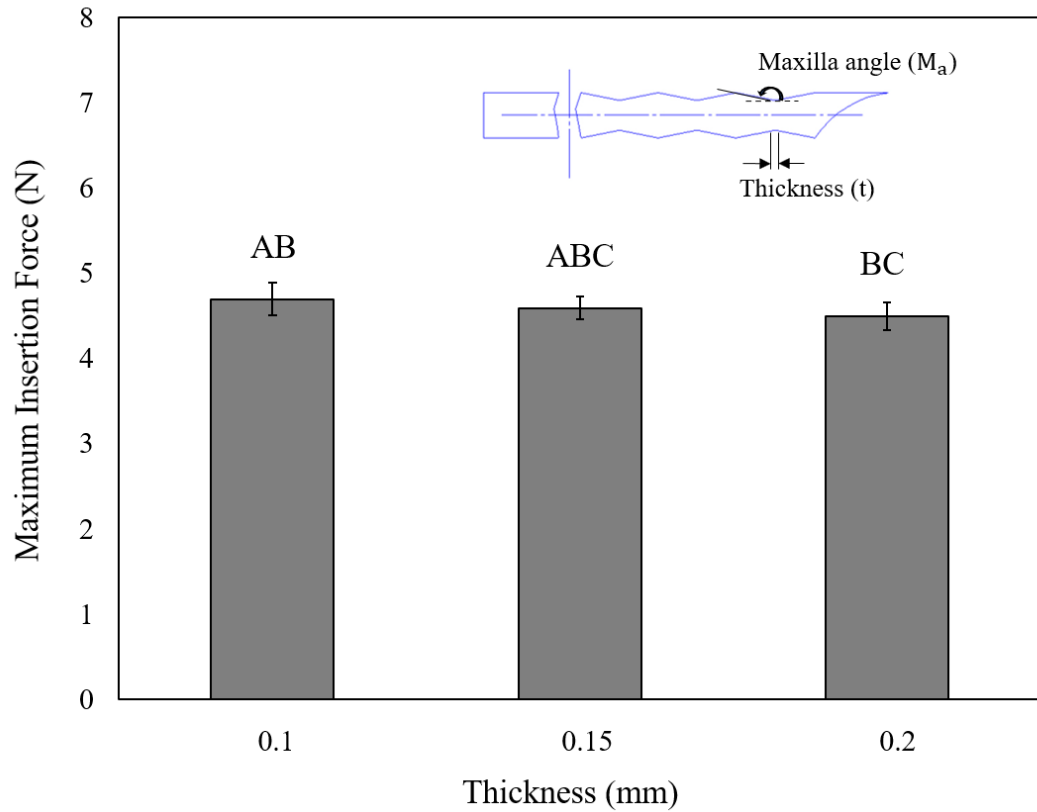


Figure 4.7. The mosquito-inspired needle design parameter on the maximum insertion force for the parameter thickness (t) in mm (no vibration, Insertion velocity = 1 mm/sec, PVC tissue phantom with $E = 6$ kPa). Bars sharing the same letters at the top of the bar graph are not significantly different at the 95% level, based on post-hoc Tukey tests.

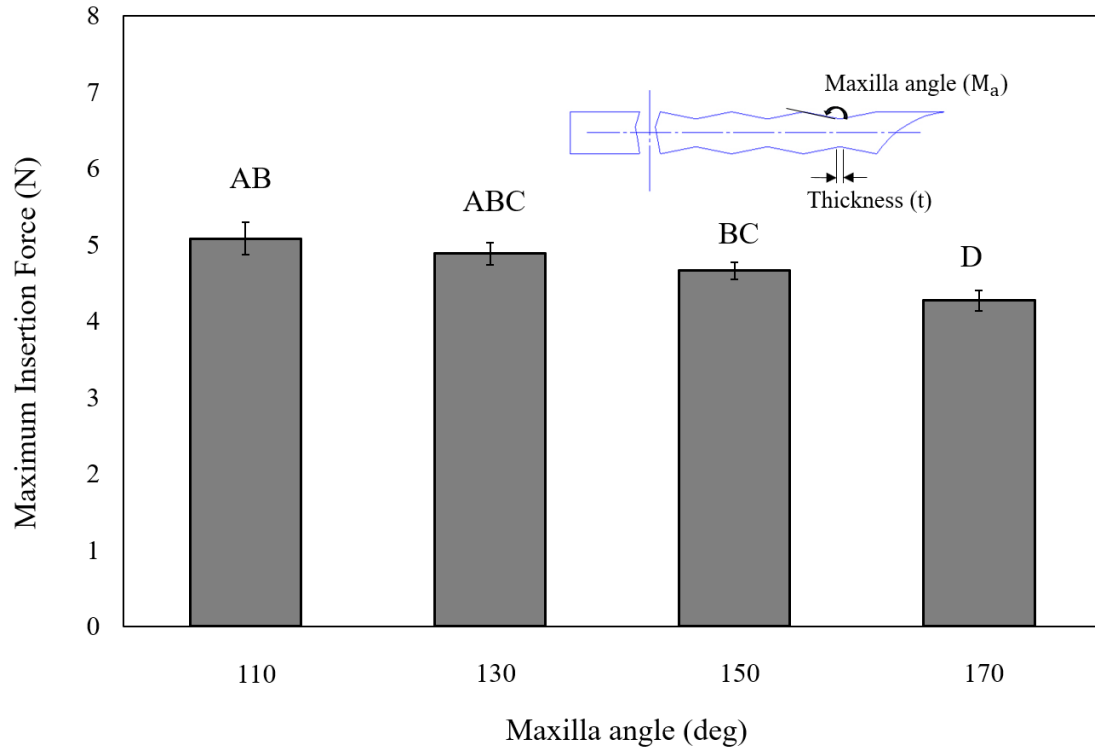


Figure 4.8. The mosquito-inspired needle design parameter on the maximum insertion force for maxilla angle (M_a) in deg (no vibration, Insertion velocity = 1 mm/sec, PVC tissue phantom with $E = 6$ kPa). Bars sharing the same letters at the top of the bar graph are not significantly different at the 95% level, based on post-hoc Tukey tests.

The influence of vibration frequencies was investigated using mosquito-inspired needles. The maximum insertion force reduced with an increase in vibration at a constant amplitude of $5 \mu\text{m}$ and insertion velocity of 1 mm/sec. The vibration frequencies ranging from 0 to 500 Hz were experimentally evaluated with the mosquito-inspired needle. The insertion tests were performed in PVC tissue phantom ($E = 6$ kPa) at an insertion depth of 60 mm (this being the maximum target in our study). As discussed in Section 4.3 (theoretical model), it is found that the influence of vibration plays a vital role in decreasing

or increasing the insertion force. From Fig 4.9, the insertion force decreases and starts to increase with the increase in vibration. At 0 Hz frequency (no vibration) the insertion force is higher, but when the vibration starts to increase, which means applied longitudinal vibration from 100 to 200 Hz, the insertion force reduces, but increases thereafter with an increase in vibration from 200 to 500 Hz. This is also shown in our model that an increase in vibration increases the insertion force [106]. The average SD values for the vibration study (see Fig 4.9) range from $0.05 \leq SD \leq 0.13$. The limitation of the vibration using a mosquito-inspired needle was at 200 Hz, which showed a reduction with an increase in insertion depth. The maximum insertion force is critical as it directs the needle to deflect and causes higher force, which is why studying the maximum insertion force is vital. In this parametric study of vibration frequency, it is experimentally seen that increasing the vibration will lead to an increase in maximum insertion force. The post-hoc Tukey tests showed a significant difference between the means of the data for different maxilla angles in Fig 4.8. The bars with the same letters showed no significance because of the slight change in angle. But the difference between the means of the data for 110 and 170 deg showed significance with a p -value (0.026) less than alpha (0.05). Moreover, the increase in the maxilla angle resulted in a lower maximum insertion force.

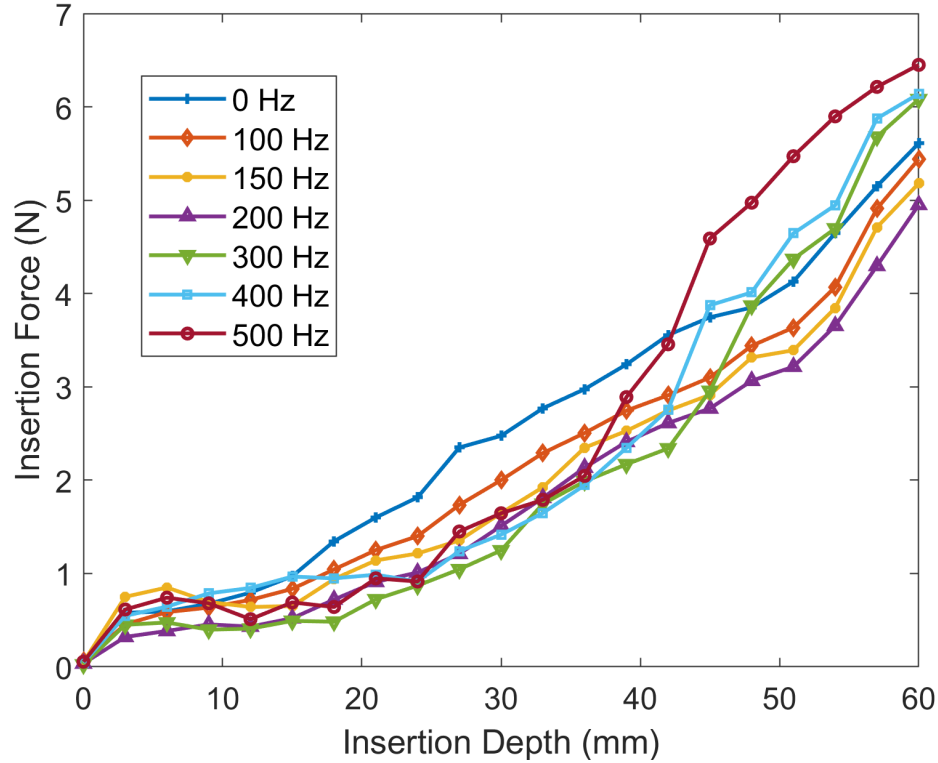


Figure 4.9. The insertion force results for different vibrational frequencies ranging from 0 to 500 Hz. (Insertion speed – 1 mm/sec, amplitude -5 μ m and depth of insertion – 60 mm)

From the experimental results shown in Fig 4.8, the maximum insertion force reduces compared to standard needles. The effect of insertion velocity was studied with mosquito-inspired needles. From Fig 4.10, the insertion force at 60 mm depth is smaller than the insertion force at 0 Hz. In the earlier Section, the vibration of 200 Hz showed a reduction in insertion force, this vibration was applied to study the effect of insertion velocity on the insertion force. The results show that increasing the velocity increases the insertion force from 1 to 10 mm/sec. The insertion force at a velocity of 1 mm/sec is lower irrespective of the insertion depth compared to the insertion velocity of 10 mm/sec. The reduction in force is due to an increased energy rate and decrease in fracture toughness [11]. Also, the

stiffness of the tissue creates extra pressure when increasing the velocity, which results in a higher force. The maximum insertion force increases with the increase in insertion velocity between 1 and 10 mm/sec, the final velocity that was utilized in our next experiments in this Chapter using standard and mosquito-inspired needles was 1 mm/sec based on our experimental results. The standard deviation values for this study ranges from $0.05 \leq SD \leq 0.14$.

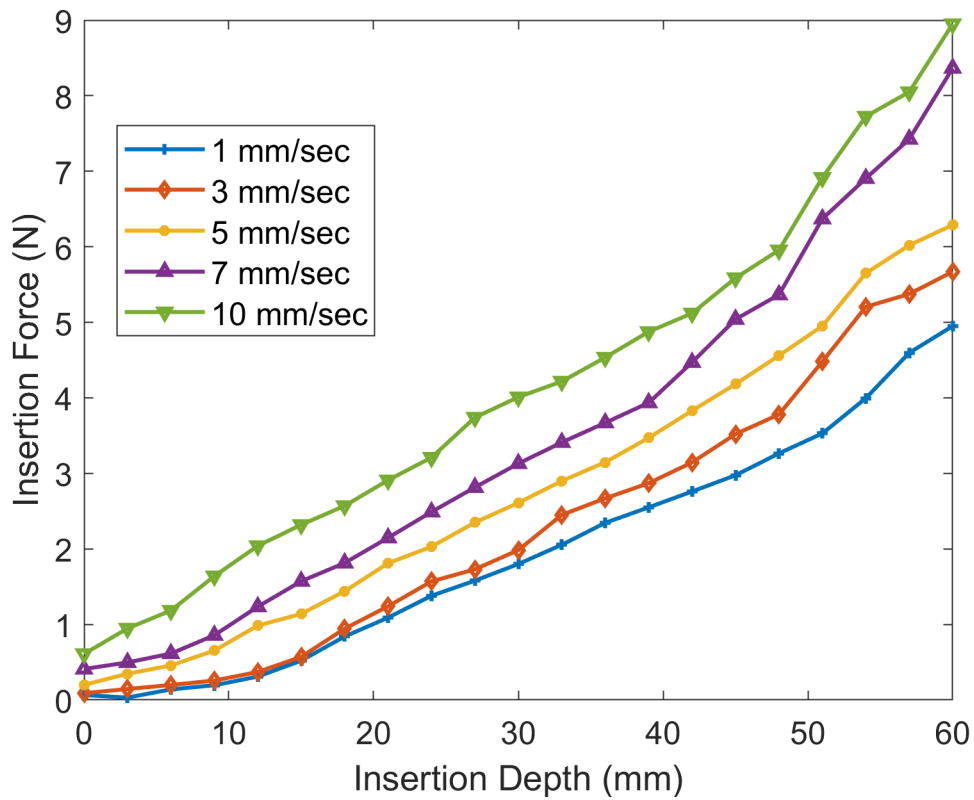


Figure 4.10. The insertion force results for mosquito-inspired needle by varying insertion velocity from 1 to 10 mm/sec with constant vibration of 200 Hz and amplitude of 5 μ m.

4.3.2 Needle Insertion Force Study

The insertion and extraction forces of the needle were studied in this Section after experimentally modifying the vibration and velocity parameters that affect the maximum insertion force along with the maxilla angle and thickness of a mosquito-inspired needle. The insertion tests were performed in PVC tissue phantom ($E = 6$ kPa) and the data presented is the average of three insertion tests. The insertion speed during needle insertion using both the needles is 1 mm/sec, depth of insertion is 60 mm, and needle diameter for both needles is 3mm. The relationship between vibration and insertion force was analyzed in Section 4.2. It is experimentally shown (see Fig 4.11) that with the effect of vibration, the maximum insertion force reduces using a standard needle.

It is conjectured that the vibration effect during needle insertion reduces the insertion force with maxilla design on the needle body and labrum-tip (see Section 4.3.3). During this insertion force study, the other important observation was the extraction force which is also reduced due to the vibration effect using a mosquito-inspired needle. The ease of extraction becomes much easier due to the path that is already created during insertion with vibration. Also, it is assumed that there is no cutting force during extraction (see Fig 4.13), only the friction force is present, which is discussed in Section 4.4.3.

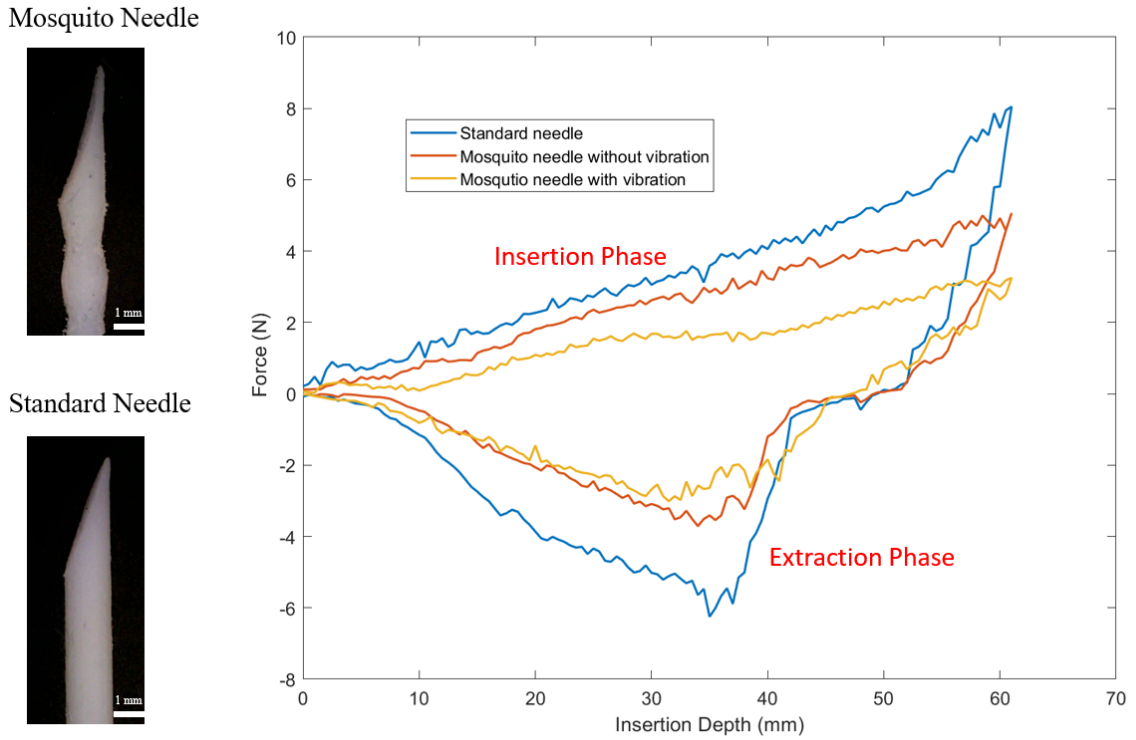


Figure 4.11. The insertion and extraction forces using standard and mosquito-inspired needles with and without vibration. (Vibration – 200 Hz, Insertion Depth – 60 mm, Insertion speed – 1 mm/sec and Amplitude – 5 μ m)

The standard deviation values for this study are in the range of $0.04 \leq SD \leq 0.12$. From Fig 4.11, the overall reduction of insertion force is 60% and the extraction force is 57% using a mosquito-inspired needle compared to the standard needle without vibration. The insertion force increases with insertion depth and the maximum insertion force values are shown in Fig 4.12. The post-hoc Tukey tests revealed a significant difference between the experimental data shown in Fig 4.12. The *p*-value (0.015) is less than the alpha (0.05) and

the mosquito-inspired needle with vibration reduced the maximum insertion force by 60% compared to the standard needle without vibration.

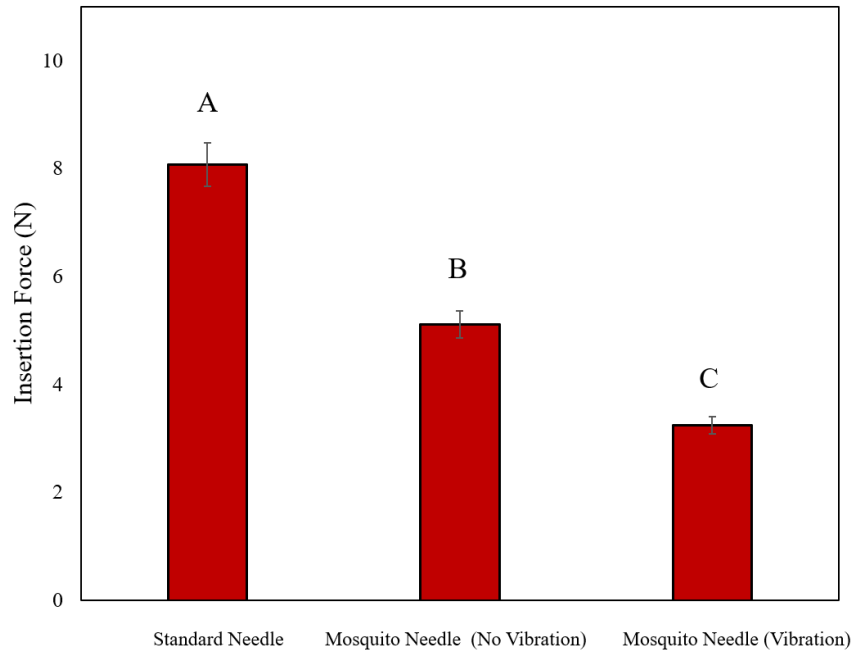


Figure 4.12. The standard deviation values for the insertion forces using standard needle without vibration and mosquito needle with vibration. Bars sharing different letters are significant at the 95% level.

4.3.3 Friction Force Study

The insertion force (cutting and friction) that occurs during needle insertion with and without vibration were discussed in the earlier Section 4.2. Therefore, this Section studies the difference between cutting and frictional force. During insertion into soft tissue, the insertion force occurs due to its contact and also the force at the needle-tip. During extraction, there is no cutting of the needle-tip, but there is friction between needle and tissue (which means only frictional force). To obtain the approximate cutting force values,

the measured extraction force was subtracted from the insertion force. For a mosquito-inspired needle with vibration of 200 Hz, the cutting force reduces or very less in number compared to the frictional force. Figure 4.13 presents the measured cutting force for the mosquito-inspired needle. The insertion force consists of friction and cutting force, and the extraction force consists of friction force (no cutting). Therefore, to measure the cutting force, the extraction force was subtracted from the insertion force, which resulted in the cutting force. The results obtained from the PVC tissue phantom and bovine liver tissue agreed with the hypothesis that maxilla design on the needle body along with vibration lowers the friction force and cutting force. The friction and cutting forces from the Fig 4.13 give us an understanding of the reduction in insertion force with vibration.

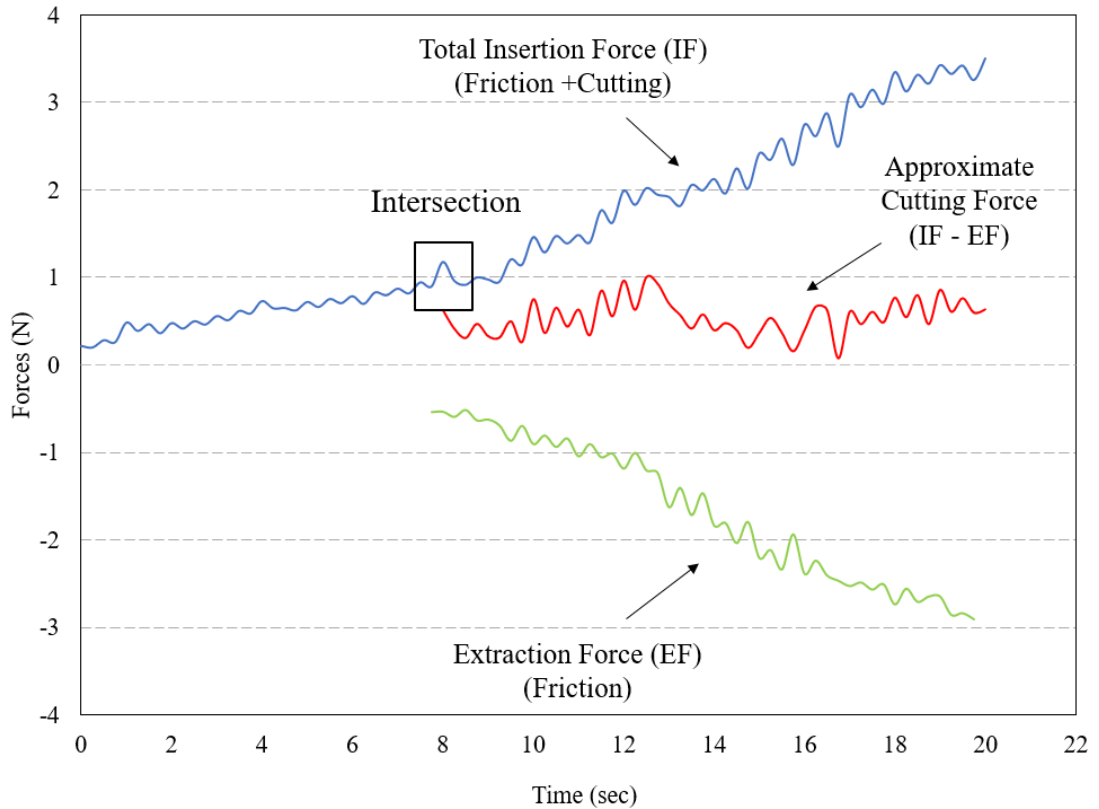


Figure 4.13. The approximation of measured cutting forces from insertion and extraction forces of the experimental data during insertion into tissue gel phantom. (vibration – 200 Hz, tissue-PVC, insertion speed– 1 mm/sec)

4.3.4 Size-Scale study

The size scale effect on insertion force was investigated using mosquito-inspired and standard needles. Since all the experiments were done using a scaled-up needle, a scaling study was also performed to validate the needle prototypes. However, this dissertation study focuses on the fundamental study of the mosquito-inspired needle with vibration, it is crucial to study the influence of vibration on the small-scale needles. The needle outer diameter in the biopsy and brachytherapy procedures are 16-gauge ($D = 1.65$ mm) and 18-

gauge ($D = 1.27$ mm) needles. The outer diameter of the needles in this study is 1.65 mm (16-gauge), 2 mm (14-gauge), and 3 mm (11-gauge). The 3D printed standard and mosquito needles are shown in Fig 4.14.

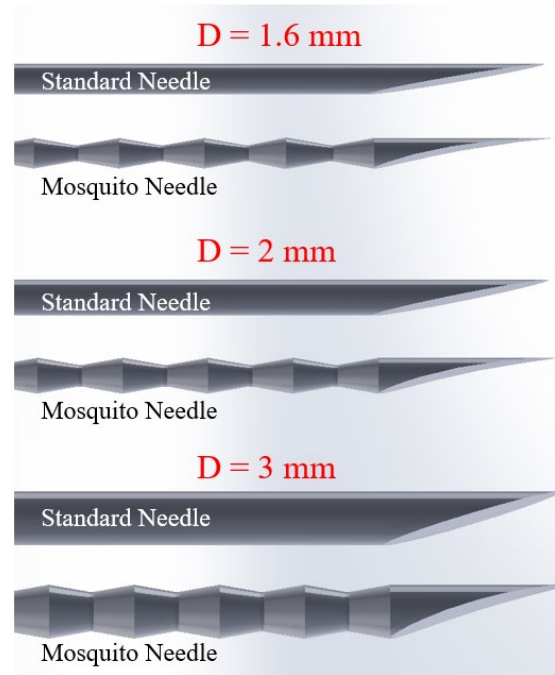


Figure 4.14. The standard and mosquito-inspired needles with different diameters (outer diameter (OD) = 1.6, 2, and 3 in mm). ($M_a = 170^\circ$, $t = 0.2$ mm, $\alpha = 40^\circ$)

The insertion tests were performed in PVC tissue phantom, which has a Young's Modulus of 1.8 kPa. The maximum insertion force decreases with the vibrating mosquito needles compared to standard needles without vibration (see Fig 4.15). The results are compared with a standard needle of the same outer diameter. The maximum insertion force is reduced by 32% using the mosquito-inspired needle with vibration for a needle diameter of 1.6mm.

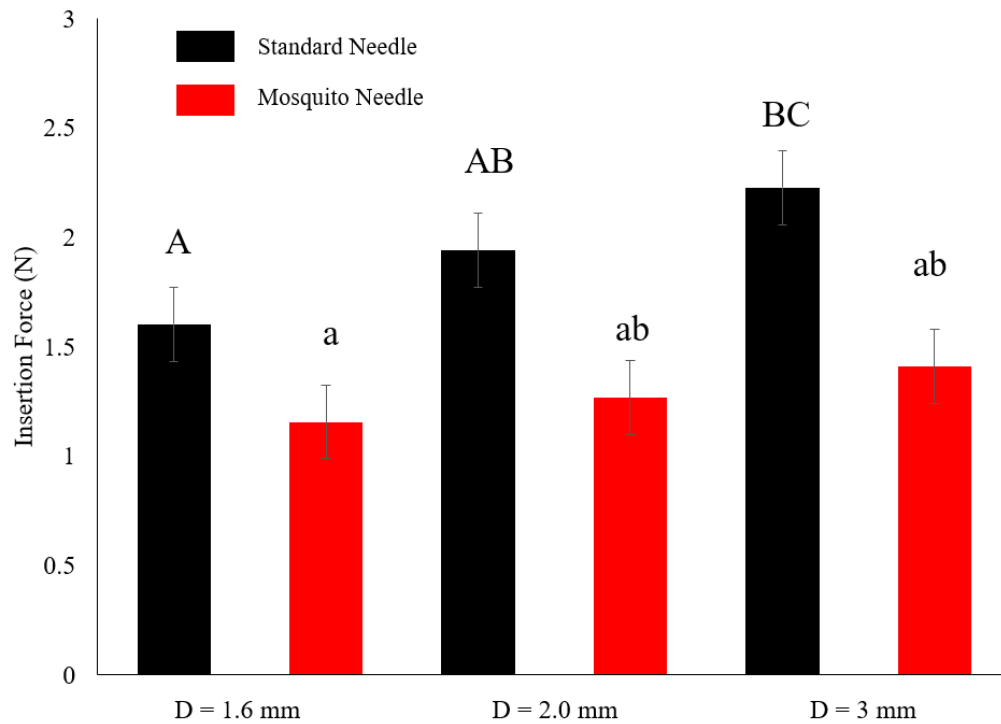


Figure 4.15. The insertion force results using standard and mosquito-inspired needles with vibration for different diameters (D) of 1.6, 2, and 3 in mm. Bars sharing the same uppercase and lowercase letters at the top of the bar graph are not significantly different at the 95% level, based on post-hoc Tukey tests.

This study also confirms that influence of longitudinal vibration results in a reduction in the maximum insertion force irrespective of the needle size. To test the significance of the data for two different groups (standard and mosquito-inspired needles), ANOVA single factor was used. The data using ANOVA were significant but to test the significance within the means of different groups, the post-hoc Tukey test was used. This test revealed a significant difference between the multiple groups. The bars with the same lowercase and uppercase letters are not significant but are significant with different letters. The *p*-value

of 0.032 is less than the alpha of 0.05. The post-hoc Tukey tests also revealed that with the change in diameter, the maximum insertion force reduced with vibration is significant at a 95% confidence level.

4.3.5 Tissue Deformation Analysis

In the earlier Section 4.3.2, the effect of vibration of a mosquito-inspired needle on the insertion force was demonstrated and showed a 60% reduction in the insertion force. From the literature, it is known that decreasing the insertion force could reduce tissue deformation [2, 74, 81]. Therefore, this study focuses on tissue deformation analysis using a magnetic sensing system (see Section 2.3). The change in the magnet position is recorded using an MTJ sensor array that measures tissue deformation changes during needle insertion. This experiment was performed with the mosquito-inspired needle with vibration and compared to a standard needle without vibration. Firstly, the tissue deformation sensing system was measured in PVC tissue phantom using both the needles for known depth of insertion. The camera observation data was also measured (which is an average of three data) parallelly during the needle insertion. The measured distance from the top of the tissue to the maximum deformation due to the standard needle was 17.5 mm, while the mosquito needle with vibration is 11.2 mm (36% reduction) (Fig 4.16). The change in magnetic field strength implies the change in position of the magnet, which means a change in the tissue deformation. The data analysis for the optical data is significant with a p -value (0.042) less than alpha (0.05). The maximum difference in tissue deformation distance with the mosquito-inspired needle with vibration is less than the standard needle without vibration.

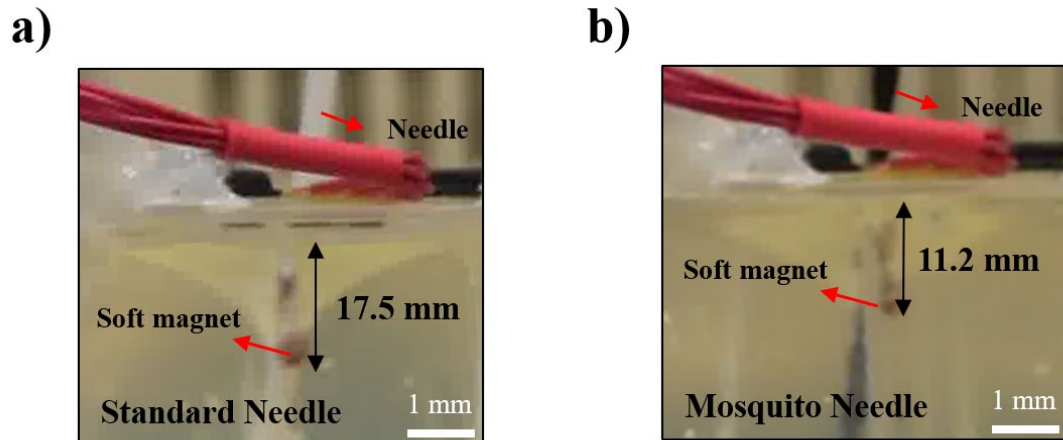


Figure 4.16. The recorded tissue deformation using a) standard needle without vibration and b) mosquito needle with vibration.

The needle insertion force increases with the increase in insertion depth (see Fig 4.12) and the maximum insertion force occurred at maximum depth, which is the maximum distance of tissue deformation. This deformation shown in Fig 4.16 was recorded with a high-speed camera and the change in the magnetic field occurred at time ($t = 10$ sec) using a mosquito-inspired needle and time ($t = 13$ sec) with the standard needle (see Fig 4.17). This decrease in deformation is due to the reduction in the insertion force with applied vibration. The tissue deformation distance (d) was decreasing with the mosquito-inspired needle compared to the standard needle. The maximum change in the magnetic field of the soft magnet for the mosquito-inspired needle with vibration was measured to be $7.112 \mu\text{T}$, whereas the standard needle exhibited $9.151 \mu\text{T}$. The lower change in the magnetic field corresponds to less tissue deformation and thus required less insertion force. This change in the magnetic field is then converted to the amount of distance from the MTJ sensor using

inverse cube law and plotted with distance on the y-axis and time on the x-axis, as shown in Fig. 4.17. To confirm the overall tissue deformation, any distorted area from the site of the needle was estimated from the picture (taken from the camera) using ImageJ. The mosquito-inspired needle with vibration indeed shows a smaller deformed area (0.24 mm^2) compared to that of standard needles (0.46 mm^2), which is a 48% reduction.

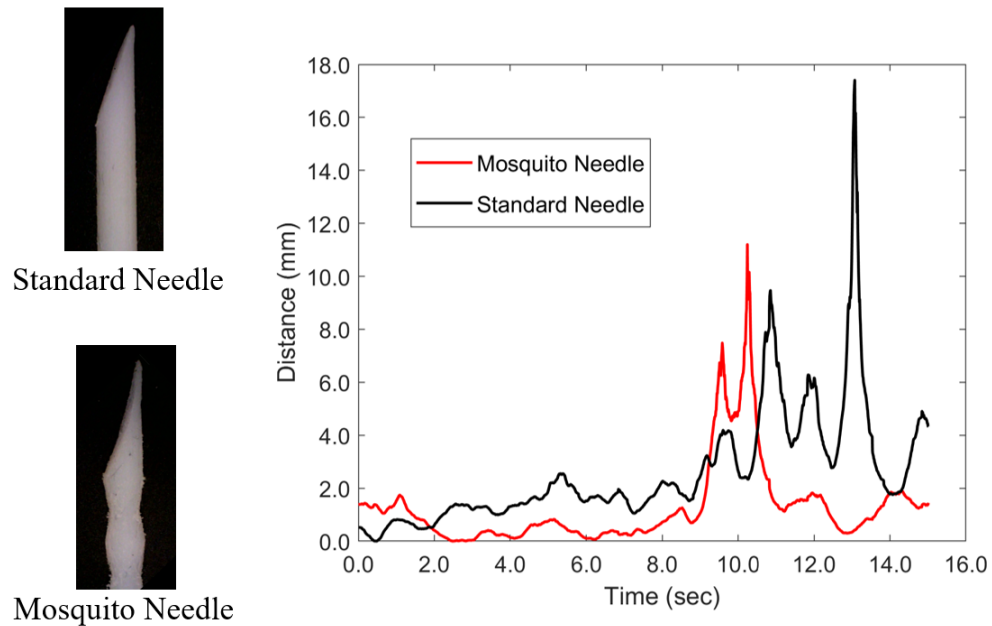


Figure 4.17. The magnetic sensing recorded tissue deformation in distance (mm) in PVC gels with a standard needle without and mosquito-inspired needle with vibration.

4.3.6 *Ex-vivo Insertion Tests into Biological Tissue*

This Section investigated the performance of the mosquito-inspired needle with vibration in bovine liver tissue. Figure 4.8 shows the average insertion force of three insertion trials into the bovine liver tissue for both standard bevel-tip needle and mosquito-inspired needle. The insertion tests into liver tissue were carried out with applied

longitudinal vibration of 200 Hz, an amplitude of 5 μm , and insertion velocity of 1 mm/sec. As shown in Fig. 4.18, the insertion force of a mosquito-inspired needle with vibration reduces compared to the standard needle without vibration. During the insertion into the tissue, both needles have different puncture force and as the needle penetrates in the tissue, the force acting on the needle increased for the standard needle and decreased for the mosquito-inspired needle. This is due to the unevenly distributed stiffness properties of the bovine liver tissue. As the depth of insertion increases, the insertion force also increased. The maximum insertion force was reduced by 39% using a mosquito-inspired needle with vibration. Also, in Fig 4.18, the insertion force was linear until 20 mm and increased after 20 mm and until 60 mm, and the inconsistency is due to the non-homogeneous properties of the bovine liver tissue, which resulted in force change and the non-linearity of force curve.

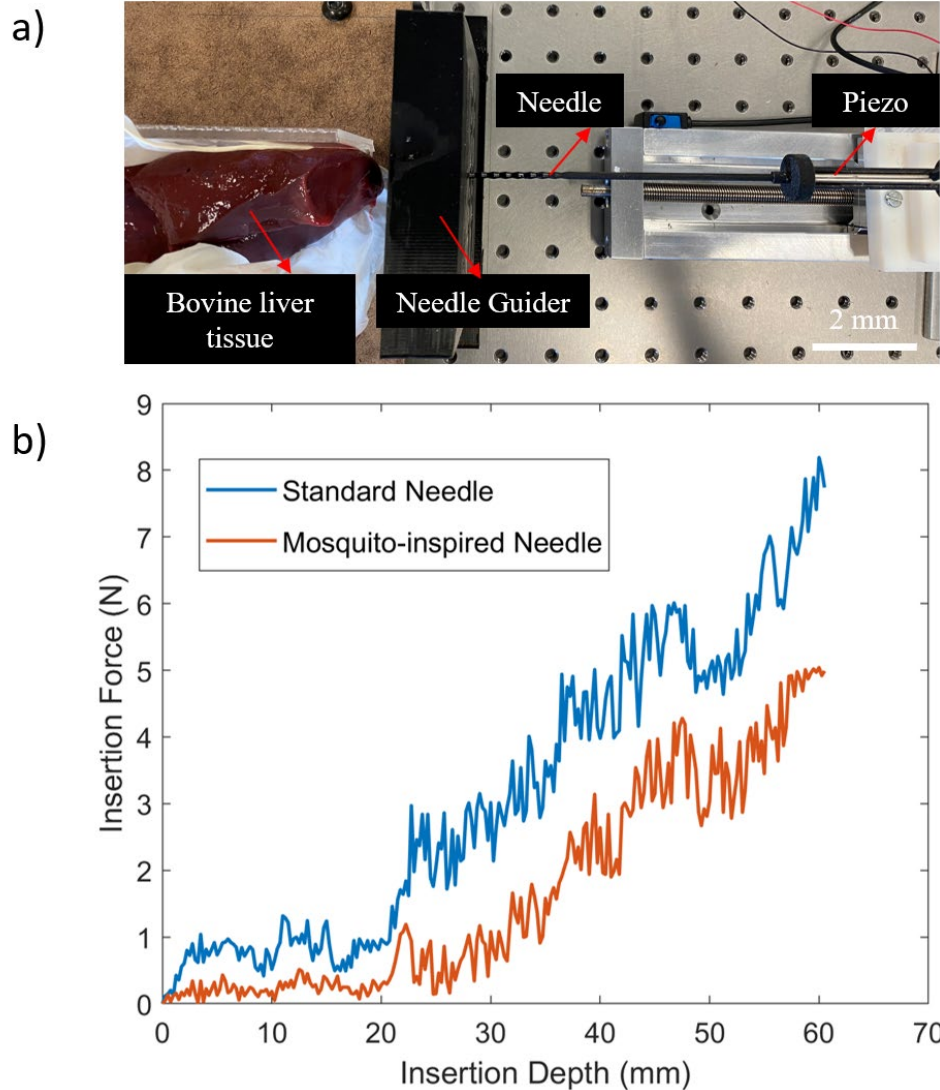


Figure 4.18. a) *Ex-vivo* insertion tests into bovine liver tissue and b) the average insertion forces obtained from insertion tests into bovine liver tissue with the vibration of 200 Hz, an amplitude of $5\mu\text{m}$, and insertion velocity of 1 mm/sec.

The insertion force increases with an increase in depth irrespective of the needle shown in Fig 4.18 b). The insertion force for mosquito-inspired needles from 0 to 60 mm was lower than the standard needle, but they increase as the insertion depth increases. It is

conjectured that the reduction in insertion force is due to the reduction in friction force during insertion into bovine liver tissue compared to the standard needle. The cutting force in the bovine liver tissue depends on the stiffness of the tissue and crack that occurred at the needle-tip, which is why the cutting force will be less than the frictional force. However, the reduction in insertion force should decrease the damage in the bovine tissue due to less pressure and less fracture [43]. The data analysis using paired *t*-test for the maximum insertion force between the standard needle and mosquito-inspired needle is significant with a *p*-value (0.037), which is less than alpha (0.05). Bars with different letters indicate that the difference between the means of the data is significant at a 95% confidence level.

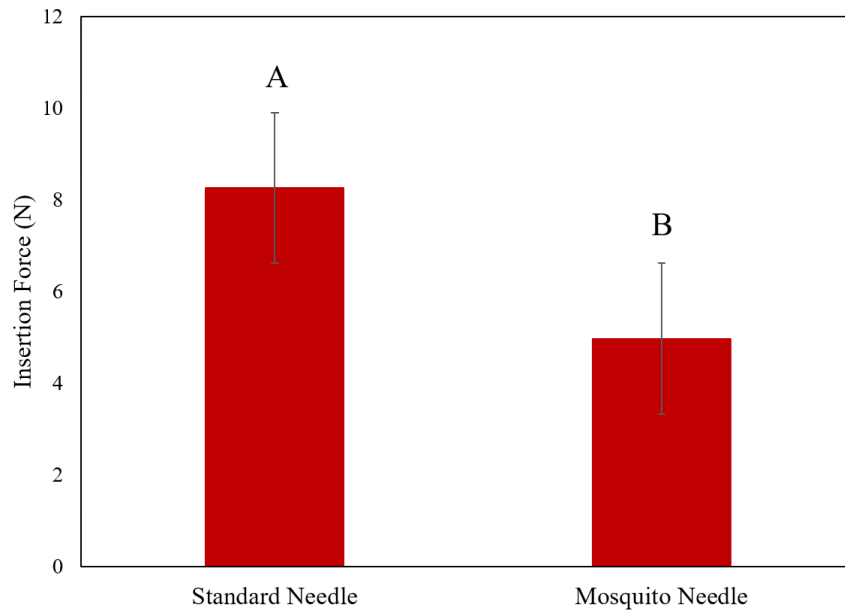


Figure 4.19. The standard deviation for insertion forces into bovine liver tissue at a depth of 60 mm using both standard and mosquito-inspired needles. Bars with different letters are significant at the 95% level.

4.3.7 Tissue Damage Analysis

The cross-sectional area of the damage caused by both standard and mosquito-inspired needles was evaluated histologically. All the standard protocols were followed during the histological evaluation, i.e., starting from insertion tests in bovine liver tissue, sample preparation, hematoxylin, and eosin staining, imaging, and analyzing the tissue damage. The insertion tests were performed in three different bovine liver tissue samples for histological evaluation [99]. The damaged area on the tissue sample was located using microscopy observation. The cross-section area of the needle paths on the stained slides was measured using ImageJ software. The statistical data presented in Table 4.3 shows the area measured in pixels using ImageJ software.

Table 4.3. The statistical data information for the area of damage in bovine liver tissue due to standard and mosquito-inspired needles.

<i>Needle type</i>	<i>Bovine liver samples damage in the area (Pixels)</i>			<i>Mean (Pixels)</i>	<i>Standard Deviation</i>
	<i>Sample 1</i>	<i>Sample 2</i>	<i>Sample 3</i>		
Standard needle	872,535	1,056,790	912,446	947,257	79,147
Mosquito needle	679,900	687,431	707,456	691,595	11,629

Figure 4.20 shows the damaged cross-sectional area caused by both the needles for three bovine liver tissue samples. The area of the damaged hole caused by both mosquito-inspired and standard needles were different because of the insertion method. It is found that the average cross-sectional area of the damage was reduced by 27% using a mosquito-inspired needle with vibration compared to the standard needle. A *t*-test was used to study the significance of the data in three liver tissue samples with the standard and mosquito-inspired needles. The mean area of the damage using a standard needle is 947,257 Pixels and with the mosquito-inspired needle is 691,595 Pixels. The significant difference of the data was tested and found that the *p*-value is 0.023, which is less than alpha (0.05). Therefore, the null hypothesis is rejected, and the data presented in Table 4.3 is statistically significant. The schematic representation of the area of the damage due to the mosquito-inspired needle was compared to the standard needle is shown in Fig 4.20 (c). The results infer that needle insertion with the vibration of a mosquito-inspired needle decreases tissue damage. This reduction implies that reducing insertion force led to a tissue damage reduction [91], which can lead to less invasive percutaneous procedures.

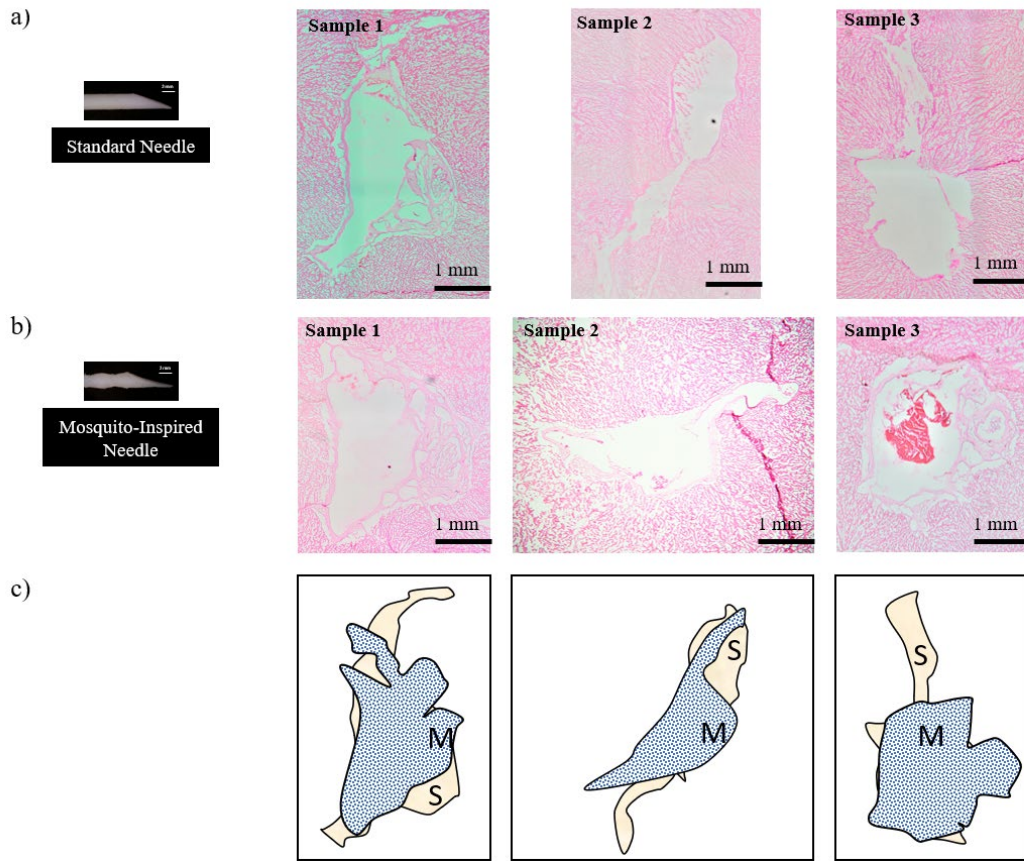


Figure 4.20. Magnified view of the damage in different bovine liver tissue samples due to a) standard needle, b) mosquito-inspired needle and c) the schematic representation of the damaged area in bovine liver tissues (M – mosquito-inspired and S – standard).

4.4 Discussions

In this Chapter, an experimental study related to the design of mosquito-inspired needle with vibration during needle insertion procedures were investigated. The ultimate goal was to provide a guideline for the surgeons to properly utilize the mosquito-inspired needle insertion for advancing the vibration-assisted clinical procedures. The study was conducted using 3D printed needles of diameter ($D = 3$ mm). The design on the needle is complex

and was unable to manufacture at the scale of 18-gauge (typical medical needle for biopsy and brachytherapy procedures). Therefore, the needles were designed and manufactured using a 3D printer, which is easy to manufacture and cost-efficient. The fundamental study of this work is to utilize the mosquito-inspired design on the needle body and apply the longitudinal vibration during needle insertion. The parametric study of maxilla angle and thickness showed that increasing the values will result in a lower maximum insertion force. Similarly, for the vibration parameter, the maximum insertion force decreases until 200 Hz and increases with an increase in vibration. This influence of vibration on insertion force is analytically studied using the LuGre friction model. The analytical model related to the insertion force (cutting and friction force) was analyzed and compared to the experimental data. The results show that the insertion force model provides an understanding of the influence of vibration on the insertion force when the vibration is increased. In fact, the experimental results are also aligned with the model data that increasing the vibration results in a higher insertion force. The vibration cutting parameters in bioinspired needle insertion needs to be studied to understand the influence of insertion forces [107]. Furthermore, a series of experiments were performed with a standard needle without vibration and a mosquito-inspired needle with vibration in PVC tissue and bovine liver tissues.

The results show that mosquito-inspired needles with vibration reduce the insertion force by 60% in PVC and 39% in the bovine liver compared to standard needles. Also, the approximate values of cutting and friction force were calculated, which gives the influence of cutting force acting on the needle-tip and friction force acting at the needle-tissue

interface. The analysis of different needle sizes implies that the application of longitudinal vibration guides in reducing the maximum insertion force irrespective of the needle size. This application of vibration-assisted mosquito-inspired needle insertion is more critical for blood sampling procedures where the insertion velocity required is very less (1 mm/sec). In blood sampling procedures, the needle has to be inserted into the skin tissue (E greater than 6 kPa) can be beneficial because of a reduction in the tissue damage. The tissue deformation from the surface to the depth of insertion also showed a reduction with the mosquito-inspired needle. The limitation in measuring the tissue deformation is the tissue. The tissue utilized for measuring the tissue deformation was PVC because the transparency and viscoelastic properties made it optically easy to record the needle insertion and compare it with the change in the magnetic field.

Furthermore, the reduction in tissue damage with vibrating mosquito-inspired needles showed a consistent reduction in the insertion force. For this reason, an insertion velocity of 1 mm/sec is recommended in our study during the needle insertion for soft tissues less than 3 kPa. The cross-sectional area of the tissue damage during the histological process followed all the standard protocols to ensure that the sectioned sample does not lose its damaged area [99]. This reduction in tissue damage suggests that the findings can be applied and extended to several blood sampling procedures and also biopsy procedures in which cannula is inserted to extract a tissue sample.

CHAPTER 5

CONCLUSION AND FUTURE WORK

5.1 Conclusion

The insertion mechanics of the honeybee-inspired needles with vibration were experimentally studied and compared with standard needles. The vibration addition during this study is inspired by mosquito-proboscis. The results obtained from the insertion tests showed that insertion force is reduced by 50% in PVC tissue phantom and 43% in chicken breast and needle-tip deflection by 47% using vibration-assisted honeybee-inspired needles compared to the standard bevel-tip needles. Furthermore, the results of the mosquito-inspired needles in PVC tissue phantom were used to experimentally modify the needle design parameters to lower the insertion and extraction force further. Our results showed that with modified parameters, the insertion force is decreased by 39% and the extraction force by 32% in PVC tissue phantom.

With the findings of the mosquito-inspired needle design effect on insertion force, the vibration was added during its insertion into tissues. The theoretical LuGre friction model was also studied to confirm the experimental results and to explain the insertion force (friction and cutting force). It was found that mosquito-inspired needles with vibration lowered the insertion force by 60%. Reducing the insertion force minimizes tissue deformation. Therefore, a novel magnetic sensing system was used to study the deformation of the tissue using vibrating mosquito-inspired needles. The tissue deformation area decreased by 48% and the distance lowered by 36% in PVC tissue phantom using a mosquito-inspired needle with vibration.

To show the relevance of insertion with vibration, insertion tests were performed into biological tissue namely bovine liver tissue using both standard and mosquito-inspired needles. The results showed that the insertion force is reduced by 39% in bovine liver tissue using the mosquito-inspired needle. Furthermore, a histological study was performed to evaluate the tissue damage using the vibrating mosquito-inspired needle. The mosquito-inspired needle with vibration was able to decrease the cross-sectional area of the tissue damage by 27% compared to a standard needle without vibration. The vibration cutting of mosquito-inspired needles in this study is beneficial for skin tissues with higher stiffness properties because the vibration influence during mosquito-inspired needle insertion can reduce the force and also the tissue damage.

5.2 Future Work

The fundamental study of the insertion mechanics (which is vital in the needle insertion force) of the honeybee and the mosquito-inspired needle has been shown to reduce the needle insertion force and tissue deformation significantly. Moreover, this reduction using bioinspired needles led to a reduction in tissue damage. The work presented in this dissertation has shown evidence that the application of bioinspired needle insertion has the potential to improve the insertion accuracy, specifically in percutaneous procedures. The future work of this fundamental study of bioinspired needle insertion will aid in further advancement of the bioinspired approach in clinical procedures by:

- 1) Investigating transverse vibration tissue cutting in tissues. The vibration effect performed in this study utilized only in the longitudinal direction (same as the axis of insertion). However, the limitation of using transverse cutting should be

challenging as the damage to the tissue cannot be increased. Therefore, transverse vibration cutting in soft tissues will be studied to determine its effect on insertion force and needle deflection.

- 2) Analyzing the bioinspired tip geometry can be optimized to reduce cutting force. The labrum-tip has been shown to lower the insertion force with and without the vibration effect. Further work is needed to understand the mechanics of bioinspired tip geometry.
- 3) Formulating computational models, to study the effect of bioinspired needle insertion is confined by soft tissue materials and also by predicting the force for force feedback to improve the target error. More parameters should be analyzed in these models especially during vibration tissue cutting.
- 4) Executing the manufacturing methods such as laser-induced plasma machining (LIPMM), metal 3D printing can be implemented to manufacture bioinspired needles, aiming to experimentally test for procedures like blood sampling and drug delivery before performing the surgery. The other aspect of this manufacturing is using biomaterials. The surface coatings on the bioinspired needle using biomaterials like polymer and composites to manufacture a biomaterial-based bioinspired needle (dual combination), which can replace stainless steel needles for better healing.

Moreover, this dissertation study will aid in developing the bioinspired needle for vibration-assisted clinical procedures. For example, in procedures like brachytherapy, if the needle insertion force and deflection are minimized, the needle can reach the site of the

procedure with minimal force. Since the vibration-assisted insertion reduced tissue damage, it can be implemented in a blood sampling procedure, where the surgeon inserts the needle into the skin tissue to acquire the blood sample. Also, developing and manufacturing the bioinspired needles for the application of surgical robotics, where high precision is required to perform the surgery. The vibration effect during bioinspired needle insertion has shown to lower the insertion force acting on the needle and the tissue damage, this reduction can be an advantage in needle-based procedures using robot surgical systems like da Vinci (Intuitive Surgical, Sunnyvale, CA) and Mako (Stryker, Kalamazoo, MI).

REFERENCES

- [1] N. Abolhassani, R. Patel, and M. Moallem, “Needle insertion into soft tissue: A survey,” *Med. Eng. Phys.*, vol. 29, no. 4, pp. 413–431, 2007. <https://doi.org/10.1016/j.medengphy.2006.07.003>
- [2] D. J. van Gerwen, J. Dankelman, and J. J. van den Dobbelsteen, “Needle-tissue interaction forces - A survey of experimental data,” *Med. Eng. Phys.*, vol. 34, no. 6, pp. 665–680, 2012, <https://doi.org/10.1016/j.medengphy.2012.04.007>
- [3] G. Dogangil, B. L. Davies, and F. Rodriguez Y Baena, “A review of medical robotics for minimally invasive soft tissue surgery,” *Proc. Inst. Mech. Eng. Part H J. Eng. Med.*, vol. 224, no. 5, pp. 653–679, 2010, <https://doi.org/10.1243/09544119jeim591>
- [4] G. Kronreif, M. Fürst, J. Kettenbach, M. Figl, and R. Hanel, “Robotic guidance for percutaneous interventions,” *Adv. Robot.*, vol. 17, no. 6, pp. 541–560, 2003, <https://doi.org/10.1163/15685530360675532>
- [5] T. K. Podder, A. P. Dicker, P. Hutapea, K. Darvish, and Y. Yu, “A novel curvilinear approach for prostate seed implantation,” *Med. Phys.*, vol. 39, no. 4, pp. 1887–1892, 2012, <https://doi.org/10.1118/1.3694110>
- [6] F. Piccinino *et al.*, “Complications following percutaneous liver biopsy,” *J. Hepatol.*, vol. 2, no. 2, pp. 165–173, 1986, [https://doi.org/10.1016/s0168-8278\(86\)80075-7](https://doi.org/10.1016/s0168-8278(86)80075-7)
- [7] S. P. DiMaio and S. E. Salcudean, “Needle insertion modeling and simulation,” *Ieee*

- Trans. Robot. Autom.*, vol. 19, no. 5, pp. 864–875, 2003, <https://doi.org/10.1109/TRA.2003.817044>
- [8] N. V. Datla and P. Hutapea, “Flexure-Based Active Needle for Enhanced Steering Within Soft Tissue,” *J. Med. Device.*, vol. 9, no. 4, p. 041005, 2015, <https://doi.org/10.1115/1.4030654>
- [9] M. Sahlabadi, S. Khodaei, and K. Jezler, “Insertion mechanics of bioinspired needles into soft tissues,” *Minim. Invasive Ther. Allied Technol.*, vol. 0, no. 0, pp. 1–8, 2017, <https://doi.org/10.1080/13645706.2017.1418753>
- [10] N. Abolhassani, R. Patel, and F. Ayazi, “Effects of different insertion methods on reducing needle deflection,” *Annu. Int. Conf. IEEE Eng. Med. Biol. - Proc.*, pp. 491–494, 2007, <https://doi.org/10.1109/iembs.2007.4352330>
- [11] M. Mahvash and P. E. Dupont, “Mechanics of dynamic needle insertion into a biological material,” *IEEE Trans. Biomed. Eng.*, vol. 57, no. 4, pp. 934–943, 2010, <https://doi.org/10.1109/tbme.2009.2036856>
- [12] M. Sahlabadi, S. Gidde, P. Gehret, K. Pourfarhangi, B. Bayarmagnai, and P. Hutapea, “Histological evaluation of tissue damage caused by bioinspired needle insertion,” *Adv. Biomater. Devices Med.*, vol. 5, no. 1, pp. 1–6, 2018.
- [13] M. Sahlabadi and P. Hutapea, “Tissue deformation and insertion force of bee-stinger inspired surgical needles,” *J. Med. Devices, Trans. ASME*, vol. 12, no. 3, pp. 12–15, 2018, <https://doi.org/10.1115/1.4040637>
- [14] S. P. DiMaio and S. E. Salcudean, “Interactive simulation of needle insertion

- models,” *IEEE Trans. Biomed. Eng.*, vol. 52, no. 7, pp. 1167–1179, 2005, <https://doi.org/10.1109/TBME.2005.847548>
- [15] N. Abolhassani, R. Patel, and F. Ayazi, “Minimization of needle deflection in robot-assisted percutaneous therapy,” *Int. J. Med. Robot. Comput. Assist. Surg.*, vol. 3, no. April, pp. 140–148, 2007, <https://doi.org/10.1002/rcs.136>
- [16] M. Giovannini, H. Ren, J. Cao, and K. Ehmann, “Study on design and cutting parameters of rotating needles for core biopsy,” *J. Mech. Behav. Biomed. Mater.*, vol. 86, pp. 43–54, 2018, <https://doi.org/10.1016/j.jmbbm.2018.06.013>
- [17] J. T. Hing, A. D. Brooks, and J. P. Desai, “Reality-based needle insertion simulation for haptic feedback in prostate brachytherapy,” *Proc. - IEEE Int. Conf. Robot. Autom.*, vol. 2006, no. May, pp. 619–624, 2006, <https://doi.org/10.1109/ROBOT.2006.1641779>
- [18] P. H. Kavi I Patel, Long Zhu, Sai Teja Reddy Gidde, Fei Ren, “Influence of Composite Polymer Coatings on the Insertion Force of Needle-Like Structure in Soft Materials,” in *Proceedings of the ASME 2020 International Mechanical Engineering Congress and Exposition*, 2020, <https://doi.org/10.1115/IMECE2020-24341>
- [19] N. Abolhassani, R. Patel, and M. Moallem, “Control of soft tissue deformation during robotic needle insertion,” *Minim. Invasive Ther. Allied Technol.*, vol. 15, no. 3, pp. 165–176, 2006, <https://doi.org/10.1080/13645700600771645>

- [20] S. T. R. Gidde and P. Hutapea, "Design and Experimental Evaluation of Mosquito-Inspired Needle Structure in Soft Materials," in *Proceedings of the ASME 2020 International Mechanical Engineering Congress and Exposition*, 2020, vol. 5, pp. 1–3, <https://doi.org/10.1115/IMECE2020-24320>
- [21] M. Mahvash and P. E. Dupont, "Fast needle insertion to minimize tissue deformation and damage," *Proc. - IEEE Int. Conf. Robot. Autom.*, pp. 3097–3102, 2009, <https://dx.doi.org/10.1109%2FROBOT.2009.5152617>
- [22] A. M. Okamura, C. Simone, and M. D. O. Leary, "Force Modeling for Needle Insertion Into Soft Tissue," vol. 51, no. 10, pp. 1707–1716, 2004, <https://doi.org/10.1109/TBME.2004.831542>
- [23] J. Stellman, "Development, production, and characterization of plastic hypodermic needles," Georgia Institute of Technology, *Master Thesis*, 2009.
- [24] O. A. Shergold and N. A. Fleck, "Experimental Investigation Into the Deep Penetration of Soft Solids by Sharp and Blunt Punches, With Application to the Piercing of Skin," *J. Biomech. Eng.*, vol. 127(5), 2005, <https://doi.org/10.1115/1.1992528>
- [25] M. A. Meltner, N. J. Ferrier, and B. R. Thomadsen, "Observations on rotating needle insertions using a brachytherapy robot.," *Phys. Med. Biol.*, vol. 52, pp. 6027–6037, 2007, <https://doi.org/10.1088/0031-9155/52/19/021>
- [26] I. Khalaji, M. Hadavand, A. Asadian, R. V. Patel, and M. D. Naish, "Analysis of needle-tissue friction during vibration-assisted needle insertion," *IEEE Int. Conf.*

Intell. Robot. Syst., pp. 4099–4104, 2013,
<https://doi.org/10.1109/IROS.2013.6696943>

- [27] R. S. Clement, E. L. Unger, O. M. Ocón-grove, T. L. Cronin, and M. L. Mulvihill, “Effects of Axial Vibration on Needle Insertion into the Tail Veins of Rats and Subsequent Serial Blood Corticosterone Levels,” *J. Am. Assoc. Lab. Anim. Sci.*, vol. 55, no. 2, pp. 204–212, 2016.
- [28] N. Abolhassani, R. Patel, and M. Moallem, “Control of soft tissue deformation during robotic needle insertion.,” *Minim. Invasive Ther. Allied Technol.*, vol. 15, no. May, pp. 165–76, 2006, <https://doi.org/10.1080/13645700600771645>
- [29] S. T. R. Gidde, T. Verissimo, N. Chen, P. Hutapea, and B.-G. Loh, “Neural network modeling of maximum insertion force of bevel-tip surgical needle,” in *ASME International Mechanical Engineering Congress and Exposition, Proceedings (IMECE)*, 2018, vol. 3, <https://doi.org/10.1115/IMECE2018-88383>
- [30] C. Yang, Y. Xie, S. Liu, and D. Sun, “Force modeling, identification, and feedback control of robot-assisted needle insertion: A survey of the literature,” *Sensors (Switzerland)*, vol. 18, no. 2, 2018, <https://doi.org/10.3390/s18020561>
- [31] J. Z. Moore, K. Malukhin, A. J. Shih, and K. F. Ehmman, “Hollow needle tissue insertion force model,” *CIRP Ann. - Manuf. Technol.*, vol. 60, no. 1, pp. 157–160, 2011, <https://doi.org/10.1016/j.cirp.2011.03.101>
- [32] M. Sahlabadi and P. Hutapea, “Novel design of honeybee-inspired needles for percutaneous procedure,” *Bioinspiration and Biomimetics*, vol. 13, no. 3, 2018,

<https://doi.org/10.1088/1748-3190/aaa348>

- [33] P. H. Mohammad Sahlabadi, David Gardell, Jonasan Younan Attia, “Design and Mechanics of Honeybee-Inspired Surgical Needles,” in *Biomedical Engineering Society Annual Meeting*, 2017.
- [34] H. Izumi, M. Suzuki, S. Aoyagi, and T. Kanzaki, “Realistic imitation of mosquito ’ s proboscis : Electrochemically etched sharp and jagged needles and their cooperative inserting motion,” *Sensors Actuators A. Phys.*, vol. 165, no. 1, pp. 115–123, 2011, <https://doi.org/10.1016/j.sna.2010.02.010>
- [35] J. Kim, S. Park, G. Nam, Y. Choi, S. Woo, and S. H. Yoon, “Bioinspired microneedle insertion for deep and precise skin penetration with low force: Why the application of mechanophysical stimuli should be considered,” *J. Mech. Behav. Biomed. Mater.*, vol. 78, no. October 2017, pp. 480–490, 2018, <https://doi.org/10.1016/j.jmbbm.2017.12.006>
- [36] T. A. Lenau, T. Hesselberg, A. Drakidis, P. Silva, and S. Gomes, “Mosquito inspired medical needles,” *Bioinspiration, Biomimetics, Bioreplication 2017*, vol. 10162, p. 1016208, 2017, <https://doi.org/10.1117/12.2261399>
- [37] M. Sahlabadi, S. Khodaei, and P. Hutapea, “Design and Evaluation of Advanced Smart Needles for Brain Biopsy,” in *Proceedings of the ASME 2017 Conference on Smart Materials, Adaptive Structures and Intelligent Systems SMASIS2017*, 2017, pp. 1–4, <https://doi.org/10.1115/SMASIS2017-3838>
- [38] J. H. Park, M. G. Allen, and M. R. Prausnitz, “Biodegradable polymer microneedles:

- fabrication, mechanics and transdermal drug delivery,” *J. Control. Release*, vol. 104, no. 1, pp. 51–66, 2005, <https://doi.org/10.1016/j.jconrel.2005.02.002>
- [39] U. Akgun, M. Karahan, and P. S. Randelli, *Knots in Orthopedic Surgery*. 2018.
- [40] J. E. L. B.D. Ratner, A.S. Hoffman, F.J. Schoen, *Biomaterials Science: An Introduction to Materials in Medicine*. 1996.
- [41] A. Chebolu, A. Mallimoggala, and Nagahanumaiah, “Modelling of Cutting Force and Deflection of Medical Needles with Different Tip Geometries,” *Procedia Mater. Sci.*, vol. 5, pp. 2023–2031, 2014, <https://doi.org/10.1016/j.mspro.2014.07.535>
- [42] M. Sahlabadi, S. Khodaei, K. Jezler, and P. Hutapea, “Study of Bioinspired Surgery Needle Advancing in Soft Tissues,” in *Proceedings of the ASME 2017 Conference on Smart Materials, Adaptive Structures and Intelligent Systems SMASIS2017*, 2017, pp. 1–4, <https://doi.org/10.1115/SMASIS2017-3915>
- [43] A. C. Barnett, “Tissue cutting mechanics of dynamic needle insertion,” *Ph.D. Thesis*, May 2016.
- [44] S. Jiang, P. Li, Y. Yu, J. Liu, and Z. Yang, “Experimental study of needle-tissue interaction forces: Effect of needle geometries, insertion methods and tissue characteristics,” *J. Biomech.*, vol. 47, no. 13, pp. 3344–3353, 2014, <https://doi.org/10.1016/j.jbiomech.2014.08.007>
- [45] M. A. Towler *et al.*, “Influence of cutting edge configuration on surgical needle penetration forces,” *J. Emerg. Med.*, vol. 6, no. 6, pp. 475–481, 1988,

[https://doi.org/10.1016/0736-4679\(88\)90403-9](https://doi.org/10.1016/0736-4679(88)90403-9)

- [46] M. Sahlabadi, “A novel bioinspired design for surgical needles to reduce tissue damage in interventional procedures,” *Ph.D. Thesis*, 2018.
- [47] A. C. Barnett, Y.-S. Lee, and J. Z. Moore, “Fracture Mechanics Model of Needle Cutting Tissue,” *J. Manuf. Sci. Eng.*, vol. 138, no. 1, p. 011005, 2015, <https://doi.org/10.1115/1.4030374>
- [48] A. A. Zadpoor, “Mechanics of biological tissues and biomaterials: Current trends,” *Materials (Basel)*, vol. 8, no. 7, pp. 4505–4511, 2015, <https://dx.doi.org/10.3390%2Fma8074505>
- [49] N. Hungr, J. A. Long, V. Beix, and J. Troccaz, “A realistic deformable prostate phantom for multimodal imaging and needle-insertion procedures,” *Med. Phys.*, vol. 39, no. 4, pp. 2031–2041, 2012, <https://doi.org/10.1118/1.3692179>
- [50] G. M. Spirou, A. A. Oraevsky, I. Alex Vitkin, and W. M. Whelan, “Optical and acoustic properties at 1064 nm of polyvinyl chloride-plastisol for use as a tissue phantom in biomedical optoacoustics,” *Phys. Med. Biol.*, vol. 50, no. 14, 2005, <https://doi.org/10.1088/0031-9155/50/14/n01>
- [51] M. Scali, D. Kreeft, P. Breedveld, and D. Dodou, “Design and evaluation of a wasp-inspired steerable needle,” *Bioinspiration, Biomimetics, Bioreplication 2017*, vol. 10162, no. April 2017, p. 1016207, 2017, <https://doi.org/10.1117/12.2259978>
- [52] K. R. Henken, P. R. Seevinck, J. Dankelman, and J. J. van den Dobbelsteen, “Manually controlled steerable needle for MRI-guided percutaneous interventions,”

- Med. Biol. Eng. Comput.*, vol. 55, no. 2, pp. 235–244, 2017,
<https://dx.doi.org/10.1007%2Fs11517-016-1490-0>
- [53] S. Misra, K. B. Reed, A. S. Douglas, K. T. Ramesh, and A. M. Okamura, “Needle-tissue interaction forces for bevel-tip steerable needles,” *Proc. 2nd Bienn. IEEE/RAS-EMBS Int. Conf. Biomed. Robot. Biomechatronics*, pp. 224–231, 2008,
<https://dx.doi.org/10.1109%2FBIOROB.2008.4762872>
- [54] S. T. R. Gidde, A. Ciuciu, N. Devaravar, R. Doracio, K. Kianzad, and P. Hutapea, “Effect of vibration on insertion force and deflection of bioinspired needle in tissues,” *Bioinspiration and Biomimetics*, vol. 15, no. 5, 2020,
<https://doi.org/10.1088/1748-3190/ab9341>
- [55] P. N. Brett, A. J. Harrison, and T. A. Thomas, “Schemes for the identification of tissue types and boundaries at the tool point for surgical needles,” *IEEE Trans. Inf. Technol. Biomed.*, vol. 4, no. 1, pp. 30–36, 2000,
<https://doi.org/10.1109/4233.826856>
- [56] A. E. Healey *et al.*, “In vivo force during arterial interventional radiology needle puncture procedures,” *Stud. Health Technol. Inform.*, vol. 111, no. May 2017, pp. 178–184, 2005.
- [57] M. Heverly and P. Dupont, “Trajectory Optimization for Dynamic Needle Insertion,” *Proc. - IEEE Int. Conf. Robot. Autom.*, no. April, pp. 1658–1663, 2005,
<https://doi.org/10.1109/ROBOT.2005.1570349>
- [58] T. B. Frick, D. D. Marucci, J. A. Cartmill, C. J. Martin, and W. R. Walsh,

- “Resistance forces acting on suture needles,” *J. Biomech.*, vol. 34, no. 10, pp. 1335–1340, 2001, [https://doi.org/10.1016/s0021-9290\(01\)00099-9](https://doi.org/10.1016/s0021-9290(01)00099-9)
- [59] Y. Kobayashi, T. Sato, and M. G. Fujie, “Modeling of friction force based on relative velocity between liver tissue and needle for needle insertion simulation,” *Proc. 31st Annu. Int. Conf. IEEE Eng. Med. Biol. Soc. Eng. Futur. Biomed. EMBC 2009*, pp. 5274–5278, 2009, <https://doi.org/10.1109/iembs.2009.5334078>
- [60] J. R. Crouch, C. M. Schneider, J. Wainer, and A. M. Okamura, “Needle Insertion with Tissue Relaxation,” *Cs.Odu.Edu*, 2005.
- [61] F. A. Urrea, F. Casanova, G. A. Orozco, and J. J. García, “Evaluation of the friction coefficient, the radial stress, and the damage work during needle insertions into agarose gels,” *J. Mech. Behav. Biomed. Mater.*, vol. 56, pp. 98–105, 2016, <https://doi.org/10.1016/j.jmbbm.2015.11.024>
- [62] P. Han and K. Ehmann, “Study of the effect of cannula rotation on tissue cutting for needle biopsy,” *Med. Eng. Phys.*, vol. 35, no. 11, pp. 1584–1590, 2013, <https://doi.org/10.1016/j.medengphy.2013.05.001>
- [63] T. J. Zuber, “Punch biopsy of the skin,” *Am. Fam. Physician*, vol. 65, no. 6, pp. 1155-1158+1164+1167, 2002.
- [64] K. Wolkowicz, J. Z. Moore, and P. Mclaughlin, “Novel pneumatic device for high speed needle insertion in brachytherapy,” *J. Med. Devices, Trans. ASME*, vol. 7, no. 3, pp. 1–2, 2013, <https://doi.org/10.1115/1.4024513>
- [65] L. Tan, X. Qin, Q. Zhang, H. Zhang, H. Dong, T. Guo, G. Liu, “Effect of vibration

- frequency on biopsy needle insertion force,” *Med. Eng. Phys.*, vol. 43, pp. 71–76, 2017, <https://doi.org/10.1016/j.medengphy.2017.02.011>
- [66] A. C. Barnett, J. A. Jones, Y. Lee, and J. Z. Moore, “Compliant Needle Vibration Cutting of Soft Tissue,” vol. 138, no. November 2016, pp. 1–9, 2018, <https://doi.org/10.1115/1.4033690>
- [67] S. Aoyagi, H. Izumi, and M. Fukuda, “Biodegradable polymer needle with various tip angles and consideration on insertion mechanism of mosquito’s proboscis,” *Sensors Actuators, A Phys.*, vol. 143, no. 1, pp. 20–28, 2008, <https://doi.org/10.1016/j.sna.2007.06.007>
- [68] Y. C. Huang, M. C. Tsai, and C. H. Lin, “A piezoelectric vibration-based syringe for reducing insertion force,” *IOP Conf. Ser. Mater. Sci. Eng.*, vol. 42, no. 1, 2012.
- [69] L. Tan, X. Qin, Q. Zhang, H. Zhang, H. Dong, T. Guo, G. Liu, “Effect of vibration frequency on biopsy needle insertion force,” *Med. Eng. Phys.*, vol. 43, pp. 71–76, 2017, <https://doi.org/10.1016/j.medengphy.2017.02.011>
- [70] W. Wu, C. Xu, C. Pan, Z. Huang, J. Zhou, and P. Huang, “Effect of vibration frequency on frictional resistance of brain tissue during vibration-assisted needle insertion,” *Med. Eng. Phys.*, vol. 86, pp. 35–40, 2020, <https://doi.org/10.1016/j.medengphy.2020.10.003>
- [71] R. K. Mobley, *Vibration Fundamentals*. Elsevier, 1999.
- [72] N. D. M. Begg and A. H. Slocum, “Audible frequency vibration of puncture-access medical devices,” *Med. Eng. Phys.*, vol. 36, no. 3, pp. 371–377, 2014,

<https://doi.org/10.1016/j.medengphy.2013.12.011>

- [73] Y. Cai, J. Moore, and Y. S. Lee, “Vibration study of novel compliant needle used for vibration-assisted needle insertion,” *Computer-Aided Design and Applications*, vol. 16, no. 4, pp. 742–754, 2019, <https://doi.org/10.14733/2019.742-754>
- [74] K. Alam, A. V. Mitrofanov, and V. V. Silberschmidt, “Experimental investigations of forces and torque in conventional and ultrasonically-assisted drilling of cortical bone,” *Med. Eng. Phys.*, vol. 33, no. 2, pp. 234–239, 2011, <https://doi.org/10.1016/j.medengphy.2010.10.003>
- [75] Ming Yang and Jeffrey D. Zahn, “Microneedle Insertion Force Reduction Using Vibratory Actuation,” *Biomed. Microdevices*, pp. 177–182, 2004, <https://doi.org/10.1023/b:bmmd.0000042046.07678.2e>
- [76] M. K. Ramasubramanian, O. M. Barham, and V. Swaminathan, “Mechanics of a mosquito bite with applications to microneedle design,” *Bioinspiration and Biomimetics*, vol. 3, no. 4, 2008, <https://doi.org/10.1088/1748-3182/3/4/046001>
- [77] M. Scali, T. P. Pusch, P. Breedveld, and D. Dodou, “Ovipositor-inspired steerable needle: design and preliminary experimental evaluation,” *Bioinspir. Biomim.*, 2017, <https://doi.org/10.1088/1748-3190/aa92b9>
- [78] M. Scali, D. Kreeft, P. Breedveld, and D. Dodou, “Design and evaluation of a wasp-inspired steerable needle,” in *Bioinspiration, Biomimetics, and Bioreplication 2017*, 2017, vol. 10162, p. 1016207, <https://doi.org/10.1117/12.2259978>
- [79] J. Ling, L. Jiang, K. Chen, C. Pan, Y. Li, W. Yuan, L. Liang, “Insertion and Pull

- Behavior of Worker Honeybee Stinger,” *J. Bionic Eng.*, vol. 13, no. 2, pp. 303–311, 2016, [https://doi.org/10.1016/S1672-6529\(16\)60303-7](https://doi.org/10.1016/S1672-6529(16)60303-7)
- [80] J. Wu, S. Yan, J. Zhao, and Y. Ye, “Barbs facilitate the helical penetration of honeybee (*Apis mellifera ligustica*) stingers,” *PLoS One*, vol. 9, no. 8, 2014, <https://dx.doi.org/10.1371/journal.pone.0103823>
- [81] A. J. Shoffstal, A. Srinivasan, M. Willis, A. M. Stiller, M. Ecker, W. E. Voit, J. J. Pancrazio, J. R. Capadona, “A Mosquito Inspired Strategy to Implant Microprobes into the Brain,” *Sci. Rep.*, vol. 8, no. 1, pp. 1–10, 2018, <https://doi.org/10.1038/s41598-017-18522-4>
- [82] M. Sahlabadi, S. Khodaei, K. Jezler, and P. Hutapea, “Insertion mechanics of bioinspired needles into soft tissues,” *Minim. Invasive Ther. Allied Technol.*, vol. 27, no. 5, pp. 284–291, 2018, <https://doi.org/10.1080/13645706.2017.1418753>
- [83] A. D. R. Li, K. B. Putra, L. Chen, J. S. Montgomery, and A. Shih, “Mosquito proboscis-inspired needle insertion to reduce tissue deformation and organ displacement,” *Sci. Rep.*, vol. 10, no. 1, p. 12248, 2020, <https://doi.org/10.1038/s41598-020-68596-w>
- [84] H. Izumi, T. Yajima, S. Aoyagi, N. Tagawa, Y. Arai, M. Hirata, S. Yorifuji, “Combined harpoonlike jagged microneedles imitating Mosquito’s proboscis and its insertion experiment with vibration,” *IEEJ Trans. Electr. Electron. Eng.*, vol. 3, no. 4, pp. 425–431, 2008, <https://doi.org/10.1002/tee.20295>
- [85] Z. L. Zhao, H. P. Zhao, G. J. Ma, C. W. Wu, K. Yang, and X. Q. Feng, “Structures,

- properties, and functions of the stings of honey bees and paper wasps: A comparative study,” *Biol. Open*, vol. 4, no. 7, pp. 921–928, 2015, <https://dx.doi.org/10.1242%2Fbio.012195>
- [86] J. Ling, Z. Song, J. Wang, K. Chen, J. Li, S. Xu, L. Ren, Z. Chen, D. Jin, L. Jiang, “Effect of honeybee stinger and its microstructured barbs on insertion and pull force,” *J. Mech. Behav. Biomed. Mater.*, vol. 68, no. January, pp. 173–179, 2017, <https://doi.org/10.1016/j.jmbbm.2017.01.040>
- [87] X. Q. Kong and C. W. Wu, “Measurement and Prediction of Insertion Force for the Mosquito Fascicle Penetrating into Human Skin,” *J. Bionic Eng.*, vol. 6, no. 2, pp. 143–152, 2009, [https://doi.org/10.1016/S1672-6529\(08\)60111-0](https://doi.org/10.1016/S1672-6529(08)60111-0)
- [88] K. Oka, S. Aoyagi, Y. Arai, Y. Isono, G. Hashiguchi, and H. Fujita, “Fabrication of a micro needle for a trace blood test,” *Sensors Actuators, A Phys.*, vol. 97–98, pp. 478–485, 2002, [https://doi.org/10.1016/S0924-4247\(01\)00872-X](https://doi.org/10.1016/S0924-4247(01)00872-X)
- [89] S. Aoyagi, H. Izumi, and M. Fukuda, “Biodegradable polymer needle with various tip angles and effect of vibration and surface tension on easy insertion,” *Proc. IEEE Int. Conf. Micro Electro Mech. Syst.*, no. January, pp. 397–400, 2007, <https://doi.org/10.1109/MEMSYS.2007.4432974>
- [90] D. Bi and Y. Lin, “Vibrating needle insertion for trajectory optimization,” *Proc. World Congr. Intell. Control Autom.*, pp. 7438–7443, 2008, <https://doi.org/10.1109/WCICA.2008.4594079>
- [91] S. T. R. Gidde, S. Islam, A. Kim, and P. Hutapea, “Vibrating Mosquito-Inspired

Surgical Needle for Reducing Tissue Deformation,” *Bioins. Biomim.*, (to be submitted 2021).

- [92] W. Li, B. Belmont, and A. Shih, “Design and Manufacture of Polyvinyl Chloride (PVC) Tissue Mimicking Material for Needle Insertion,” *Procedia Manuf.*, vol. 1, pp. 866–878, 2015, <https://doi.org/10.1016/j.promfg.2015.09.078>
- [93] M. Sahlabadi and P. Hutapea, “Tissue Deformation and Insertion Force of Bee-Stinger Inspired Surgical Needles,” *J. Med. Device.*, pp. 1–12, 2018, <https://doi.org/10.1115/1.4040637>
- [94] K. Yan, W. S. Ng, K. V. Ling, T. I. Liu, Y. Yu, and T. Podder, “High frequency translational oscillation & Rotational drilling of the needle in reducing target movement,” *Proc. IEEE Int. Symp. Comput. Intell. Robot. Autom. CIRA*, pp. 163–168, 2005, <https://doi.org/10.1109/CIRA.2005.1554271>
- [95] C. S. McGill, J. A. Schwartz, J. Z. Moore, P. W. McLaughlin, and A. J. Shih, “Effects of insertion speed and trocar stiffness on the accuracy of needle position for brachytherapy,” *Med. Phys.*, vol. 39, no. 4, pp. 1811–1817, 2012, <https://doi.org/10.1118/1.3689812>
- [96] V. Egorov, S. Tsyuryupa, S. Kanilo, M. Kogit, and A. Sarvazyan, “Soft tissue elastometer,” *Med. Eng. Phys.*, vol. 30, no. 2, pp. 206–212, 2008, <https://doi.org/10.1016/j.medengphy.2007.02.007>
- [97] S. Islam, V. Shah, S.T.R. Gidde, P. Hutapea, S.H. Song, J. Picone, A. Kim, “A Machine Learning Enabled Wireless Intracranial Brain Deformation Sensing

- System,” *IEEE Trans. Biomed. Eng.*, vol. 67, no. 12, pp. 1–1, 2020, <https://doi.org/10.1109/TBME.2020.2990071>
- [98] A. Michaud, “On The Magnetostatic Inverse Cube Law and Magnetic Monopoles,” *Int. J. Eng. Res.*, vol. 7, no. 5, pp. 50–66, 2013.
- [99] M. Slaoui and L. Fiette, “Histopathology procedures: from tissue sampling to histopathological evaluation.,” *Methods Mol. Biol.*, vol. 691, no. 1979, pp. 69–82, 2011, https://doi.org/10.1007/978-1-60761-849-2_4
- [100] S. T. R. Gidde, S. Acharya, S. Kandel, N. Pleshko, and P. Hutapea, “Bioinspired Needle Insertion Into Soft Tissue : A Tissue Damage Study,” *Ann. Biomed. Eng.*, (to be submitted 2021)
- [101] R. Tsumura, Y. Takishita, Y. Fukushima, and H. Iwata, “Histological evaluation of tissue damage caused by rotational needle insertion,” *Proc. Annu. Int. Conf. IEEE Eng. Med. Biol. Soc. EMBS*, vol. 2016-Octob, pp. 5120–5123, 2016, <https://doi.org/10.1109/embc.2016.7591879>
- [102] C. Simone and A. M. Okamura, “Modeling of needle insertion forces for robot-assisted percutaneous therapy,” *Proc. 2002 IEEE Int. Conf. Robot. Autom. (Cat. No.02CH37292)*, vol. 2, no. May, pp. 2085–2091, 2002, <https://doi.org/10.1109/ROBOT.2002.1014848>
- [103] M. Khadem, C. Rossa, R. S. Sloboda, N. Usmani, and M. Tavakoli, “Mechanics of Tissue Cutting during Needle Insertion in Biological Tissue,” *IEEE Robot. Autom. Lett.*, vol. 1, no. 2, pp. 800–807, 2016, <https://doi.org/10.1109/LRA.2016.2528301>

- [104] J. R. Crouch, C. M. Schneider, J. Wainer, and A. M. Okamura, “A velocity-dependent model for needle insertion in soft tissue,” *Lect. Notes Comput. Sci. (including Subser. Lect. Notes Artif. Intell. Lect. Notes Bioinformatics)*, vol. 3750 LNCS, pp. 624–632, 2005, https://doi.org/10.1007/11566489_77
- [105] C. Canudas-de-Wit, “A new model for control of systems with friction,” *IEEE Trans. Automat. Contr.*, vol. 43, no. 8, pp. 1189–1190, 1998, <https://doi.org/10.1109/9.376053>
- [106] H. Olsson, K. J. Åström, C. Canudas De Wit, M. Gäfvert, and P. Lischinsky, “Friction Models and Friction Compensation,” *Eur. J. Control*, vol. 4, no. 3, pp. 176–195, 1998, [https://doi.org/10.1016/S0947-3580\(98\)70113-X](https://doi.org/10.1016/S0947-3580(98)70113-X)
- [107] S. T. R. Gidde, S. Acharya, S. Al-Safadi, K. Patel, P. Hutapea, “Effect of Cutting Parameters in Vibration-Assisted Bioinspired Needle Insertion”, *J. Med. Dev.* (to be submitted 2021)

APPENDIX A

COMPRESSION TESTS FOR PVC AND GELATIN PHANTOMS

The compression tests were performed on the tissue-mimicking materials that were used in the dissertation study. The tissue-mimicking materials were utilized according to their viscoelastic properties. The gelatin tissue phantom was used to study the needle deflection, as there was a lack of tissue damage seen in PVC material. But most of the studies used in this dissertation were PVC tissue phantom. Many studies have been used PVC tissue material to study the insertion force and its effects.

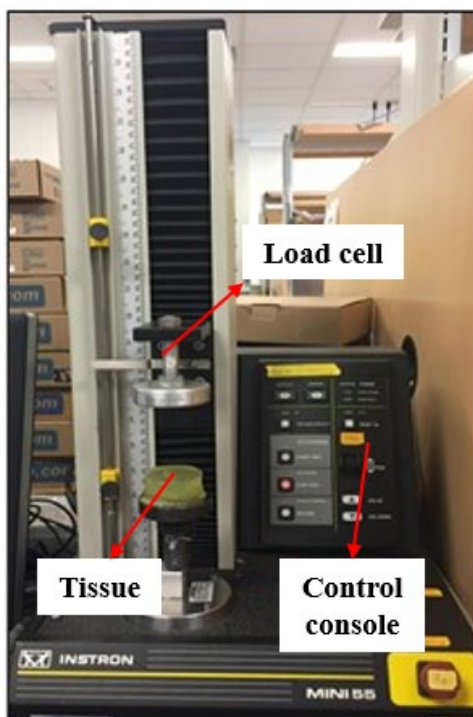


Figure A1. The compression test setup to determine the Young's Modulus of the tissue phantoms.

To determine the Young's Modulus of the different phantom gel, an Instron (Mini 55) Universal Testing System to perform a compression test as shown in Fig A1 was utilized. This is a standard method from the literature to acquire stress-strain relationships. The resolution of the load cell for the Instron machine is 0.112 mN. The tissue samples of each tissue-mimicking material were cut into a cylindrical shape with a thickness of 10 mm and a diameter of 50 mm. Due to the viscoelastic properties of the tissue phantoms, they were compressed with a 5 N load by small increments of 0.5 mm at a rate of 0.5 mm/s and then allowing the tissue to relax for 10 sec, this was repeated until the tissue reaches its strain condition and the minimum values for each compression and strain gave us the Young's Modulus. The most linear portion was used to find a line of best fit and the calculated slope was determined to be the Young's Modulus. The 11.1% of gelatin had Young's Modulus value of 4.2 kPa which was a sufficient model for healthy breast tissue. The PVC tissue phantom has a Young's Modulus of 1.8 and 6 kPa.

Table A1. The Young's Modulus and insertion force values for different tissue-mimicking materials used in this study.

<i>Material</i>	<i>Young's Modulus (E) kPa</i>	<i>The average insertion forces (N)</i>
(Polyvinyl chloride) PVC	1.3	1.99 ± 0.09 (No vibration)
	1.8	1.2 ± 0.11 (Vibration)
	6	3.25 ± 0.06 (No vibration)
Gelatin	4.2	2.94 ± 0.08 (Vibration)

APPENDIX B

MATLAB CODE FOR THEORETICAL MODEL

```
clc

clear all

close all

%the parameters that were chosen with respect to the properties of the needle for the
model and the needle used in the experiment for this theoretical analysis

Fco = 1.0611; %coulomb friction

Fs = 0.294; %static friction

sigma_0 = 0.0521; %stiffness coefficient

sigma_1 = 0.0145; %damping coefficient associated with z

sigma_2 = -0.0051; %viscous damping coefficient

alpha = 40; % needle-tip angle

E_T = 0.0026; %stiffness of the crack surface

E_R = 0.0557; %stiffness modulus

omega = linspace(0, 500,11);

% omega represents the vibration frequency

%divides the elements into 11 from 1 to 500 vibration frequency
```

```

%experimental data using 16-gauge standard bevel-tip needle into PVC %tissue (E = 6
kPa)

A = [2.14 1.40 1.27 1.14 1.69 2.49 3.12 4.02 4.35 4.87 5.05];

err = [0.08 0.108 0.09 0.11 0.106 0.092 0.086 0.1095 0.0958 0.086 0.075];

% The standard deviation (SD) values for the maximum insertion force at each
%vibration frequency from 0 to 500 Hz

errorbar(A, err);

for i = 1 : length(omega)

    F(i) = insertion(Fco, Fs, sigma_0, sigma_1, sigma_2, omega(i));

end

F = abs(F);

errorbar(omega, A,err,'x')

hold on

plot(omega, F)

hold off

xlim([0 500])

%%ylim([0 10] %if the force needs to be limited

xlabel ('Vibration(Hz)');

ylabel('Insertion Force (N) ');

legend("Experimental","Model");

```

```

set(gca,'FontSize',12);

set(legend,'position',[0.2 0.7 0.15 0.15],'FontSize',12)

print('Force', '-dpng', '-r300'); % save figure in PNG format with dpi

% Friction force:

%function below is the friction force formula that includes vibration

%effect on friction force (Ff) and cutting Force (Fc)

%F1 is the force acting on the needle

%F2 is the cutting (Fc) and friction force (Ff)

%F is the total insertion force

% The function for
function [F] = insertion(Fco, Fs, sigma_0, sigma_1, sigma_2, omega)

gamma = 0.0078;

vi = 1; %insertion speed

a = 0.475; %amplitude at the tip with respect to the change in units

t = 60; %time at insertion occurs during insertion into tissue

alpha = 30; % needle-tip angle

E_T = 0.0026; %stiffness of the crack surface

E_R = 0.0026; %stiffness modulus

%sinusoidal form of vibration

% V represents the total velocity, which means the summation of %insertion vibration
and insertion speed

```

```

V = 2*pi*a*omega*cos(2*pi*omega*t) +vi; %mm/sec
g = Fco + (Fs - Fco)*exp(-gamma*abs(vi)); % N/mm
z = g*sign(V); %N/sec
zdot = vi - sigma_0*(abs(V)/g)*z;
Fc = (4*tan(alpha/2)*(E_R)^2)/b*E_T;
Ff = ((sigma_0*z + sigma_1*zdot + sigma_2*V)- (0.009));
F2 = Fc+Ff;
F1 = 2.01;
F = F1 + F2;
end

```